A STUDY INTO THE FUNDAMENTAL UNDERSTANDING OF IRON-TRANSFORMATIONS AND THE EFFECT OF IRON AS FLUXING AGENT ON HIGHVELD FINE COAL SOURCES DURING GASIFICATION

A dissertation submitted to North-West University, Potchefstroom Campus, in fulfilment of the requirements for the degree of M.Eng (Chemical Engineering)

By

Christoffel Bernardus Prinsloo

B.Eng (Chem)(NWU)(2006)

Supervisor: Prof. F.B. Waanders

Co-supervisor: Dr. J.C. van Dyk

School of Chemical and Minerals Engineering

North-West University

Potchefstroom

South Africa

November 2008

SOLEMN DECLARATION

I, Christoffel Bernardus Prinsloo, declare that my work contained in this dissertation is my own original study and has not been previously published or submitted to any academic institution for a degree and that the necessary credit is given in the references.

CB Prinsloo

CB Prinsloo

2009-05-22

Date

ACKNOWLEDGEMENTS

I would firstly like to thank and praise my Creator who made all this possible for me. Without the ability and the love I received from the Lord I would not have been able to complete this project successfully. He deserves all the praise.

Secondly, I would like to thank my father Tolla, mother Christine, brother Johan and sister Suné for all their love, support and encouragement during this time. It really pulled me through!

I would also like to thank Prof. Waanders for his excellent guidance and his willingness to provide help and go the extra mile! I really appreciate it.

Dr. Van Dyk also provided valuable inputs and good advice which I greatly appreciate.

Ben Ashton and Jan Oosthuizen for help with experimental work.

Lastly, I want to thank Merica for all her tireless efforts to help and encourage me when everything did not go according to plan. You really are my strength!

I would like to dedicate this dissertation to my family and Merica. I love you all dearly!

~ Soli Deo Gloria ~

ABSTRACT

Coal, as energy resource, possesses numerous characteristics and properties which all have an influence on its gasification behaviour. The two properties considered critically important when evaluating a coal source for gasification are its mineral content and slagging behaviour. Research has indicated that slag formation can be inhibited or even prevented by the addition of a fluxing agent. It is thus of great importance to understand the mineral interaction during gasification, in order to select a suitable fluxing agent for the prevention of slagging and clinker formation in the gasifier.

The aim of this dissertation is to evaluate the slagging properties of a coal source with the addition of iron as a fluxing agent and to study the transformation of the mineral and added iron during gasification.

A pre-determined amount of elemental iron (between 2 and 20 percentage by mass) was added to three different coal samples obtained from Sasol's operations in South Africa. The transformation of the iron in conjunction with the possible iron-containing minerals present in the coal was studied by means of Mössbauer spectroscopy. Typical characterisation analyses were also carried out on the original coal samples. The ash fusion temperature analyses (AFT) were used to study the slagging behaviour of the iron-spiked coal samples. Even though AFT analyses only provide an average flow property, it gives a good indication of the changes that the iron addition induces in coal properties. FactSage modelling was carried out in conjunction with the Mössbauer and AFT analyses.

The AFT analysis on all of the samples indicated that the iron addition led to a 20% decrease in the AFT of all three the coal samples. The decrease observed, can be attributed to three main reasons: Formation of lower melting iron-containing phases, bridging of oxygen bonds by FeO and Fe_2O_3 and the lowering of the viscosity by the iron-oxides, mainly hematite.

Mössbauer spectra of the three original coal samples indicated that pyrite was the only iron-bearing mineral present.

In the three original ash samples it was observed that two components were present due to the transformation of the pyrite: hematite and an iron (Fe^{2+}, Fe^{3+}) containing glass. Spectra of ash samples containing a large amount of iron (>10 wt%) showed almost only hematite with a small amount of the iron (Fe^{2+}, Fe^{3+}) containing glass visible. This dominance of the hematite in the spectra was due to the transformation of the elemental iron which was present in a far greater quantity than the pyrite.

Initial simulations with the aid of the FactSage modelling package were carried out and it indicated that the partial oxygen pressure played a significant role in the transformation of pyrite in particular. The simulation showed that with the addition of iron to the coal samples there was a whole range of possible iron species that might form.

Key words: Gasification; mineral transformation; fluxing agent; elemental iron; AFT; Mössbauer spectroscopy; FactSage modelling

SINOPSIS

Steenkool, as energiebron, besit verskeie eienskappe wat elkeen 'n rol speel tydens die vergassingsproses. Die twee eienskappe wat as kritiek belangrik geag word wanneer 'n steenkoolbron vir vergassing geëvalueer word, is die mineraalinhoud van die bron, sowel as moontlike slakvorming. Navorsing het aangetoon dat slak geïnhibeer of selfs verhoed kan word deur die byvoeging van 'n vloeimiddel. Dit is dus uiters belangrik om *mineraalinteraksies tydens die vergassingsproses te verstaan, om sodoende 'n ingeligte* keuse te kan maak rakende die vloeimiddel vir die voorkoming van slak en klinkervorming in die vergassers.

Die doel van hierdie tesis is om die slakeienskappe van 'n steenkoolbron te evalueer indien yster bygevoeg word as vloeimiddel, asook om die transformasie van die mineraal sowel as die bygevoegde yster te bestudeer.

'n Voorafbepaalde hoeveelheid yster (tussen 2 en 20 massa%) is gevoeg by drie steenkoolmonsters verkry vanaf Sasol se operasionele bedrywighede in Suid-Afrika. Die transformasie van die bygevoegde yster, sowel as moontlike ysterbevattende minerale is bestudeer deur gebruik te maak van Mössbauer-spektroskopie. Die standaard karakteriseringstegnieke is uitgevoer op die oorspronklike steenkoolbronne. As-smeltingstemperatuur (AFT)-analises is gebruik om die slakeienskappe van die monsters met ysterbyvoeging te bestudeer. Gewone AFT-analises voorsien slegs 'n gemiddelde vloei-eienskap van die steenkoolbron, maar gee nogtans 'n goeie aanduiding van die veranderinge wat in steenkooleienskappe plaasvind as gevolg van die ysterbyvoeging. FactSage-modellering is ook uitgevoer.

Die resultate van die AFT-analises het aangedui dat die byvoeging van yster tot 'n verlaging van 20% in die AFT van die onderskeie steenkoolbronne lei. Hierdie verlaging kan aan drie redes toegeskryf word, naamlik: vorming van laer smeltende yster-bevattende fases, oorbrugging van suurstofbindings deur FeO en Fe_2O_3 en die verlaging van die viskositeit deur die yster-oksiedes, veral hematiet.

Mössbauer-spektra van die drie oorspronklike steenkoolmonsters het aangetoon dat *piriet die enigste yster-bevattende mineraal teenwoordig is.*

In die drie oorspronklike as-monsters is twee komponente waargeneem in die spektra: hematiet en 'n yster (Fe^{2+}, Fe^{3+})-bevattende glas. Spektra van die as-monsters met 'n groot hoeveelheid yster-byvoeging (>10 massa%) toon feitlik net hematiet met 'n klein hoeveelheid van die yster (Fe^{2+}, Fe^{3+})-bevattende glas nog sigbaar. Hierdie dominansie van die hematiet in die spektra kan toegeskryf word aan die transformasie van die suiwer bygevoegde yster wat in 'n groter hoeveelheid as die piriet teenwoordig is.

Simulasies met die FactSage-modelleringspakket het aangetoon dat die parsiële suurstofdruk 'n belangrike rol speel in veral piriet-transformasie. Die simulasies het ook aangetoon dat die byvoeging van yster kan lei tot die moontlike vorming van 'n hele reeks ysterspesies.

Sleutelwoorde: Vergassing; mineraal transformasie; vloeimiddel; yster; AFT; Mössbauer-spektroskopie; FactSage modellering

TABLE OF CONTENTS

CHAPTER 1 - INTRODUCTION 1
1.1 Background 1
1.2 Aim of dissertation 1
1.3 Hypothesis 2
1.4 Scope of investigation 2
1.5 Structure of dissertation 2
CHAPTER 2 – LITERATURE STUDY 3
2.1 Introduction 3
2.2 Overview of coal 3
2.2.1 Definition and formation of coal 3
2.2.2 Composition of coal 6
2.2.2.1 Vitrinite 8
2.2.2.2 Exinite 9
2.2.2.3 Inertinite 9
2.2.3 Mineral matter in coal 11
2.3 Gasification 17
2.3.1 Fixed bed gasifier 17
2.3.2 Fixed bed gasification process 19
2.3.3 High temperature gasification 22
2.4 Fusibility of coal ash 25
2.5 Fluxing properties of coal minerals 34
2.6 Transformation of mineral matter 37
CHAPTER 3 - EXPERIMENTAL SETUP 42
3.1 Samples 42
3.2 Proximate analysis 42
3.3 Ultimate analysis 43
3.4 Ash composition 44
3.5 Scanning microscopy analyses (SEM) 44
3.6 AFT analysis 45
3.7 Mössbauer spectroscopy 47
3.7.1 Introduction to Mössbauer spectroscopy 48
3.8 FactSage modelling 53

CHAPTER 4 – RESULTS & DISCUSSION 55
4.1 Introduction 55
4.2 Characteristics of coal samples 55
4.2.1 Proximate analysis 55
4.2.2 Ultimate analysis 55
4.2.3 Ash composition analysis 56
4.2.4 SEM results 58
4.3 AFT analysis 59
4.3.1 Analysis of original samples 59
4.3.2 Results for AFT experiments on iron addition samples under oxidizing conditions 60
4.3.3 Results of the AFT experiments conducted on the iron addition samples, under reducing conditions 64
4.3.4 Discussion of the AFT results 67
4.4 Mössbauer spectroscopy 72
4.4.1 Sample A 74
4.4.2 Sample B 77
4.4.3 Sample C 79
4.5 FactSage modelling 81
CHAPTER 5 – SUMMARY & CONCLUSIONS 86
5.1 AFT analysis 86
5.2 Mössbauer spectroscopy 87
5.3 FactSage modelling 87
REFERENCES 89
APPENDIX – EXPERIMENTAL RESULTS i
A.1 Ash and coal composition i
A.2 AFT analysis on iron – added samples iii
A.3 Mössbauer spectroscopy vi

LIST OF TABLES

CHAPTER 2 – LITERATURE STUDY

Table 2.1: Distinction between peat and brown coal....4

Table 2.2: Classification and properties of brown coal....5

Table 2.3: Overview of the different macerals....7

Table 2.4: Properties of the main mineral groups....13

CHAPTER 4 – RESULTS & DISCUSSION

Table 4.1: Proximate analysis for the three coal samples received (on a mass percentage basis)....55

Table 4.2: Ultimate analysis for the three coal samples received....56

Table 4.3: Ash composition analysis for the three coal samples received....57

Table 4.4: AFT results of the original samples under oxidizing conditions....60

Table 4.5: AFT results of the original samples under reducing conditions....60

Table 4.6: Percentage difference in AFT induced by iron addition....67

Table 4.7: Room temperature Mössbauer parameters of the various Fe species present in the coal....72

Table 4.8: Room temperature Mössbauer parameters of the various Fe species present in the coal ash....73

APPENDIX – EXPERIMENTAL RESULTS

Table A. 1: Composition of the coal in percentage elements present....i

Table A. 2: Composition of the coal ash in percentage elements present....ii

Table A. 3: Result of AFT analysis conducted on sample with 2 mass percentage iron added under oxidizing conditions....iii

Table A. 4: Result of AFT analysis conducted on sample with 5 mass percentage iron added under oxidizing conditions....iii

Table A. 5: Result of AFT analysis conducted on sample with 10 mass percentage iron added under oxidizing conditions....iv

Table A. 6: Result of AFT analysis conducted on sample with 15 mass percentage iron added under oxidizing conditions....iv

Table A. 7: Result of AFT analysis conducted on sample with 20 mass percentage iron added under oxidizing conditions....iv

Table A. 8: Result of AFT analysis conducted on sample with 2 mass percentage iron added under reducing conditions iv
Table A. 9: Result of AFT analysis conducted on sample with 5 mass percentage iron added under reducing conditions v
Table A. 10: Result of AFT analysis conducted on sample with 10 mass percentage iron added under reducing conditions v
Table A. 11: : Result of AFT analysis conducted on sample with 15 mass percentage iron added under reducing conditions v
Table A. 12: Result of AFT analysis conducted on sample with 20 mass percentage iron added under reducing conditions v

LIST OF FIGURES

CHAPTER 2 – LITERATURE STUDY

Figure 2.1: Process of coalification.....6
Figure 2.2: The three different maceral groups.....10
Figure 2.3: Schematic illustration of intrinsic and extrinsic mineral formation.....12
Figure 2.4: SEM image of a kaolin – coal – tonstein.....14
Figure 2.5: SEM image of calcite.....15
Figure 2.6: SEM image op epigenetic pyrite deposited into cleats.....16
Figure 2.7: Clastic quartz grains in coal.....17
Figure 2.8: A schematic representation of a Sasol – Lurgi gasifier.....18
Figure 2.9: A moving or fixed bed with temperature profile.....20
Figure 2.10: Schematic representation of a fixed – bed gasifier with all the distinctive zones indicated.....21
Figure 2.11: Graph depicting the increase in reaction rate with in crease in temperature.....23
Figure 2.12: Schematic representation of a GE gasifier.....24
Figure 2.13: Schematic illustration of a slagging Lurgi gasifier.....25
Figure 2.14: A ternary phase diagram for the $SiO_2 – Al_2O_3 – CaO$ system.....30
Figure 2.15: The effect of Al_2O_3, SiO_2 and TiO_2 on the AFT of a coal source.....36
Figure 2.16: Mineral matter transformation mechanism.....37

CHAPTER 3 – EXPERIMENTAL SETUP

Figure 3.1: Schematic illustration of a SEM apparatus.....45
Figure 3.2: Schematic illustration of the four observed changes during a standard AFT test.....46
Figure 3.3: The Halder Mössbauer apparatus used for experimental purposes.....47
Figure 3.4: Events occurring in Mössbauer spectroscopy.....48
Figure 3.5: Schematic illustration of a Mössbauer apparatus.....50
Figure 3.6: Schematic representation of the isomer shift observed in a Mössbauer spectrum.....51
Figure 3.7: Schematic representation of a qaudrupole splitting observed in a Mössbauer spectrum.....52

Figure 3.8: Schematic representation of a typical hyperfine magnetic splitting as observed in a Mössbauer spectrum.....53

CHAPTER 4 – RESULTS & DISCUSSION

Figure 4.1: SEM image of Sample C with 15 mass percentage iron addition.....58
Figure 4.2: SEM image of sample B with 20 mass percentage iron addition.....58
Figure 4.3: SEM image of Sample C ash with 15 mass percentage iron addition.....59
Figure 4.4: AFT results of Sample A and those to which different amounts of iron were added under oxidizing conditions.....61
Figure 4.5: AFT results of Sample B and those to which different amounts of iron were added under oxidizing conditions.....61
Figure 4.6: AFT results of Sample C and those to which different amounts of iron were added under oxidizing conditions.....62
Figure 4.7: Complete AFT results of Sample A showing all four deformation temperatures under oxidizing conditions.....62
Figure 4.8: Complete AFT results of Sample B showing all four deformation temperatures under oxidizing conditions.....63
Figure 4.9: Complete AFT results of Sample C showing all four deformation temperatures under oxidizing conditions.....63
Figure 4.10: AFT results of Sample A and those to which different amounts of iron were added under reducing conditions.....64
Figure 4.11: AFT results of Sample B and those to which different amounts of iron were added under reducing conditions.....65
Figure 4.12: AFT results of Sample C and those to which different amounts of iron were added under reducing conditions.....65
Figure 4.13: Complete AFT results of Sample A showing all four deformation temperatures under reducing conditions.....66
Figure 4.14: Complete AFT results of Sample A showing all four deformation temperatures under reducing conditions.....66
Figure 4.15: Complete AFT results of Sample C showing all four deformation temperatures under reducing conditions.....67

Figure 4.16: AFT results for an ash sample with added Fe_2O_3 68
Figure 4.17: The ternary phase diagram for the three component system Al_2O_3-FeO-SiO_2 69
Figure 4.18: A ternary phase diagram for the three component system Al_2O_3-Fe_2O_3-SiO_2 70
Figure 4.19: The Mössbauer spectrum of Sample A coal (0 mass percent Fe added) 74
Figure 4.20: The Mössbauer spectrum of Sample A coal (20 mass percentage Fe added) 74
Figure 4.21: The Mössbauer spectrum of Sample A ash (0 mass percentage Fe added) 75
Figure 4.22: The Mössbauer spectrum of Sample A ash (20 mass percentage Fe added) 76
Figure 4.23: The Mössbauer spectrum of Sample B coal (0 mass percentage Fe added) 77
Figure 4.24: The Mössbauer spectrum of Sample B coal (20 mass percentage Fe added) 77
Figure 4.25: The Mössbauer spectrum of Sample B ash (0 mass percentage Fe added) 78
Figure 4.26: The Mössbauer spectrum of Sample B ash (20 mass percentage Fe added) 79
Figure 4.27: The Mössbauer spectrum of Sample C coal (0 mass percentage Fe added) 79
Figure 4.28: The Mössbauer spectrum of Sample C coal (20 mass percentage Fe added) 80
Figure 4.29: The Mössbauer spectrum of Sample C ash (0 mass percentage Fe added) 80
Figure 4.30: The Mössbauer spectrum of Sample C ash (20 mass percentage Fe added) 81
Figure 4.31: Phase diagram depicting possible phases as the result of pyrite subjected to combustion conditions 82
Figure 4.32: FactSage diagram illustrating the transformation of pyrite to pyrrhotite at a constant oxygen partial pressure 83

Figure 4.33: FactSage diagram illustrating the transformation of
pyrite to hematite at a constant oxygen partial pressure 84
Figure 4.34: FactSage diagram depicting iron transformation
during gasification 85

APPENDIX A – EXPERIMENTAL RESULTS
Figure A.1: The Mössbauer spectrum for the calibration sample
(100 mass percentage Fe) vi
Figure A.2: The Mössbauer spectrum for Sample A coal
(2 mass percentage Fe added) vi
Figure A.3: The Mössbauer spectrum for Sample A coal
(5 mass percentage Fe added) vii
Figure A.4: The Mössbauer spectrum for Sample A coal
(10 mass percentage Fe added) vii
Figure A.5: The Mössbauer spectrum for Sample A ash
(2 mass percentage Fe added) viii
Figure A.6: The Mössbauer spectrum for Sample A ash
(5 mass percentage Fe added) viii
Figure A.7: The Mössbauer spectrum for Sample A ash
(10 mass percentage Fe added) ix
Figure A.8: The Mössbauer spectrum for Sample A ash
(15 mass percentage Fe added) ix
Figure A.9: The Mössbauer spectrum for Sample B coal
(2 mass percentage Fe added) x
Figure A.10: The Mössbauer spectrum for Sample B coal
(5 mass percentage Fe added) x
Figure A.11: The Mössbauer spectrum for Sample B coal
(10 mass percentage Fe added) xi
Figure A.12: The Mössbauer spectrum for Sample B coal
(15 mass percentage Fe added) xi
Figure A.13: The Mössbauer spectrum for Sample B ash
(2 mass percentage Fe added) xii
Figure A.14: The Mössbauer spectrum for Sample B ash
(5 mass percentage Fe added) xii

Figure A.15: The Mössbauer spectrum for Sample B ash
(10 mass percentage Fe added) xiii
Figure A.16: The Mössbauer spectrum for Sample B ash
(15 mass percentage Fe added) xiii
Figure A.17: The Mössbauer spectrum for Sample C coal
(5 mass percentage Fe added) xiv
Figure A.18: The Mössbauer spectrum for Sample C coal
(10 mass percentage Fe added) xiv
Figure A.19: The Mössbauer spectrum for Sample C coal
(15 mass percentage Fe added) xv
Figure A.20: The Mössbauer spectrum for Sample C ash
(2 mass percentage Fe added) xv
Figure A.21: The Mössbauer spectrum for Sample C ash
(5 mass percentage Fe added) xvi
Figure A.22: The Mössbauer spectrum for Sample C ash
(10 mass percentage Fe added) xvi
Figure A.23: The Mössbauer spectrum for Sample C ash
(15 mass percentage Fe added) xvii

CHAPTER 1 INTRODUCTION

1.1 Background

Coal is widely regarded as one of the most important energy sources currently available for exploitation. This rock originates from the fossilised remains of plant debris, which has undergone numerous physical and chemical changes throughout millions of years (Falcon & Snyman, 1986). Coal, however, cannot be classified as a homogeneous material due to the presence of organic and inorganic constituents (Falcon & Falcon, 1987). The inorganic constituents within the coal are often referred to as the mineral matter. This mineral matter (inorganic constituents) plays a major role during the gasification of a coal source as it is responsible for the majority of the operational problems experienced (Govender, 2005). Operational problems, such as channel burning which originates from the melting of the mineral matter (also known as slagging) in the coal lead to insufficient gasification and pressure drop within the gasifier (Govender, 2005; Van Dyk 2006).

Sasol is currently the largest commercial user of the gasification technologies known. This gasification is mainly used for the production of synthesis gas (a gas consisting of H_2 and CO) which is utilized in the Fischer-Tropsch process in order to produce fuels and chemicals. Sasol's gasifiers receive mainly a low-rank inertinite-rich coal, which is the type of coal commonly found in South Africa. The properties of the coal used may differ, depending on the area from which it originates (Van Dyk, 2006).

In order to operate gasifiers effectively, a fundamental understanding regarding the composition of the coal, as well as the transformation undergone by the mineral matter is crucial. This understanding will help identify possible problem areas, as well as in assisting in the resolution of operational problems.

1.2 Aim of dissertation

The main aim of this dissertation is to study the transformation of the minerals containing iron in coal during heating, in order to closely simulate the gasification process. The second objective is to establish what effect the addition of an iron-fluxing agent will have on the slagging properties of a coal source.

1.3 Hypothesis

Research conducted by Van Dyk (2006) indicates that iron has a definite effect on the ash fusion temperature (the temperature at which the mineral matter melts) and generally tends to decrease this temperature. Thus, it is expected that the addition of an iron-fluxing agent will enhance slag formation during gasification.

1.4 Scope of investigation

Three different coal samples will be used for the experimental work. Sub-samples will be made up from these three samples and a certain amount of pure elemental iron will be added to each. A standard ash fusion temperature (AFT) test will be conducted on each of the sub-samples, in order to establish the effect of adding a certain amount of iron to a coal source. Mössbauer spectroscopy will be used to study the transformation of the iron in the sub-samples, as well as the iron-free samples. Finally, limited FactSage modelling will be carried out, in order to compare simulated and experimental results.

1.5 Structure of dissertation

A review of the literature that relates to this project is provided in Chapter 2. In Chapter 3 the experimental method and procedures are discussed while the experimental results and a discussion are given in Chapter 4. Chapter 5 completes this dissertation with the most important conclusions reached in this project.

CHAPTER 2 LITERATURE STUDY

2.1 Introduction

In this chapter an overview of the most relevant literature is given. Firstly a broad overview is given in which the origin of coal and the different components that form the constituents of coal, are discussed. The different characteristics of coal are also incorporated in this overview. Following this overview an introduction to the gasification process and the gasification vessel is given. Finally, a discussion about the mineral matter in coal, as well as topics that can be linked to minerals, i.e. slagging and the viscosity of slag is presented. The role of fluxing agents in slag formation and the influence of these fluxing agents on coal properties are also addressed.

2.2 Overview of coal

This section deals with the development process coal undergoes from peat stage to the bituminous stage, which is the coal used in the study, and how this process of forming the coal influences slagging and combustion properties of a coal source.

2.2.1 Definition and formation of coal

Coal is defined by Falcon & Snyman (1986) as a material that is fundamentally composed of the fossilised remains of plant debris in which progressive physical and chemical changes have taken place over an extended period of time. Neavel (1981) defines coal as a sedimentary rock accumulated as peat, composed mainly of macerals such as vitrinite, exinite and inertinite and subordinately of minerals. Water and gases are also present within the submicroscopic pores of the coal (Neavel, 1981).

Coalification is a term developed to describe the process of coal formation. Thus, it includes all the stages during coal formation which, according to Falcon and Ham (1988), are: peat → lignite (brown coal) → bituminous coal → semi-anthracite → anthracite → graphite

The level which a certain coal has reached in this coalification process (for example the bituminous stage) is called the rank of that particular coal (Falcon & Snyman 1986). Thus, the initial phase of coal formation is the peat stage. Peat can be described as the piece of earth located just under or partially above, the surface of a swamp environment. The optimum conditions for the creation of peat are obtained in stagnant water, over a period of one year, above or just beneath the surface, in order to prevent plant decay (Stach, *et al.*, 1982). The characteristics of a swamp environment are an abundance of water and a rich plant life. Some of the swamp environment was located at the coast where sea water dammed up fresh water running off the land (Stach *et al.*, 1982).

Over an extended period of time dead plant material had been buried beneath the surface of the swamp and thereby peat formed. This is a continuous process, which ensures that the peat of a swamp area keeps growing each year. It has been estimated that peat can grow up to 2 mm annually (Stach *et al.*, 1982). In this peat stage, plant material started to degrade due to the presence of fungi and bacteria which first degraded the protoplasm and enzyme substances. This degradation then continued to also include the storage foods (starch, sugars, etc.) and the lignin and cellulose found in the cell walls of the plant material. All of these degradations are known as the biochemical degradation stage. Once all of the plant material has been buried at a depth of 1 m the degradation switches to geochemical coalification or maturation (Falcon & Snyman, 1986). The next stage in coal formation is known as lignite or brown coal formation. In the transition, at a depth of about 200-400 m, between the two stages a noticeable decrease in the volume of the material within the peat can be observed. This can be ascribed to the compression, which increased as the material was further buried under soil. An estimated 2 400 to 3 000 years are needed to form just 1 m of brown coal (Stach, *et al.* 1982). The main distinctions between peat and brown coal are listed in Table 2.1.

Table 2.1: Distinction between peat and brown coal (Stach *et al.*, 1982)

Parameter	Peat	Brown coal
% Moisture	> 75	<75
% Carbon	Mostly < 60	Mostly > 60
Free cellulose	present	Not present
Can be easily cut?	yes	no

An increase in the burial depth leads to a decrease in the porosity of the coal and also the moisture content of the coal, as can be seen in Table 2.1. This brown coal or lignite phase can be subdivided into three different sub-phases, i.e. soft brown coal, dull brown coal and bright brown coal. The last two brown coals mentioned, namely dull and bright brown coal, are also known as sub-bituminous coal. In Table 2.2 the differences between the three different brown coals are highlighted.

Table 2.2: Classification and properties of brown coal (Stach et al., 1982)

Rank of coal	Megascopic	Microscopic	Physical composition
Soft brown coal	Brown and dull	Large pore volumes, gelification is rare, open cell lumens	75-35% H_2O 60 -70% C (daf*)
Dull brown coal	Dark brown to black, dull to low brightness	Less pore volume, stronger gelification open cell lumens are rare	35–25% H_2O Approximately 71% C (daf*)
Bright brown coal	Black and bright	Gelification completed	Usually 8–10% H_2O 71-77% C (daf*)

*= dry, ash-free basis

The formation of bituminous coal is the next stage in the coalification process. This stage in coal formation requires extreme burial depth in order to form. It is suggested that depths of at least 1 500 m are necessary for the formation of bituminous coals. A further increase in the burial depth of the coal leads to a further increase in the rank of the coal. The final two phases of the coalification process are known as the anthracite and graphite phases, respectively. Coalification is completed once the graphite phase is reached. Thus, graphite is the last stage in this process and this stage is sometimes used as an index for rock metamorphism (Stach *et al.*, 1982).

This whole coalification process is illustrated in Figure 2.1.

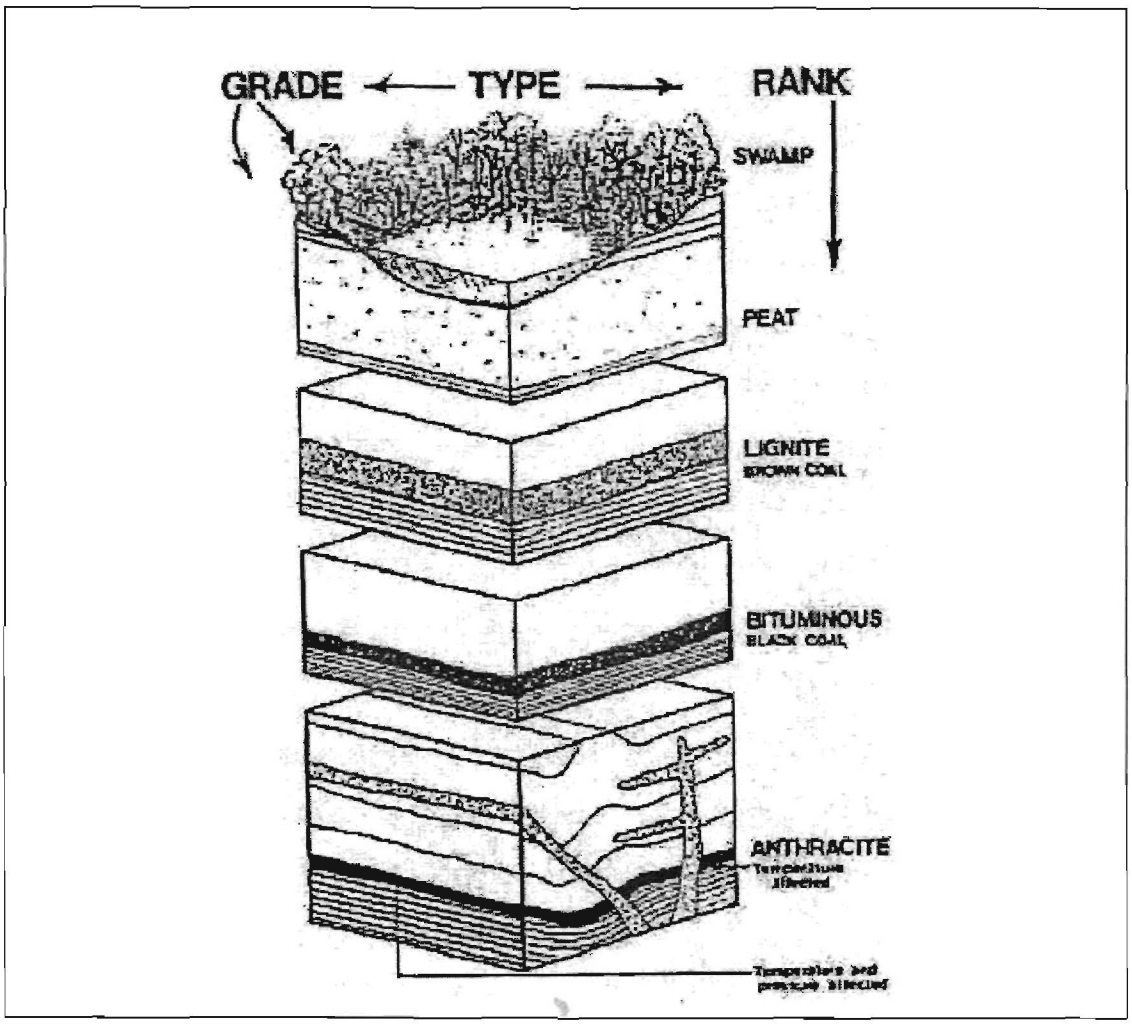


Figure 2.1: Process of coalification (Falcon & Ham, 1988)

2.2.2 Composition of coal

Generally, coal can be divided into organic and inorganic constituents when viewed on a microscopic level and is thus not a homogeneous substance. The organic constituents are mainly plant remains as described in the previous section, while mineral matter makes up the inorganic constituents. Organic constituents that are recognisable at the microscopic level are known as macerals and can be roughly divided into three groups, i.e. liptinite (exinite), inertinite and vitrinite. This classification is done, based on the chemical and physical differences between the organic constituents of a certain coal (Falcon & Ham, 1988., Stach *et al.*, 1982). In Table 2.3 an overview of the origin, properties and the technological characteristics of each of the three macerals is given.

Table 2.3: Overview of the different macerals (Falcon & Snyman, 1986, Falcon & Ham,1988)

Maceral group	Plant origin	Description	Chemical properties	Technological characteristics
Vitrinite	Woody trunks, branches, stems	Dark to medium grey	Oxygen rich	Combusts rapidly, Pyrolysis, Hydrogenation/liquefaction
	Stalks, bark, leaf tissue	Pale grey	Decreasing amount of volatiles upon heating	Combusts with little smoke
		White	Decreasing amount of volatiles upon heating	Combusts with no smoke
Exinite	Cuticles, spores, resin bodies	Black-brown to dark grey	Hydrogen rich	Combusts very rapidly, Pyrolysis
	Algae	Pale grey to white shadows	Hydrogen rich	Hydrogen/liquefaction, bitumen production
Inertinite	Same as for vitrinite, and oxidized detrital organic humus	Medium grey	Carbon rich	Combusts slowly, maintains flame, relatively inert in coking
		Pale grey to white and yellow white	Carbon rich	Combusts slowly, maintains flame, relatively inert in coking

A further in-depth discussion regarding the three different macerals now follows. Specific emphasis is placed on the behaviour of each of these macerals during combustion, in order to provide a platform from where behaviour during gasification can be modelled and explained.

2.2.2.1 Vitrinite

Vitrinite is defined by Falcon & Snyman (1986) as a group of microscopically recognisable constituents originating from cell wall material, as well as the cell fillings of the so-called woody tissue of plants, i.e. trunks, branches, etc. The name vitrinite is the group name under which certain macerals are listed. Three different macerals are distinguishable in this group and are known as telinite, collinite and vitrodetrinite. The vitrinite maceral group is the most frequently found maceral group and is usually present in bituminous coal (Stach *et al.*, 1982).

Properties of this maceral group, as well as the other maceral groups, are known to change with an increase in rank. With an increase in rank, the aromaticity and carbon content decrease in an almost linear trend while the hydrogen content initially increases and then decreases (Stach *et al.*, 1982). The main criterion for aromaticity is to comply with Hückel's $4n + 2$ rule. This rule states that a molecule is aromatic only if it has planar, monocyclic system of conjugation in which there is a total number of $(4n + 2)\pi$ electrons present with n being an integer, i.e. $n = 0, 1, 2,...$
The π-electrons refer to the electrons that are involved in π-bonding which is the result of two unhybridized p-orbitals overlapping sideways (McMurry, 2000).

The density of vitrinite varies between 1.3 and 1.8 g/ml, depending on the rank of the coal. In the process of combustion, the vitrinite maceral group exhibits a behaviour which is known as reactive behaviour. When vitrinite is heated, it degasifies with the volatiles, enhancing ignition. The coal ignites and combusts relatively easily. In the stage of devolatilization, in which the volatiles are removed, the coal of this maceral group softens, becomes plastic and swells to produce a porous char, leaving a larger area for the combustion process. In low rank coals vitrinite macerals are known to oxidize readily with a high tendency towards spontaneous combustion. Vitrinite macerals in low rank coals can readily be hydrogenated and liquefied, while high rank coals require certain special processes. Low rank vitrinite is further identified as being one of the most suitable feedstocks for the pyrolysis process (Falcon & Snyman, 1986).

2.2.2.2 Exinite

The exinite maceral group includes all of the chemical distinct parts of the plants, i.e. spores, cuticles, resins, etc. Macerals that are listed in this group are sporinite, cutinite, alginite, resinite and liptodetrinite. Exinite macerals can be described as aliphatic-aromatic skeletons having aliphatic side chains. When heated, this maceral group releases more volatile matter than any of the other maceral groups (Falcon & Snyman, 1986). Macerals of this group are known to yield exceptionally high proportions of tar and bitumen in the sub-bituminous and low rank bituminous coals. In high rank bituminous coal, exinite becomes indistinguishable from vitrinite (Falcon & Snyman, 1986).

Exinite macerals are the lightest of all of the macerals. The density for this group of macerals varies between 1.18 and 1.25 g/ml, depending on the rank. When heated, the exinite macerals exhibit the same behaviour as the vitrinite macerals, i.e. degasifies and the ignition being enhanced by the volatiles. When the heating of this coal is at an early stage, thus at low temperatures, a rapid release of bitumen and tar is observed which results in great carbon losses. The flame can, therefore, not be maintained. Concerning the oxidizability of this maceral group, it is not well-known what the rate of potential oxidation could be. Exinite is regarded as a very suitable feedstock for hydrogenation due to its high hydrogen content in, especially, low-rank coals. Low rank exinite is also one of the most suitable feedstocks for pyrolysis (Falcon & Snyman, 1986).

2.2.2.3 Inertinite

The inertinite maceral group originates from plant material that has been modified and degraded in oxidation conditions during the peat stage of coal formation. The plant material mentioned, is the same as the material from which vitrinite originates. Degradation in this oxidation condition occurs on an aerobic or sub-aerobic basis (Falcon & Snyman, 1986). The term inert in the name of this maceral group indicates the relatively low and in some cases non-reactivity of this group. In this maceral group the following macerals can be found: fusinite, semifusinite, macrinite, inertodetrinite, micrinite and sclerotinite. Micrinite, however, is not inert but has traditionally been listed in the inertinite maceral group (Stach *et al.*, 1982).

When comparing inertinite to the other two maceral groups in low rank coals it is observed that inertinite is much more aromatic than the other groups. An increase in rank does not really alter the physical and chemical properties of inertinite. Inertinite contains a large amount of oxygen and a small amount of hydrogen. The oxygen content of inertinite reduces rapidly with an increase in the rank of the coal (Falcon & Snyman, 1986).

The density of the inertinite group macerals falls roughly in the same range as that of the vitrinite macerals (1.35 – 1.7 g/ml) and hardly changes with a difference in rank. With regard to the combustion of this maceral group, the behaviour is in direct contrast with that of the other two maceral groups. Inertinite group macerals do not soften, degasify or become porous upon heating. A reduced surface for combustion is the result when these maceral groups are heated, which makes it difficult to ignite and slower to burn out. A higher oxygen feed and higher temperatures are needed to initiate the combustion process. It is believed that inertinite oxidizes at a far slower rate than the other maceral groups. Hydrogenation of this maceral group is not possible, due to its low hydrogen content. Furthermore, inertinite is not very suitable for pyrolysis, as very low yields would result if they were to be used as feedstock (Falcon & Snyman, 1986). Figure 2.2 shows images of the three different maceral goups.

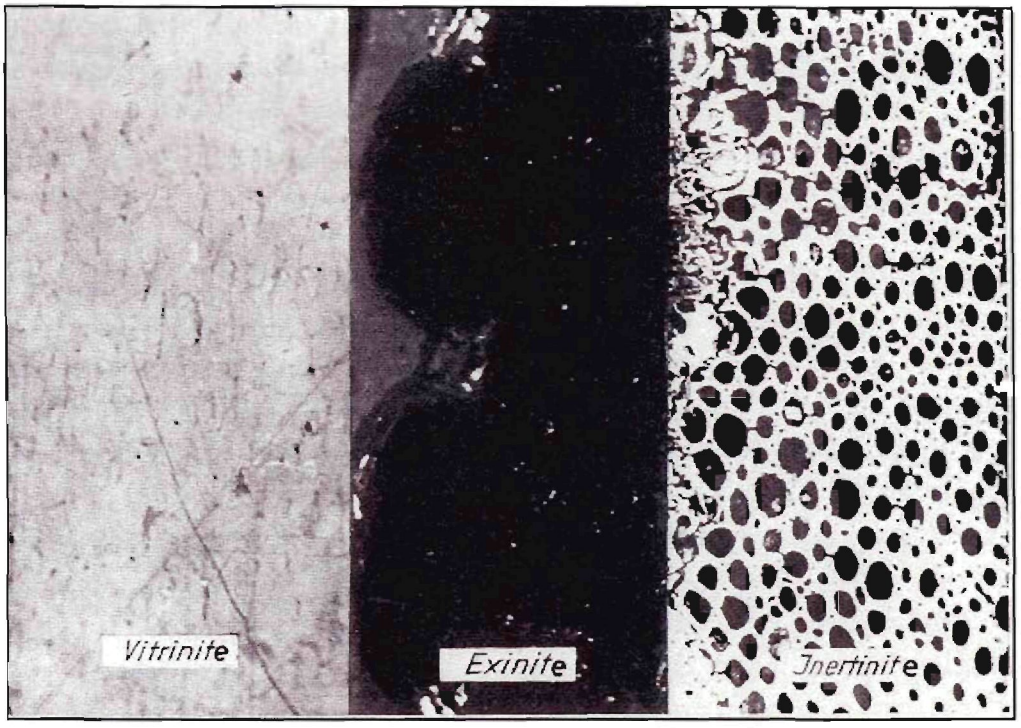


Figure 2.2: The three different maceral groups (Stach et al., 1982)

2.2.3 Mineral matter in coal

Mineral matter is regarded as the inorganic constituent of coal. Ward (2002) defines mineral matter as the sum of the minerals and other inorganic material within coal.

Stach *et al.* (1982) divides inorganic matter into three groups, based on their origin, with the three groups being:

- Inorganic matter from the original plants.
- Minerals that have been formed during the first stage of the coalification process or have been introduced by wind and water into the coal deposits. This group also contains the inorganic-organic complexes.
- Minerals that have been deposited during the second stage of the coalification process. Solutions in this coal deposit enter into cracks and cavities which lead to the introduction of inorganic matter into the coal deposit.

Minerals that are introduced during the first stage of the coalification are usually observed to be fine-grained and intimately grown with the coal, while minerals introduced during the second stage are neither fine-grained nor intimately grown (Stach *et al.*, 1982). Several authors each defines different categories for coal mineral matter. Renton (1982) states that mineral matter present in coal can be subdivided into three categories, i.e. detrital, vegetal and chemical.

According to Renton (1982) mineral matter in the detrital category was derived from a source that is external to the original swamp. This detrital mineral matter entered the swamp by means of wind and water. Vegetal mineral matter originated from the minerals found in the original swamp plants. Minerals in the chemical category originated from species that had once been part of an aqueous solution. These species could have entered the coal by direct precipitation or by chemical reactions between the aqueous solution and inorganic material already present in the coal-forming swamp (Renton, 1982).

Falcon and Snyman (1986), on the other hand, suggest that coal can be divided into two categories, i.e. intrinsic and extrinsic inorganic matter.

The intrinsic inorganic matter category of Falcon and Snyman (1986) compares well with the vegetal category of Renton (1982) in that it includes the inorganic matter that was present in the original living plant tissue of the swamp plants. These inorganic particles were embedded in the peat-forming swamp and got trapped in the form of sub-microscopic particles and organo-metallic complexes. Extrinsic inorganic matter, on the other hand, had been introduced into the peat forming swamp by means of wind, water, etc. This category is subdivided into primary/syngenetic and secondary/epigenetic categories. Primary or syngenetic inorganic matter includes all of the minerals that accumulated during the peat-forming phase.

This accumulation was achieved by means of wind, water and in-situ precipitation. The epigenetic or secondary category includes the minerals deposited by water into fractures or cavities and pores within this peat-forming swamp. Fractures present in the coal gave groundwater, containing mineral-forming ions, the opportunity to enter the coalbed and deposit mineral matter (Falcon & Snyman, 1986; Renton, 1982).

Figure 2.3 shows a schematical representation of the difference between intrinsic and extrinsic inorganic matter.

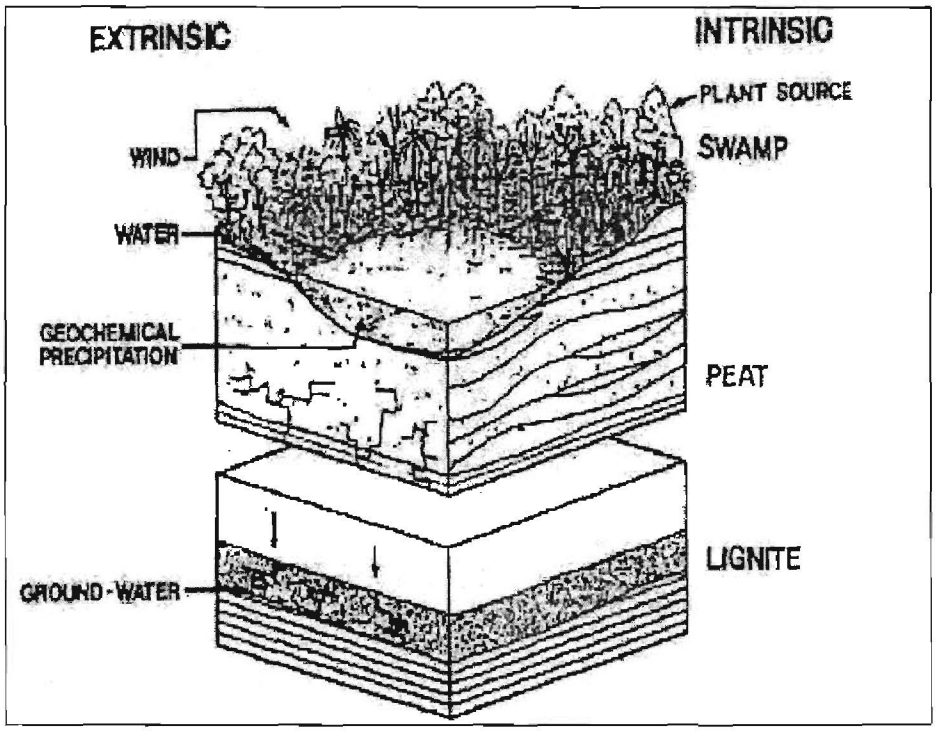


Figure 2.3: Schematic illustration of intrinsic and extrinsic mineral formation (Falcon & Snyman, 1986)

Vassilev *et al.* (1995) state that coal minerals (for Bulgarian coal) in the crystalline matter can be divided into major minerals (> 5 volume percent) and minor minerals (1 – 5 volume percent). The minerals in the major minerals category are: quartz, kaolinite, illite, feldspar, calcite, pyrite and gypsum. In the minor mineral category the minerals are: cristobalite, montmorillonite, mica, chlorite, zeolites, hematite, goethite, diaspore, borite, apatite, brucite, barytocalite, dolomite, siderite, marcasite, jarosite, alunite and hexahydrite. It should however be noted that the abundance of minerals are source dependant and that the type of minerals as well as the quantity in which they are found may more than likely vary in South African coal.

Alpern *et al.* (1983) states that the general agreement in literature is that clays, sulphides, carbonates and quartz can be regarded as the most common minerals in coal. Table 2.4 provides the different mineral groups with some of the common minerals listed in that group, together with the basic properties of each group.

Table 2.4: Properties of the main mineral groups (Alpern *et al.*, 1983; Falcon & Snyman, 1986)

Minerals	Formula	Colour	Anisotropism	Physical disposition and hardness
Clays				
Kaolinite	$Al_2\{Si_2O_5\}(OH)_4$	Dark grey to black	Isotropic	Scaly, soft
Illite	$KAl_2(AlSi_3O_{10})(OH)_2$			
Montmorillonite	$(Al,Mg)_2((Al,Si)_4O_{10})(OH)_2$			
Carbonates				
Siderite	$Fe(CO_3)$	Yellow-brown	Highly anisotropic	Rhombohedral cleavage, medium hardness
Ankerite	$Ca(Mg,Fe,Mn)(CO_3)_2$	Colour-less to white-yellow brownish		
Calcite	$Ca(CO_3)$			
Dolomite	$CaMg(CO_3)_2$			
Sulphides				
Pyrite	FeS_2	Yellow to bronze	Isotropic	Granular or massive, hard
Marcasite	FeS_2	Pale bronze – yellow	Highly anisotropic	Tabular, hard

Oxides				
Hematite	Fe_2O_3	White to blue-red, Steel grey	Strong anisotropism	Tabular, hard
Quartz	SiO_2	Dark to grey black	Weakly anisotropic	Granular, hard

Falcon and Snyman (1986) lists clays, carbonates, sulphides, quartz and glauconite as the most common minerals found in South Africa. A short discussion of each member of this important mineral group will now be given, in order to provide sufficient background information on these minerals.

Clays

This mineral group is the most important since it is the most abundant mineral found in coal. Normally, this mineral group makes up 60 – 80 mass percent of the total coal mineral content. Clays are usually found in one of two fundamental forms, either as finely dispersed inclusions in coal or as kaolin – coal tonstein. The most common minerals in this group are known to be: kaolinite, illite and sericite, while chlorite is the least abundant mineral in this group. Kaolinite rich coal is known to originate from a freshwater depositional environment. This kaolinite-rich coal usually has a higher ash fusion temperature (AFT) due to the fluxing properties of the kaolinite (Falcon & Snyman, 1986; Renton, 1982; Stach *et al.*, 1982). Figure 2.4 shows a SEM image of crystalline kaolin – coal tonstein which is better known as asflint clay in certain countries (Loughnan, 1978).

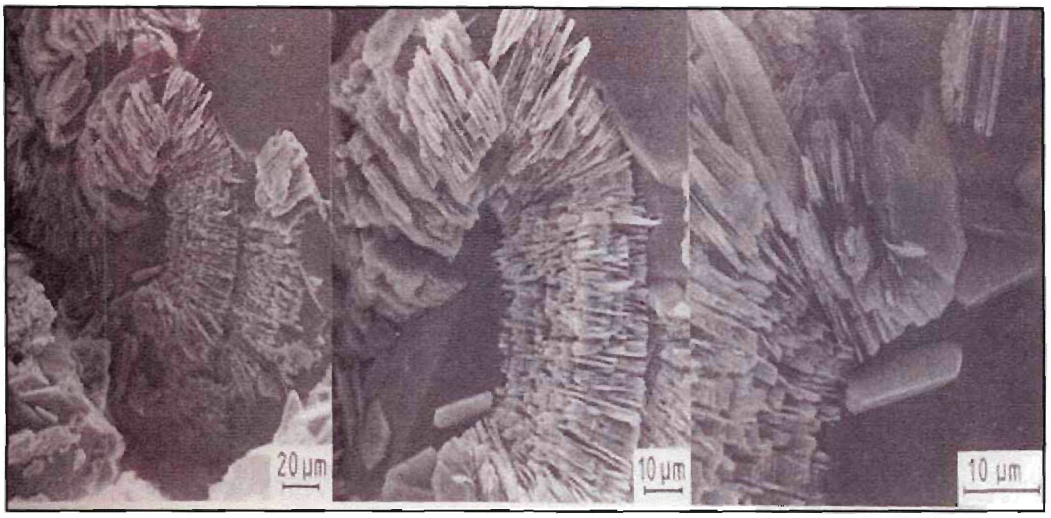


Figure 2.4: SEM image of a kaolin – coal – tonstein (Stach *et al.*, 1982)

Carbonates

Carbonates are the second most abundant mineral group after clay minerals and are known to be chemical in origin. These minerals are thought to have been formed during the late syngenetic and epigenetic phases of coal formation. Calcite, deposited during the second stage of coalification, is the most abundant mineral in this group. Dolomite and ankerite, on the other hand, are the least common (Falcon & Snyman, 1986; Renton, 1982; Stach *et al.*, 1982).

Figure 2.5 shows a SEM image of the mineral calcite in coal.



Figure 2.5: SEM image of calcite (Stach *et al.*, 1982)

Sulphides

The most commonly found minerals in this group are pyrite and marcasite and are omnipresent in Southern African coals. Marcasite is usually limited to coals in which there is a sulphur content of more than 1 mass percent (Falcon & Snyman, 1986; Renton, 1982; Stach *et al.*, 1982).

The mineral pyrite can be classified into five different types, i.e. (Renton, 1982):

- Framboids
- Isolated euhedral crystals
- Nonspherical aggregates of euhedral crystals

- Irregular shapes
- Fracture fillings

Figure 2.6 shows a SEM image of epigenetic pyrite deposited into cleats or fracture fillings.

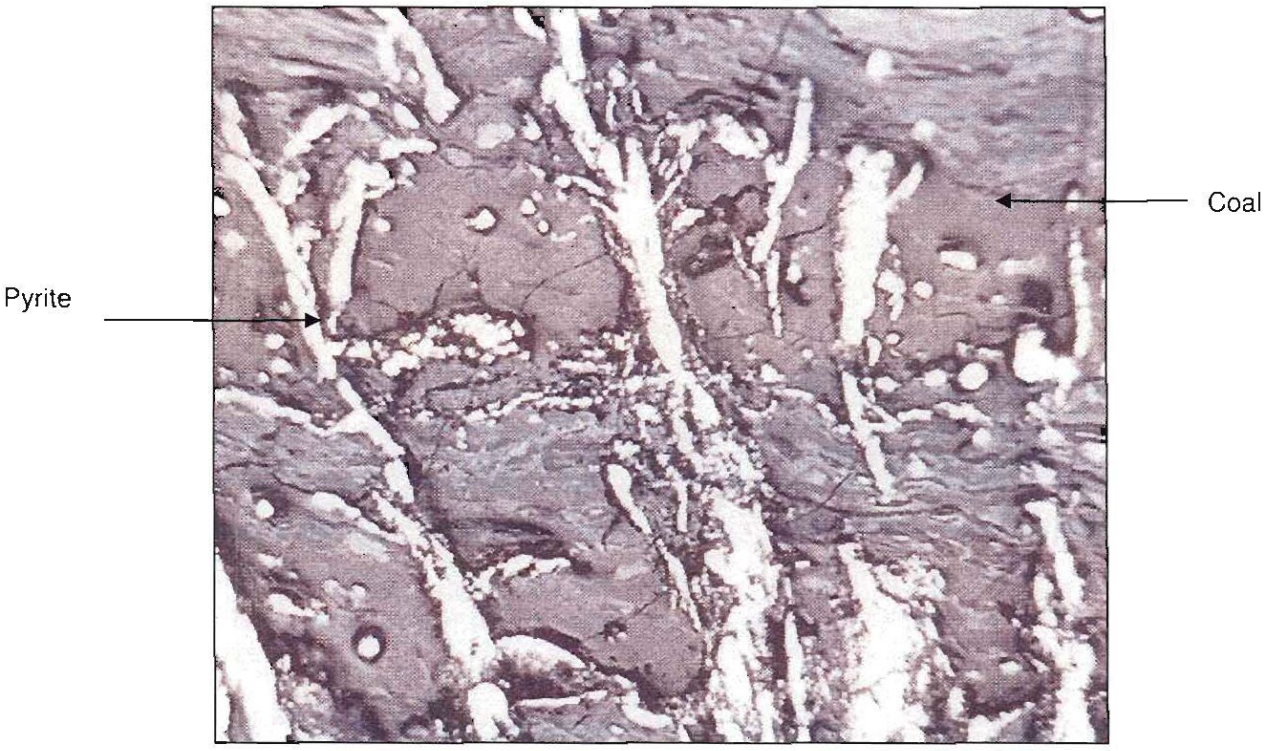


Figure 2.6: SEM image op epigenetic pyrite deposited into cleats (Stach et al., 1982)

Quartz

Quartz is by far the most important mineral in the oxide group. As mentioned earlier, quarts is one of the most common minerals found in coals around the world. Despite its abundance, it is only found in small quantities (Falcon & Snyman, 1986).

According to Renton (1982), quartz can be of vegetal, chemical or detrital origin. Quartz usually occurs as either rounded grains or as a fine crystalline structure in coal (Stach *et al.*, 1982).

Figure 2.7 illustrates clastic quartz grains. Clastic quartz was brought by water or wind and is present as more or less rounded grains (Stach *et al.*, 1982).



Figure 2.7: Clastic quartz grains in coal (Stach *et al.*, 1982)

2.3 Gasification

Gasification can be regarded as the core of Sasol's operations and can be defined as the conversion of a solid or a liquid into a gas. In coal gasification combustible gas or syngas (binary mixture of H_2 and CO), as it is commonly known, is produced. In gasification technology three basic designs exist: Fixed bed (or moving bed), fluidised bed and entrained flow gasifiers. The fixed bed and fluidised gasifiers are operated at moderate temperatures which are usually less than the ash fusion temperature (AFT) of the coal source. Entrained flow gasifiers are operated at high temperatures and the ash is removed in a molten state (Crnomarkovic *et al.*, 2007; Kristiansen, 1996; Probstein & Hicks, 2006)

In sections 2.3.1 and 2.3.2 fixed bed gasifiers will be discussed, with high temperature gasification being covered in section 2.3.3.

2.3.1 Fixed bed gasifier

Coal gasification by means of a Lurgi gasifier dates as far back as 1934 when the first of these gasifiers was erected in Germany (Nowacki, 1981; Yong, 2007). When Sasol started operations in 1950 Sasol 1, located in Sasolburg, was equipped with ten gasifiers called Mark III gasifiers. These gasifiers had an internal diameter of 3.66m. In 1966 three additional Mark III gasifiers were added to the existing ones. The total number of gasifiers was increased when three Mark IVs, with an internal diameter of 4m, were added in 1978. In 1980 another gasifier, with an internal diameter of 5m, the so-called Mark V gasifier, was brought into production (Van Dyk, 2006). Sasol currently utilizes 84 Mark IV gasifiers with 80 of them being located at the two plants in Secunda (Van Dyk, 2006).

Fixed bed gasifiers can basically be operated in one of two ways, i.e. the ash produced during the gasification process can be in either a dry state or a molten liquid (slag) (Nowacki, 1981; Schilling *et al.*, 1979).

Sasol utilizes Sasol–Lurgi Fixed bed dry bottom (FBDB) gasifiers which imply that the ash is removed in a dry state (Van Dyk, 2006). The Sasol–Lurgi gasification process is a medium temperature and pressure process. Coal is gasified at a pressure of 3 MPa and at temperatures ranging from 300℃ to 1500℃. In order to comply with these temperatures and pressures, the Sasol–Lurgi gasifiers are designed and built to be double–walled, water-cooled steel vessels. No refractory lining is present in these gasifiers (Van Dyk, 2006). Figure 2.8 shows a schematic representation of a Sasol–Lurgi gasifier.

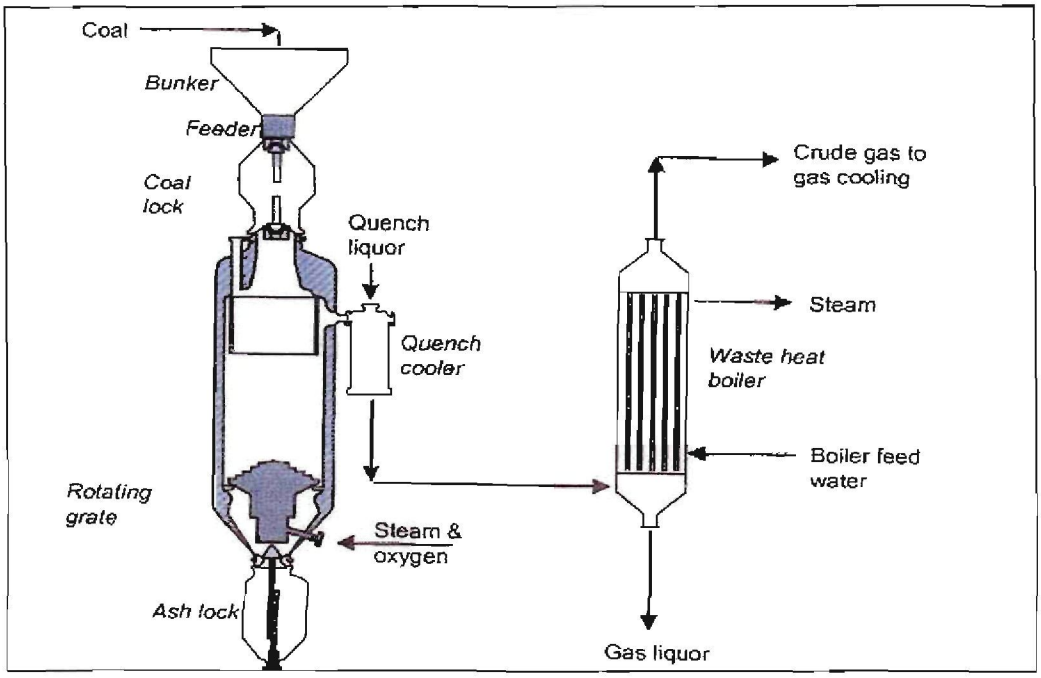


Figure 2.8: A schematic representation of a Sasol – Lurgi gasifier (Collot, 2002)

2.3.2 Fixed bed gasification process

As mentioned earlier in this section, gasification is the production of syngas from coal which is used as feedstock. During the gasification process the coal is brought into contact with a reactive gas, usually a mixture of steam and oxygen/air. The syngas that results from this reaction is further processed by the Fischer–Tropsch process to produce automotive fuel, as well as a wide range of chemicals (Van Dyk, 2006).

The Sasol–Lurgi gasifiers are operated using lump-sized coal. The coal is firstly crushed before it is screened to separate the different size fractions. Once the screening has taken place, the coal enters the gasifier via a lock–hopper system. As the coal descends down the gasifier, it comes in contact with the rising reactive gases which enter the gasifier at the bottom. The heat of the rising reactant gases removes first all the moisture from the coal before it forces the release of the volatile matter. A so-called char is what remains once all the volatile matter has been released. The char then descends further down the gasifier where it is burned to ash. The Sasol–Lurgi gasifiers are equipped with a rotating ash grate at the bottom which removes the ash from the gasifiers in a batchwise mode of operation (Bunt, 2006; Govender, 2005; Van Dyk, 2006).

Several scrapers are present in the ash grate to assist with the removal of the ash from the vessel into the rotating ash grate (Van Dyk, 2006). Figure 2.9 illustrates a fixed bed gasifier with an accompanying temperature profile.

Five distinctive zones have been identified in the Sasol – Lurgi gasifiers. These zones are (Nowacki, 1981; Schilling *et al.*, 1979; Slaghuis, 1993).

:

- Drying zone
- Devolatilization zone
- Reduction zone
- Combustion zone
- Ash bed

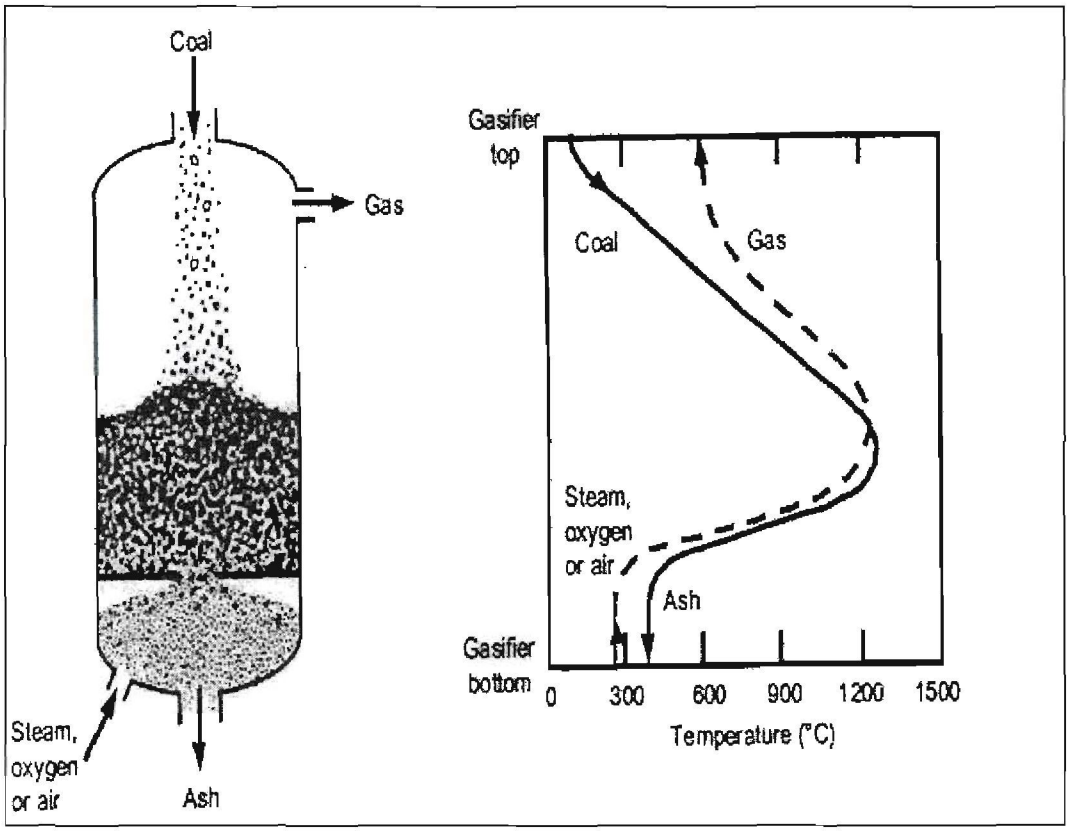


Figure 2.9: A moving or fixed bed with temperature profile (Van Dyk, 2006)

In the **drying zone** the moisture present in the coal is released once the coal comes in contact with the hot reactant gases rising from the bottom of the gasifier.

The coal's volatile matter is removed in the **devolatilization zone** resulting in the transformation of the coal into char. This zone is also known as the stage where pyrolysis takes place. The next zone is the **reduction zone** where the bulk of the reactions are endothermic reactions while the reactions in the **combustion zone** are mainly exothermic. All the ash is removed from the bottom of the **ash bed** located at the bottom of the gasifier (Bunt, 2006; Govender, 2005; Van Dyk, 2006).

Figure 2.10 shows a fixed - bed gasifier with all the distinctive zones indicated.

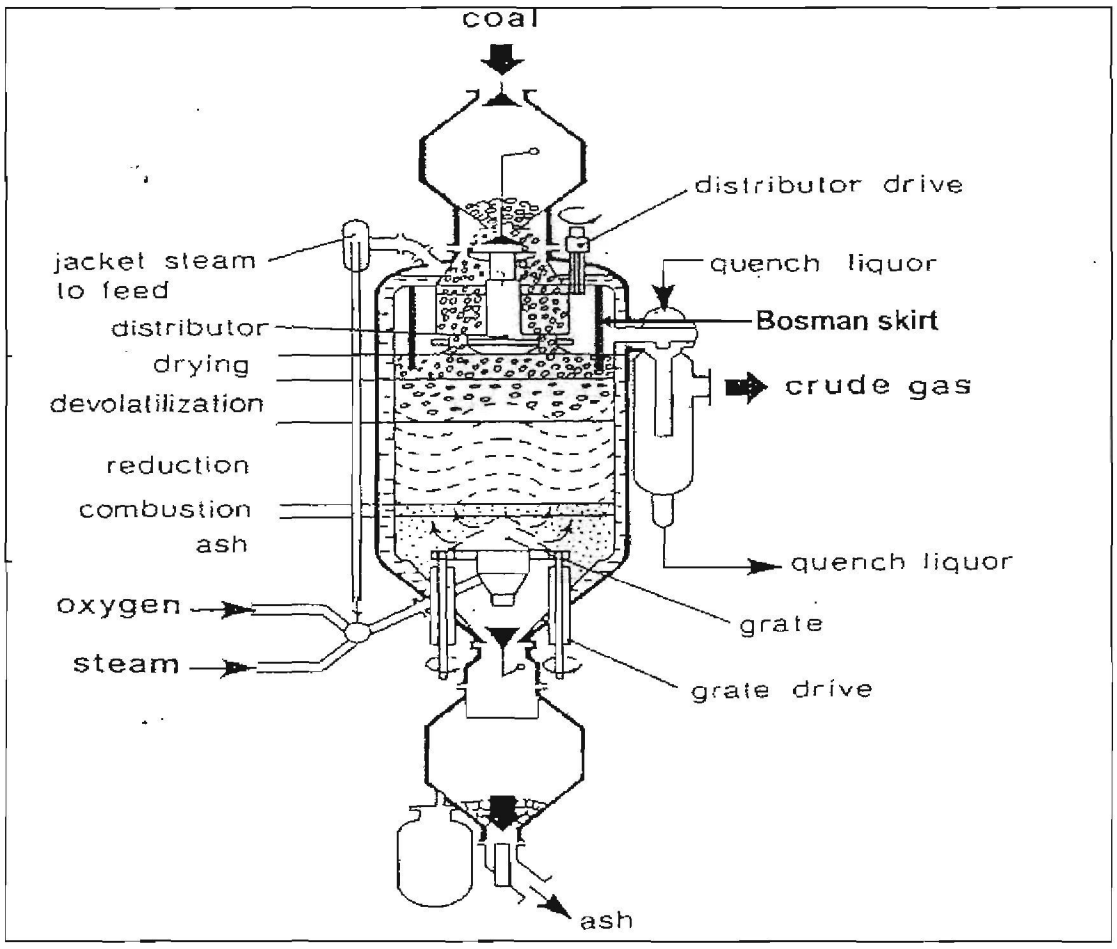


Figure 2.10: Schematic representation of a fixed – bed gasifier with all the distinctive zones indicated (Bunt, 2006)

The counter–current manner, in which Sasol–Lurgi gasifiers are operated, enhances the thermal efficiency. This is obtained by heat exchanging that takes place in the gasifier. According to Schilling *et al* (1979) and Nowacki (1981) the hot ash that exits the combustion zone of the gasifier exchanges heat with the cold incoming reactant gases. The same scenario is found at the top of the gasifier where the heat

exchanging takes place between the hot product gases and the cold incoming coal. This ensures that the material leaving the gasifiers (product gas and ash) does so at relatively low temperatures (Van Dyk, 2006).

The chemistry of gasification is extremely complex as stated by Van Dyk (2006) and Bunt (2006). Some of the most important reactions that take place during gasification can be closely related to gas reforming reactions (Bunt, 2006; Van Dyk, 2006).

According to Nowacki (1981) and Slaghuis (1993) the coal will first loose its moisture in the drying zone of the gasifier, where after the dried coal will start to devolatilize at temperatures ranging between 350 and 400 °C. In this zone the production of gases, oils and tars will occur.

The process of pyrolysis also occurs during this stage due to the destructive action of the heat on the coal. The course of this destruction process can be described by the following reaction (Bunt, 2006; Van Dyk, 2006):

$$C_m H_n \rightarrow (\frac{n}{4})CH_4 + \left[\frac{(m-n)}{4}\right]C \qquad (2.1)$$

Where: m = number of C atoms and n = number of H atoms

The second stage in coal gasification is termed char gasification and can be represented by the following reactions (Bunt, 2006; Guo et al., 2007; Van Dyk, 2006):

$C + CO_2 \rightarrow 2CO$	ΔH = 159.7 kJ/mol	(2.2)
$C + H_2O \rightarrow CO + H_2$	ΔH = 118.9 kJ/mol	(2.3)
$C + O_2 \rightarrow CO_2$	ΔH = -405.9 kJ/mol	(2.4)
$CO + H_2O \leftrightarrow CO_2 + H_2$	ΔH = -40.9 kJ/mol	(2.5)
$C + 2H_2 \rightarrow CH_4$	ΔH = -87.4 kJ/mol	(2.6)

2.3.3 High temperature gasification

High temperature gasification is a relatively new development in gasification technology. The operation of gasifiers at high temperatures has several advantages: increase in the

production of syngas which is the result of better carbon conversion, suppression of CO_2 and methane formation and better steam utilization is obtained (Kristiansen, 1996; Probstein & Hicks, 2006). This is illustrated in Figure 2.11 where it is clearly illustrated that an increase in temperature, results in a higher reaction rate.

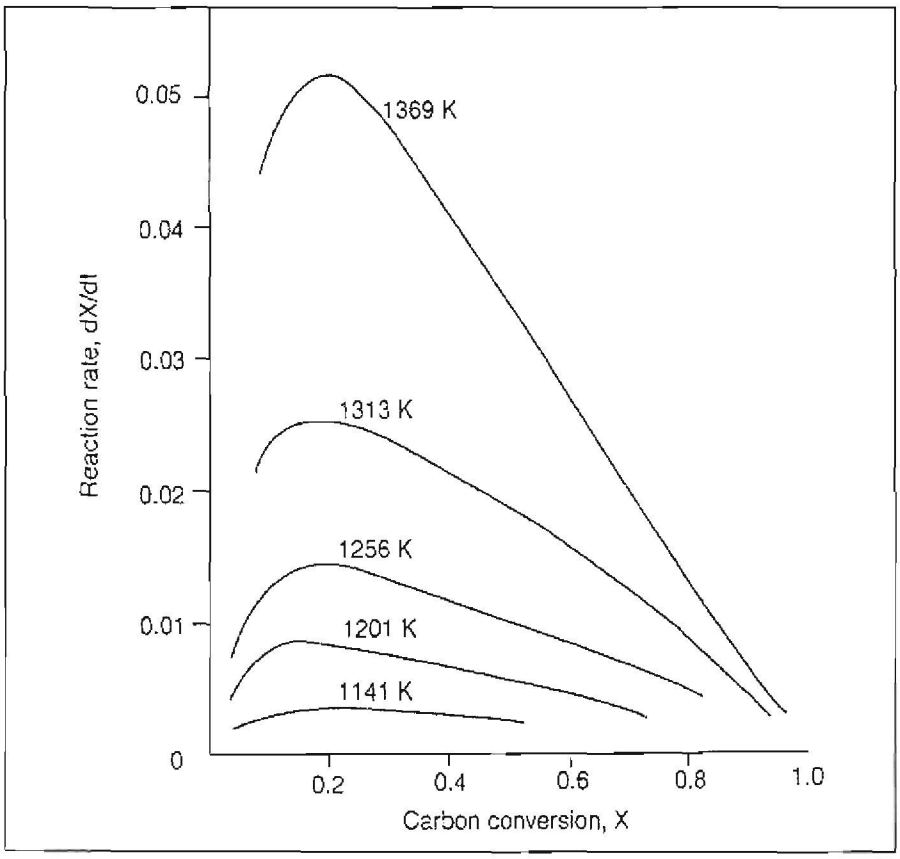


Figure 2.11: Graph depicting the increase in reaction rate with in crease in temperature (Kristiansen, 1996)

Kristiansen (1996) states that an increase in temperature will lead to a decrease in the surface area of the micropores, as well as mesopores of coal chars. This, in turn, has an effect on the gasification rate.

Entrained flow gasifiers are well-known high temperature gasifiers and are employed by companies such as General Electric (GE), formerly Texaco, and Shell (Kristiansen, 1996). Figure 2.12 gives a schematic representation of a GE entrained flow gasifier.

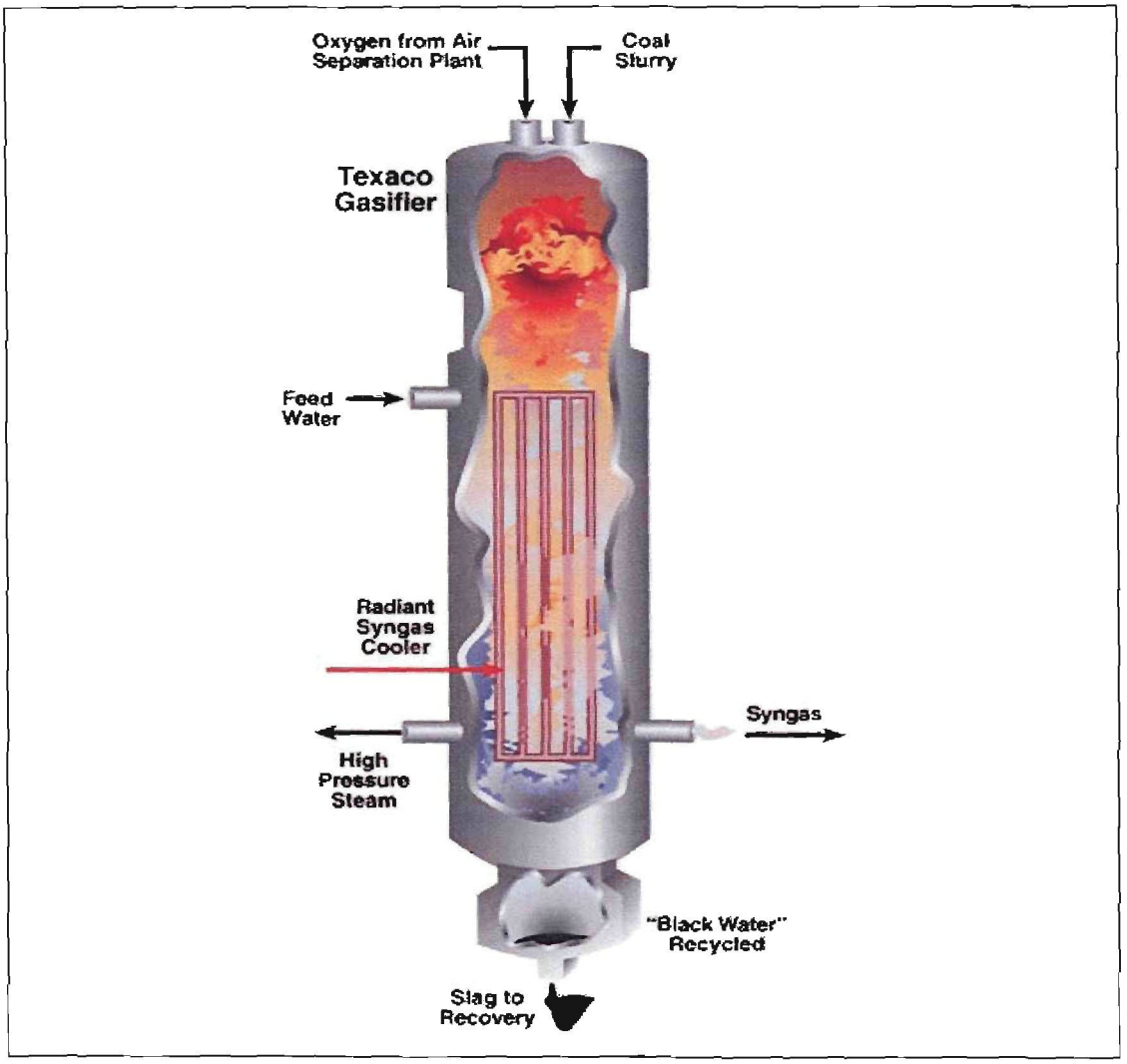


Figure 2.12: Schematic representation of a GE gasifier
(National Energy Technology Laboratory, 2008)

The entrained flow gasifiers receive coal that has been pulverised to a size of more or less 75 µm. Reactant gases for these gasifiers are normally O_2 or air together with steam. One of the main features that make these gasifiers increasingly popular is the fact that they can receive any type of coal and are not seriously affected by the rank of the coal. The residence time in these gasifiers is also considerably less than in any other types of gasifiers, which implies that a higher throughput can be achieved. There are, however, disadvantages to entrained flow gasifiers. Due to the high temperature operation all the volatile matter in the coal source is oxidised, which leads to a relatively large oxygen consumption. The high temperature also ensures that severe operating conditions within the gasifier and the molten slag cause operating problems due to the difficulty of handling, as well as removal of the slag (Kristiansen, 1996; Probstein & Hicks, 2006).

As mentioned in section 2.3.1 fixed bed gasifiers can also be operated at high temperatures with the result that the ash is removed as a slag. Figure 2.13 is an illustration of a slagging Lurgi gasifier.

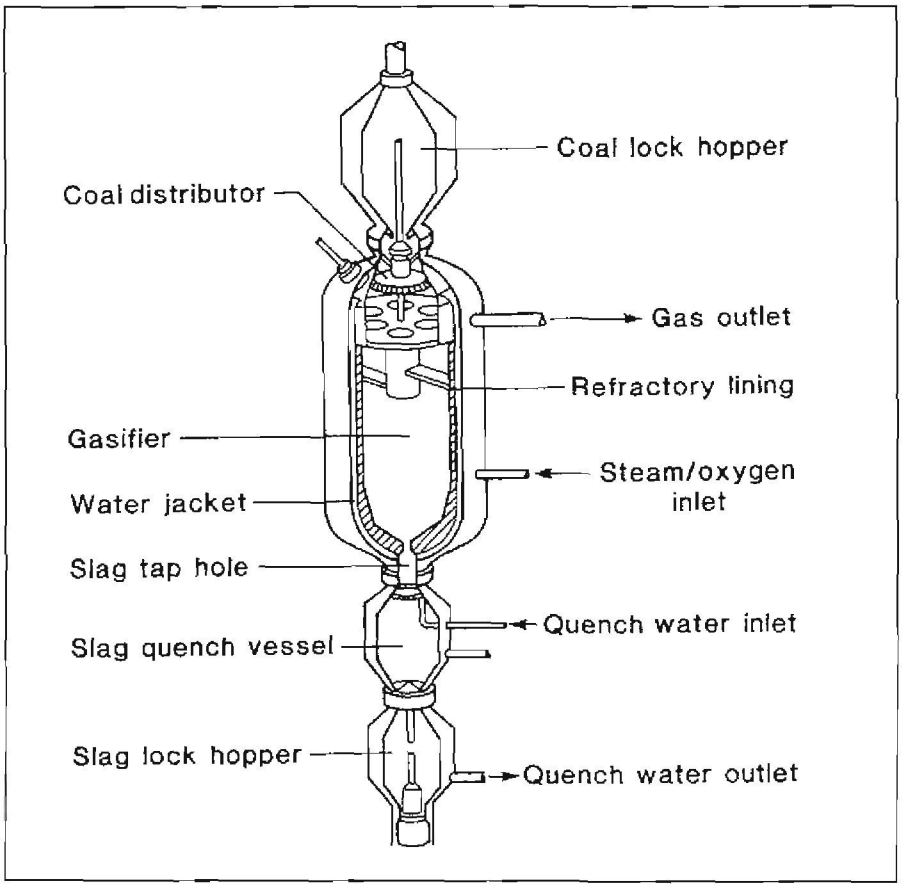


Figure 2.13: Schematic illustration of a slagging Lurgi gasifier (Probstein & Hicks, 2006)

2.4 Fusibility of coal ash

The tendency of coal ash to slag under high temperatures is a serious matter of concern for companies that utilizes gasifiers and boilers. Melting of the inorganic material in coal is responsible for the slagging and clinker formation that is observed when coal is subjected to high temperatures. Clinker formation can lead to channel burning, resulting in pressure drop within a gasifier, which ultimately results in an unstable gasifier (Van Dyk *et al.*, 2005). Slagging occurs when the ash heats up to a point where particles within the ash start to sinter and fuse. Eventually, a liquid slag is produced (Wall *et al.*, 1996). Removal of slag within a non–slagging gasifier, as

well as clinkers, forces the gasifiers out of production, resulting in a loss of production time which in turn results in profit loss.

It is thus critically important to develop a model that can be used to predict the fusing characteristics and potential of the coal source being used. Several authors have spent a lot of time researching and developing such models.

From the research conducted, it is evident that it is possible to correlate the composition of the coal ash with the ash fusion temperature of that particular coal. However, the development and application of a model to simulate fusibility of coal is a procedure filled with obstacles. This can be ascribed to the fact that the fusibility characteristics of coal are extremely difficult to measure or determine exactly. Coal is not a homogeneous substance, as mentioned earlier, which implies that it does not have a sharp melting point like a pure substance would have (Slegeir *et al.*, 1988). Several authors, like Sleiger *et al.* (1988) and Seggiani (1999), state that the acid/base ratio is the most frequent used parameter for correlating the contents of the coal ash with the slagging and fusibility characteristics of that particular coal. This ratio considers all the components in the coal ash to be oxides and then divide them in two groups, i.e. an acid and a base group (Slegeir *et al.*, 1988).

The oxides in the base group are Na_2O, K_2O, CaO, MgO and Fe_2O_3. All these oxides are normalized so that (Slegeir *et al.*, 1988):

$$\% \text{ Base} = \% Na_2O + \% K_2O + \% CaO + \% MgO + \% Fe_2O_3 = 100\% \qquad (2.7)$$

In the acid group, the following oxides are found: SiO_2, Al_2O_3 and TiO_2. These oxides are also normalized by the same procedure as in the case of the base group, so that (Slegeir *et al.*, 1988):

$$\% \text{ Acid} = \% SiO_2 + \% Al_2O_3 + \% TiO_2 = 100\% \qquad (2.8)$$

This normalization is to ensure that there is adequate adjustment for any deficiencies that may be present in the minor components, standardization differences that may occur between laboratories and to serve as a correction for sulphur concentrations in laboratory ash (Slegeir *et al.*, 1988).

From this acid/base ratio an iron index can be calculated. This is done by the following equation (Govender, 2005):

$$\text{Iron index} = \frac{Fe_2O_3}{(acid/base\ ratio)} \quad (2.9)$$

A silica factor was also developed, since silica tends to form lower melting species with basic components in the ash. The equation to calculate the silica factor is given by (Govender, 2005):

$$\text{Silica factor} = \frac{SiO_2}{SiO_2 + Fe_2O_3 + CaO + MgO} \quad (2.10)$$

In conjunction with the silica factor a dolomite ratio, as well as an acidity ratio, is calculated. These two equations are shown in equations 2.11 and 2.12 respectively (Govender, 2005).

$$\text{Dolomite ratio} = \frac{CaO + MgO}{Fe_2O_3 + CaO + MgO + K_2O + Na_2O} \quad (2.11)$$

$$\text{Acidity} = \frac{SiO_2 + Al_2O_3}{Fe_2O_3 + CaO + MgO + Na_2O + K_2O} \quad (2.12)$$

A so-called Attig and Duzy factor has been developed for eastern USA coals in which the slagging probability is calculated as a factor. This factor is calculated as shown in equation 2.13 (Govender, 2005)

$$\text{Slagging factor} = \left(\frac{\%Base}{\%Acid}\right) \times \%\ \text{dry sulphur} \quad (2.13)$$

$$\text{Fouling factor} = \left(\frac{\%Base}{\%Acid}\right) \times Na_2O \quad (2.14)$$

Equation 2.13 has been proven to be ineffective for Australian coal since the slagging factor uses sulphur as a replacement for iron which is found in the form of pyrite in USA coals. In Australian coals, however, iron is present mostly as siderite.

Thus, a new slagging index had to be developed for Australian coal, as is shown in equation 2.15 (Govender, 2005).

$$\text{New slagging index} = \left(\frac{\%Base}{\%Acid}\right) \times Fe_2O_3 \qquad (2.15)$$

This clearly illustrates the difficulty of developing a universally applicable model to describe the fusibility or slagging behaviour of coal due to the difference in composition of different coal sources.

This acid/base ratio has been proven accurate with a small number of samples with similar composition. If the number of samples is large and the compositions of the coal sources differ, this ratio is known to be far less effective (Segiani, 1999).

From an experimental perspective the standard ash fusion temperature (AFT) test is conducted in order to establish the possibility of a coal source to form a slag or to produce clinkers during gasification (Govender, 2005; Jak, 2002 Van Dyk *et al.*, 2005). In the AFT test four different temperatures are measured and the fusibilty of a coal source is then determined, based on the four measured values. The AFT test, however, has many shortcomings, such as accuracy and the uncertainty regarding reproducibility of results (Van Dyk, 2006).

This ash fusion temperature (AFT) of a coal source is influenced by numerous factors. According to Renton (1982), silica, sulphur and iron are known to have the biggest influence on the AFT of a coal source during combustion. An increase in the silica content will result in a higher AFT, while an increase in the amounts of iron and sulphur will lead to a lower AFT. The effect of the iron, however, depends on the valency state of the iron. Ferrous iron oxide is known to suppress the AFT more than ferric iron oxide. Iron is identified by various authors to be the controlling component in fouling and slagging of coal sources during combustion (Mayoral *et al.*, 2002; Ram *et al.*, 1995). Mayoral *et al.* (2002) state that pyrite plays a major role in slagging due to formation of low melting FeS–FeO intermediates, together with the fluxing effect of aluminosilicates.

In the combustion process the most operational problems are experienced with the alkali elements sodium, potassium and the alkali–earth metals calcium, magnesium (Renton, 1982). Zevenhoven–Onderwater *et al.* (2001) confirm this behaviour and state that these metals can react with the bed material present in the thermal conversion system, leaving a coated layer on the surface. It is also known that clays can react with sodium to produce components with a higher melting point than sodium silicates or sulfates (Van Dyk, 2006).

Jak (2002) investigated the possibility of predicting the AFT of coal sources. The main goal of this investigation was to see whether the AFT of a coal source could be correlated with the liquidus temperature (the temperature at which the first solid just starts to precipitate on the cooling of a so–called slag–liquid oxide melt) (Jak, 2002). In this study, Jak (2002) fixed the contents of the ash to be a multi – component system consisting of Al–Ca–Fe–Si. By using the thermodynamic computer package F*A*C*T it was possible to find a linear correlation between the AFT of a coal source and the liquidus temperature of that source. This simple correlation is shown in equation 2.16 (Jak, 2002)

$$AFT = a + bT_{liquidus} \qquad (2.16)$$

In this equation a and b are parameters, while $T_{liquidus}$ is the liquidus temperature of the coal source.

A simple compositional correlation was also developed and compared to the results obtained from equation 2.16. This correlation is shown in equation 2.17 (Jak, 2002).

$$AFT = A_{SiO2}X_{SiO2} + A_{Al2O3}X_{Al2O3} + A_{CaO}X_{CaO} + A_{Fe2O3}X_{Fe2O3} \qquad (2.17)$$

A_{SiO2}, A_{Al2O3}, A_{CaO} and A_{Fe2O3} are empirical parameters, while X_{SiO2}, X_{Al2O3}, X_{CaO} and X_{Fe2O3} are ash compositions (in mass percent) normalized to 100%. When the results of equation 2.17 are compared with equation 2.16 it is seen that equation 2.16 gives a better correlation and is more accurate. By using equation 2.16 it was observed that 53% of the AFTs fell within an agreement of 20°C, while only 30% of the AFTs of equation 2.17 fell in this agreement. If the difference between the AFTs is increased to 40°C the amount of points within this agreement for equation 2.16 increased to 87% and for equation 2.15 to 43%. It is evident from this that equation 2.16 gives a better correlation and is far more accurate than equation 2.17 (Jak,

2002). Another predictive tool that can be used for the prediction of possible slagging and clinkering behaviour is the use of phase diagrams. Phase diagrams can also be used to predict the probable composition of the clinkers (Magasiner *et al.*, 2001).

The liquidus temperature, as mentioned earlier in this section, can also be predicted by means of a phase diagram. In this diagram another temperature is also predicted, the so-called solidus temperature, which is the temperature where the solid will start to melt. At the liquidus temperature (usually defined as Lc) the first crystallization is observed and at the solidus temperature (Sc) the crystallization is completed. Thus, the cooling liquidus temperature will give an indication of the likely occurrence of clinker formation (Magasiner *et al.*, 2001). A binary, ternary or quaternary phase diagram can be used, depending on the number of components present within the ash. The phase diagram is normally selected, based upon the dominant components in the ash (Magasiner *et al.*, 2001). In Figure 2.14 an example of a phase diagram for the $SiO_2 - Al_2O_3 - CaO$ system is shown. Each vertex of the triangle represents 100 mass percent of a specific component.

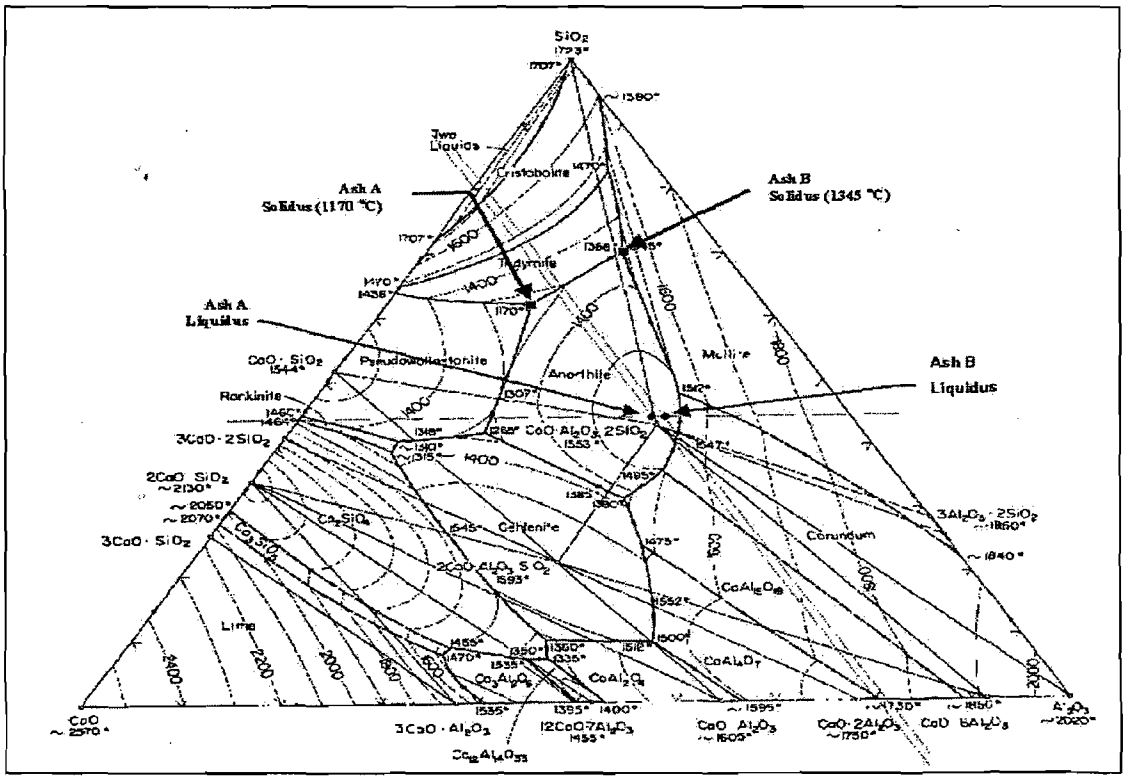


Figure 2.14: A ternary phase diagram for the $SiO_2 - Al_2O_3 - CaO$ system (Verein Deutscher Eisenhüttenleute, 1995)

Viscosity of coal ash slags is an area of great interest for researchers, mainly for the reason to maintain slag flow in wet bottom boilers (Kalmanovitch & Frank, 1988). Various authors have suggested several models, but most of these models have the original Urbain model as basis, which was originally developed for metallurgical slags (Kalmanovitch & Frank, 1988; Kondratiev & Jak, 2001). It was noticed that the Urbain model gave a reasonable fit with the experimental data obtained from the bulk flow properties of low–rank coal ash slags. The main motivation, however, for using this model as a basis is the fact that it has a theoretical basis and not an empirical one, as is the case for other models (Kalmanovitch & Frank, 1988).

Kondratiev and Jak (2001) investigated the slag characteristics of an Al_2O_3–CaO–FeO–SiO_2 system, in order to predict these characteristics. Within this system, it is possible to predict the slagging characteristics by means of the Weymann – Frenkel equation as shown in equation 2.18 (Kondratiev & Jak, 2001).

$$\eta_L = \mathrm{AT}\exp(10^3 \frac{B}{T}) \qquad (2.18)$$

In equation 2.18, A and B are model parameters, while T is the temperature in Kelvin. From this equation, the behaviour of the liquid slag at any temperature can be predicted since the viscosity of the liquid phase is temperature dependant (Kondratiev & Jak, 2001).

The parameters A and B in equation 2.16 are linked to each other by means of equation 2.19 (Kondratiev & Jak, 2001).

$$-\ln A = mB + n \qquad (2.19)$$

In equation 2.19 m and n are both model parameters. According to Kondratiev and Jak (2001), the model parameter B is described by a polynomial function of the slag composition. In their model they classify the slag components into three groups, i.e. glass formers (for example SiO_2), amphoteric oxides (for example Al_2O_3) and modifier oxides (for example CaO, FeO, MgO, etc.). The limiting temperature and viscosity requirements for most gasifiers concerning the temperature and viscosity are 1100 – 1500°C and 5 – 25 Pa.s respectively, which serve as extra motivation for predicting viscosity behaviour of a slag (Kondratiev & Jak, 2001).

Kalmanovitch and Frank (1988) base their model also on the original Urbain model, where the original Urbain model treats slags as complex silicate melts. In conjunction to the Urbain model, the network former model of glasses is also used. In this model the various oxide components that are present within the melt are classified as network formers, network modifiers or amphoteric oxides (Kalmanovitch & Frank, 1988).

Network formers (SiO_2 and TiO_2) form long stable polymers that are responsible for a high viscosity slag. Network modifiers (CaO, MgO, Na_2O, K_2O, FeO and P_2O_5) are responsible for reducing the stability of the network by bridging the oxygen bonds within the network former. This action of the network modifiers results in a lower viscosity. The amphoteric oxides (Al_2O_3 and Fe_2O_3) can have both the characteristics of the network formers and the network modifiers, depending on the composition of the melt (Kalmanovitch & Frank, 1988).

The two equations developed in the Urbain model for the modelling of slag viscosity are shown in equations 2.20 and 2.21 (Kalmanovitch & Frank, 1988).

$$\ln [A] = -(0.2693*B + 11.6725) \quad (2.20)$$

$$\text{Viscosity} = A*T*\exp\left(1000*\frac{B}{T}\right) \quad (2.21)$$

In these two equations A and B are model parameters with A being the key parameter that is calculated by means of equation 2.20. The algorithm developed to calculate viscosity is shown below (Kalmanovitch & Frank, 1988).

Step 1: The mole fraction of all the components, as oxides, should be determined, based on the chemical composition of the melt. (Fe_2O_3 should be converted to the equivalent FeO)

Step 2: The model parameter M should be calculated where:

$$M = CaO + MgO + Na_2O + FeO + 2Ti_2O_2 + 3SO_3 \text{ mole fractions} \quad (2.22)$$

Step 3: Alpha to be used in equation 2.23 should now be calculated, where:

$$\text{Alpha} = \frac{M}{M + Al_2O_3 + Fe_2O_3} \text{ mole fractions} \qquad (2.23)$$

For actual calculation purposes FeO, as mentioned in step 1, replaces Fe_2O_3

Step 4: Model parameter B, as seen in eq. 2.21 should now be calculated. This is done in the following manner:

$$B = B0 + (B1 * SiO_2) + (B2 * (SiO_2)_2) + (B3 * (SiO_2)^3) \qquad (2.24)$$

$$B0 = 13.8 + 39.9355 * \text{alpha} - 44.049 * (\text{alpha})^2 \qquad (2.25)$$

$$B1 = 30.481 - 117.1505 * \text{alpha} + 129.9978 * (\text{alpha})^2 \qquad (2.26)$$

$$B2 = -40.9429 + 234.0486 * \text{alpha} - 300.04 * (\text{alpha})^2 \qquad (2.27)$$

$$B3 = 60.7619 - 153.9276 * \text{alpha} + 211.1616 * (\text{alpha})^2 \qquad (2.28)$$

Step 5: Calculate A by making use of equation 2.21

Step 6: By simple mathematical manipulation of equation 2.22, the natural log of the viscosity at any temperature can be calculated as follows:

$$\ln(\text{viscosity}) = \ln(A) + \ln(T) + 1000\left(\frac{B}{T}\right) \qquad (2.29)$$

Kalmanovitch and Frank (1988) performed a linear regression on Machin's data (Machin & Hanna, 1945; Machin *et al.*, 1952) and came up with new values for the parameters shown in equation 2.21 for the calculation of A. Equation 2.21 is the equation for a straight line and can thus be written as (Kalmanovitch & Frank, 1988):

$$\ln(A) = (\text{slope} * B + \text{constant}) \qquad (2.30)$$

As was seen in equation 2.21 the values for the slope and the constant in the original Urbain equation are 0.27 and 11.6 respectively. The linear regression performed by

Kalmanovitch and Frank (1988) provided the values 0.28 for the slope and 11.8 for the constant. This corrected Urbain model can predict, with a fair amount of accuracy, the viscosity of bulk coal ash melts, as well as simple oxide glasses (Kalmanovitch & Frank, 1988).

2.5 Fluxing properties of coal minerals

Fixed bed gasifiers need to be operated below the AFT of a coal source in order to prevent slag formation. One of the suggestions being made on how this can be achieved is by varying the oxygen load to the gasifier. This method, however, is not preferred, due to the fact that a decrease in the oxygen feed will ultimately result in the reduction of the amount of gas produced. The preferred option in most of the Lurgi gasifiers is to vary the steam consumption (Van Dyk & Waanders, 2007).

The other option regarding slag formation in a gasifier is to add certain additives to the coal in order to manipulate the AFT of that particular coal. Various authors mentioned that the addition of mineral species will influence the viscosity of the slag in slagging gasifiers, as well as manipulating the AFT of coal the source during gasification (Kondratiev & Jak, 2001; Ninomiya & Sato, 1997; Patterson & Hurst, 2000; Vassilev *et al.*, 1995). According to Van Dyk (2006) the addition of minerals as fluxing agents to coal has numerous advantages such as:

- Lower consumption of steam during the gasification process.
- Improvement in carbon utilization resulting from lower steam consumption.
- Less gasifier trips that was due to the sintering of the coal ash, as well as higher temperatures of the gases leaving the gasifiers.
- Less CO_2 production due to a lower H_2/CO ratio.

In slagging gasifiers, the main aim is to control the viscosity of the slag. A slag that has too high or too low a viscosity will seriously influence the effectivity of the gasifier. Fluxing agents play a key role in controlling the viscosity of the slag within these gasifiers. The general agreement in the literature is that the viscosity of a coal slag will decrease with an increase in the amount of fluxing agents added. This decrease in viscosity can be ascribed to the reduction of solids by the presence of the fluxing agents (EPRI, 1980; Kondratiev & Jak, 2001; Ninomiya & Sato, 1997).

Calcium and iron containing components are the most commonly used fluxing agents for both slag control and manipulation of the AFT. Oxides of these two elements that are used include $CaCO_3$, Fe_2O_3, CaO, FeO etc. (Ninomiya & Sato, 1997; Kondratiev & Jak, 2001). Calcium in the coal is known to be completely assimilated within the aluminosilicate glass of the ash. An "effectiveness" of 1 has, therefore, been assigned to calcium as a fluxing agent. Iron, on the other hand, has a variable degree of assimilation and, therefore, the "effectiveness" assigned to iron will vary, depending on the size and the distribution of the pyrite within the coal.

Pyrite, present within the coal as part of a mixed mineral matter consisting also of clay, has a greater chance of forming an iron–rich glass than a pure pyrite particle would have on its own. Unassimilated iron may occur as crystalline magnetite within this glass structure (Gibb, 1996).

Gibb (1996) proposes a new slagging index, based on CCSEM analysis that takes into account the degree of assimilation which occurs with the oxides CaO and Fe_2O_3 when used as fluxing agents. This index is shown in equation 2.31 (Gibb, 1996).

$$Index = \sum_{\substack{all\ mineral \\ occurences}} [mass\ fraction \times (CaO + Fe_2O_3 \times (1 - 0.5 \times \frac{Fe_2O_3}{Fe_2O_3 + Al_2O_3 + SiO_2}))] \quad (2.31)$$

This index is also based on the assumption that pure pyrite particles have an "effectiveness" of 0.5 as fluxing agents, while a pyrite/clay mixture has an "effectiveness" of between 0.5 and 1, depending on the amount of clay present (Gibb, 1996). Jak (2002) was also able to predict the behaviour of coals with added fluxing agents by means of the F*A*C*T software package.

Van Dyk and Waanders (2007) state that certain minerals such as kaolinite, alumina, silica and titania can be added to a coal source to increase the AFT of that coal. Kaolinite contains high concentrations of Si and Al, which makes it possible for this mineral to react with sodium to produce a component with a significantly higher melting point. Thus, a higher AFT is obtained by adding kaolinite (Van Dyk & Waanders, 2007). A higher AFT is related to increased silica content, while a lower AFT is due to a decrease in silica content, as well as an increase in the presence of sulphate and oxide minerals (Vassilev et al., 1995).

Van Dyk and Waanders (2007) conducted a study in which the effectiveness of Al_2O_3, SiO_2 and TiO_2 as fluxing agents was investigated. From this study it became evident that Al_2O_3 had the most noticeable effect on the AFT of the coal ash. An increase in the amount of Al_2O_3 added to the coal clearly led to higher AFTs (Van Dyk & Waanders, 2007).

The effect of these three fluxing agents is illustrated in Figure 2.15.

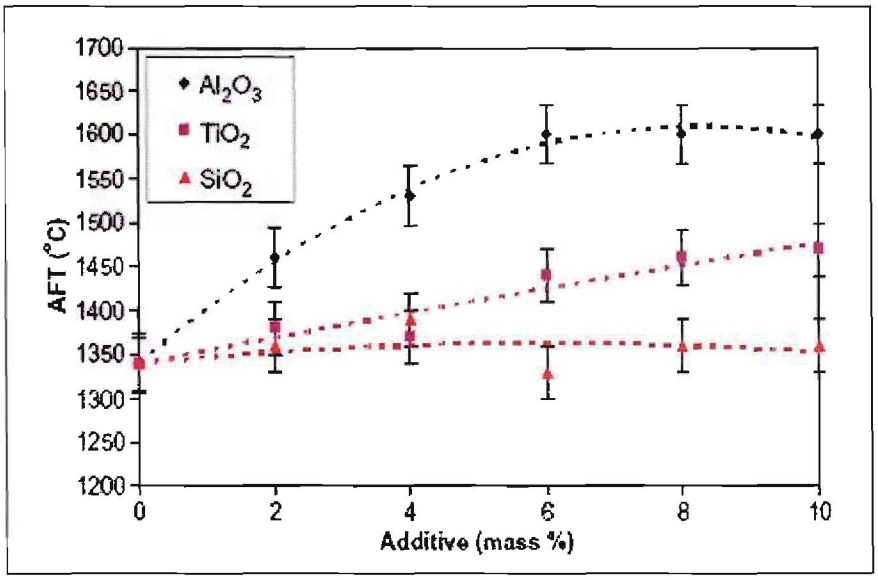


Figure 2.15: The effect of Al_2O_3, SiO_2 and TiO_2 on the AFT of a coal source (Van Dyk & Waanders, 2007)

Thus, from Figure 2.15 it can be concluded that the AFT increases with an increase in fluxing agent added, up to an optimum point where it stabilizes.

The choice of fluxing agents more often than not is based upon factors other than the influence of these agents on coal properties. These factors include flux cost, refractory resistance, type of gasifier, etc. (Kondratiev & Jak, 2001). Another important factor to consider is the trade–off that exists between the cost of adding the flux versus the increased efficiency and reliability of operating at a lower temperature (Patterson & Hurst, 2000).

A first critical step, when selecting a fluxing agent, is to study the phase equilibria of the system present within the coal (Kondratiev & Jak, 2001).

Blending different coal sources is an alternative to fluxing agents. The blending of a coal source, in order to prevent slagging and to optimize coal properties, is a common practice and is known to be the best method to adjust silica to alumina ratios. It is, however, extremely difficult to select the combination of the coals that should be used, as well as the proportions in which they should be mixed (Kondratiev & Jak, 2001; Patterson & Hurst, 2000).

2.6 Transformation of mineral matter

The study of the transformation of mineral matter is of great importance, since it is one of the specific properties that also provide information regarding the slagging potential of a coal source or sources (Van Dyk *et al.*, 2006). Transformation of the mineral matter embedded in coal is a complex process that involves decomposition, phase changes and interaction with inorganic matter (Benson, 1987). Tomeczek and Palugniok (2002) suggest a mineral matter transformation mechanism illustrated in Figure 2.16.

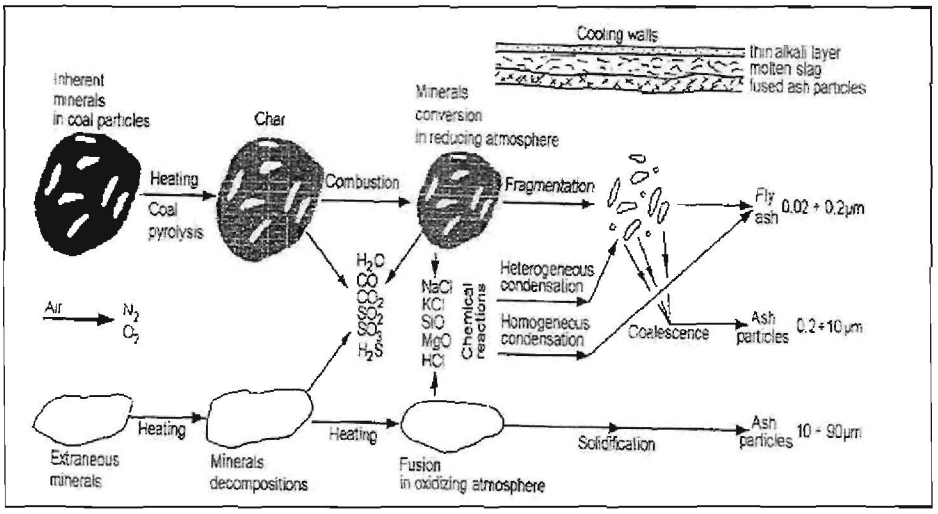


Figure 2.16: Mineral matter transformation mechanism
(Tomeczek & Palugniok, 2002)

Mineral matter transformation is widely covered by various authors in the literature. In this section a summary of the transformations of the main mineral groups is given.

Quartz

Quartz at room temperature is known as low quartz. Upon heating, a phase transformation occurs at a temperature of 573°C where the low quartz is converted into high quartz. High quartz produces tridymite at a temperature of 867°C. Tridymite is a relatively stable compound which does not undergo any change between 867°C and 1470°C. The last transformation occurs at 1470°C where the tridymite is converted into cristobalite (Benson, 1987; Reifenstein *et al.*, 1999).

Clay minerals

The main clay minerals present in coal are kaolinite, illite and montmorillonite. Kaolinite firstly starts to decompose at a temperature of 450°C due to the loss of the OH unit and forms a component known as metakaolinite. Metakaolinite is a stable compound and remains unaltered up to a temperature range between 950–1000°C.

When heated above this temperature range, the metakaolinite will convert to either γ–alumina or combination of mullite and cristobalite. A further increase will result in more of the α–alumina converting to mullite. At temperatures above 1500°C mullite is the only stable compound (Reifenstein *et al.*, 1999; Ward, 2002). The transformation of the kaolinite in oxidizing conditions can be illustrated by reaction 2.32 (Alpern *et al.*, 1983).

$$Al_2Si_2O_5(OH)_4 \rightarrow Al_2O_3.2SiO_2 + 2H_2O \qquad (2.32)$$

When kaolinite is thermally treated with nitrogen, the transformation process that occurs, is shown in reaction 2.33 (Alpern *et al.*,1983).

$$3(Al_2O_3.2SiO_2.2H_2O) \xrightarrow[800\,°C]{450\,°C} 3(Al_2O_3.2SiO_2) + 6H_2O \xrightarrow[1000\,°C]{850\,°C} Al_6O_5(SiO_4)_2 + 6H_2O \qquad (2.33)$$

Illite and the other clay components also firstly loose the OH–unit when heated. At a temperature of between 950°C and 1050°C the illite minerals transform into spinel and mullite. Upon further heating (> 1200°C) the components fuse to produce glassy components (Benson, 1987; Ward, 2002).

When illite is thermally treated with nitrogen, the transformation that takes place is illustrated in reaction 2.34 (Alpern *et al.*,1983).

$$KAl_2(AlSi_3O_{10}).(OH)_2 \xrightarrow[620°C]{370°C} KAl_2(AlSi_3O_{11}) + H_2O \xrightarrow[1050°C]{940°C} Al_2O_3 + KAlSi_2O_6 + SiO_2 + H_2O \qquad (2.34)$$

Alpern *et al.* (1983) summarizes the decomposition and transformation of the clay minerals as:

- Loss of absorbed water at 50–150°C.
- Loss of endothermic water:
  Kaolinite at 500-600°C.
  Illite at 370–620°C.
  Montmorillonite at 600–730°C.
- Destruction of the lattice at 850–1000°C.

Carbonates

The decomposition of carbonates in an oxidizing or neutral atmosphere usually implies the loss of CO_2 and a residue consisting of oxides (Alpern *et al.*, 1983).

Calcite is one of the most commonly found carbonate minerals. Pure calcite usually decomposes in the temperature range of 675–950°C. In this temperature range,metastable polymorphs such as aragonite ($CaCO_3$) or vaterite ($CaCO_3$) are formed. Calcite also partially decomposes into lime (CaO).

At very high temperatures (> 1600°C) calcite is fully decarboxylated to lime and CO_2 (Reifenstein *et al.*, 1999). This decomposition of calcite was already observed by Alpern *et al.* (1983) at between 850°C and 900°C as shown in reaction 2.35.

$$CaCO_3 \xrightarrow[900\ °C]{850°C} CaO + CO_2 \qquad (2.35)$$

Other common carbonate minerals include siderite and dolomite. The transformation reaction of siderite is shown in reaction 2.36 and that of dolomite in reaction 2.37 (Alpern *et al.*, 1983).

$$FeCO_3 \xrightarrow[610°C]{425°C} FeO + CO_2 \qquad (2.36)$$

$$MgCa(CO_3)_2 \xrightarrow[900°C]{780°C} MgO + CaO + 2CO_2 \qquad (2.37)$$

Sulphides

Pyrite is the most commonly found mineral in this group. With regard to combustion processes and slagging potential, it is also one of the more important minerals. The transformation of pyrite, as well as the other minerals in this group, depends largely on the atmosphere in which the heating is taking place. In oxidizing conditions SO_3 and SO_2 gases are produced and the final residue is hematite. Reducing conditions, on the other hand, forces the production of H_2S gas and pyrrhotite as final the residue is formed (Alpern *et al.*, 1983; Benson, 1987; Ward, 2002).

Vassileva and Vassilev (1996) state that the production of pyrrhotite seems to be a product of incomplete pyrite oxidation. The transformation reaction of pyrite under oxidizing conditions is shown in reaction 2.38 and for reducing conditions in reaction 2.39.

$$2FeS_2 + 3/2O_2 \rightarrow Fe_2O_3 + 2SO_2 \quad (2.38)$$

$$FeS_2 + H_2 \rightarrow FeS + H_2S \quad (2.39)$$

According to Tomeczek and Palugniok (2002) the decomposition of pyrite starts at more or less at 700K (430°C) and can be divided into two parts. In the first part $Fe_{1.25}S$ is produced, which is later converted to Fe and S_2 in the second part, at a temperature of 1000K (730°C). In oxidizing conditions the combustion reaction of pyrite starts at 600K (330°C) (Tomeczek & Palugniok, 2002).

The decomposition of pyrite reaches a maximum at 540°C from where it slows down to a temperature of approximately 580°C. Then decomposition increases up to 640°C, where it again reaches a maximum (Van Dyk, 2006).

Sulphates

Sulphates are not very common minerals in coal and are present as gypsum in the most coals. Gypsum is always destroyed in high temperature processes. The two products of gypsum transformation under oxidizing conditions are CaO and SO_3, while under reducing conditions the products are CaS and CO_2 (Alpern *et al.*, 1983).

CHAPTER 3 EXPERIMENTAL SETUP

In this Chapter the different experimental techniques, used during the course of this project, as well as the samples used are discussed.

3.1 Samples

Three different coal samples were obtained from Sasol's operations in the Highveld area of South Africa. The three samples were classified as: Sample A, B and C and none of the samples were subjected to any pre-treatment. Sample C originated from the overflow stream of a centrifuge and was obtained in the form of fines. Sample B was taken from the underflow of a thickener tank and was received in the form of a slurry. The slurry was first dried and then crushed to obtain a uniformly fine coal sample. Sample A was obtained from the Sasol plant's slurry section and not from a specific unit like the other two samples and the same procedure that were followed with Sample B were repeated for this sample.

The three samples received, were first subjected to the various characterisations. Elemental iron was then added to the three samples in amounts of 2, 5, 10, 15 and 20 mass percentages. These sub-samples (15 in total) were then subjected to AFT analyses, as well as Mössbauer spectroscopy. The aim of the AFT analyses was to establish the effect of the added iron to the slagging behaviour of the coal samples and whether iron could be used as a fluxing agent. Mössbauer analysis, on the other hand, was used to investigate the transformation of the mineral iron originally present in the coal, as well as the coal with added iron.

3.2 Proximate analysis

Proximate analysis is used to determine the composition of a coal sample in terms of moisture, ash content, volatile matter content and fixed carbon in relative amounts (Falcon & Ham, 1988; Govender, 2005; Mayoral *et al.*, 2001). This analysis is also widely used to establish the rank of a coal, to obtain the ratio between combustible and incombustible gases or to evaluate the coal for a certain process or purpose (Mayoral *et al.*, 2001).

The moisture content that is measured in this analysis is the water that is present within the pores and cracks of the coal sample after all of the surface water has been removed (Falcon & Ham, 1988). The moisture content within the coal is determined by the standard procedures as set out in standard ISO 1171 (ISO 1171, 1997).
The ash content of a coal sample can be defined as the residue that remains after combustion of the sample has taken place.

The amount of ash gives a fair indication of the amount of inorganic matter present within the coal and is measured by using the standard procedure set out in standard ISO 1171 (Falcon & Ham, 1988; Govender, 2005; ISO 1171, 1997). Volatile matter within a coal source is basically derived from two sources, i.e. from organic matter and mineral matter.
The presence and quantity of volatile matter present an indication of the reactivity of the coal, as well as the possible production rates of tar and oils during gasification (Falcon & Ham, 1988; Govender, 2005). The volatile matter contents are obtained by the standard procedure set out in standard ISO 562 (ISO 562, 1998). The fixed carbon is defined as the solid remains after the volatile matter, ash and moisture have been removed (Falcon & Ham, 1988). The amount of fixed carbon is calculated by difference.

3.3 Ultimate analysis

During an ultimate analysis, the coal is decomposed into its ultimate chemical components, namely carbon, hydrogen, sulphur, nitrogen and oxygen. Each of these elements plays a vital role in a number of calculations and evaluations. The hydrogen and carbon contents, as determined by the ultimate analysis, are used for material balance calculations, as well as coal conversion calculations. Nitrogen, on the other hand, is used to monitor the potential formation of harmful nitrogen oxides. The sulphur analysis is used to evaluate sulphur emissions, coal preparation and coal quality (Falcon & Ham, 1988; Govender, 2005).

The total sulphur content of a coal sample is obtained by the standard procedure set out in standard ASTM D4239, while the procedures of obtaining the carbon, hydrogen and nitrogen contents are set out in standard ASTM D5373 (ASTM D4239, 2005; ASTM D5373, 2002). The oxygen content is obtained by difference.

3.4 Ash composition

The ash remaining after the coal samples have been combusted, consists mainly of mineral species. As part of the characterization of the coal samples the ash must also be analysed in order to gain insight into the types of minerals present. The procedures as set out in standard ASTM D3682 were used to obtain the composition of the ash in terms of the oxides of Si, Al, Fe, Ti, P, Ca, Mg, Na, K and S (ASTM D3682, 2001).

3.5 Scanning microscopy analyses (SEM)

For all SEM analyses a FEI Quanta 200 ESEM Scanning Electron Microscope fitted with an Oxford Inca 400 energy dispersive x–ray spectrometer was used.

The main motivation for the utilisation of the SEM apparatus was that it aided in the investigation of the iron transformation. This apparatus can be used to study coal ash in which it can determine the size, shape and chemistry of individual ash particles. The determination of these quantities is made possible by a highly focused electron beam that is able to produce a variety of signals consisting of backscattered and secondary electrons. It is possible to scan the sample at a certain position by using the co-ordinates together with the energy intensity at the chosen position. A digital image can then be obtained from that location (Kamer *et al.*, 1994; Tiedt & Pretorius, 2006).

The secondary electrons are the most commonly used type of signal utilized in SEM studies. A high resolution image is obtained from the sample, due to the fact that the secondary electrons signal is emitted in close proximity to the incident beam. These electrons possess less than 50eV of kinetic energy, which gets lost when the electrons are scattered. Only electrons that have sufficient energy to surmount the surface barrier energy will make a contribution to a detectable signal (Tiedt & Pretorius, 2006).

Backscattered electrons, on the other hand, are the product of collisions between a large number of incident electrons and the sample being studied with the electrons being re-emitted by the surface of the sample. The atomic number provides the key to the intensity of the backscattered signal. A darker image corresponds to the

higher atomic number elements, whereas lighter images indicate heavier atoms (Tiedt & Pretorius, 2006).

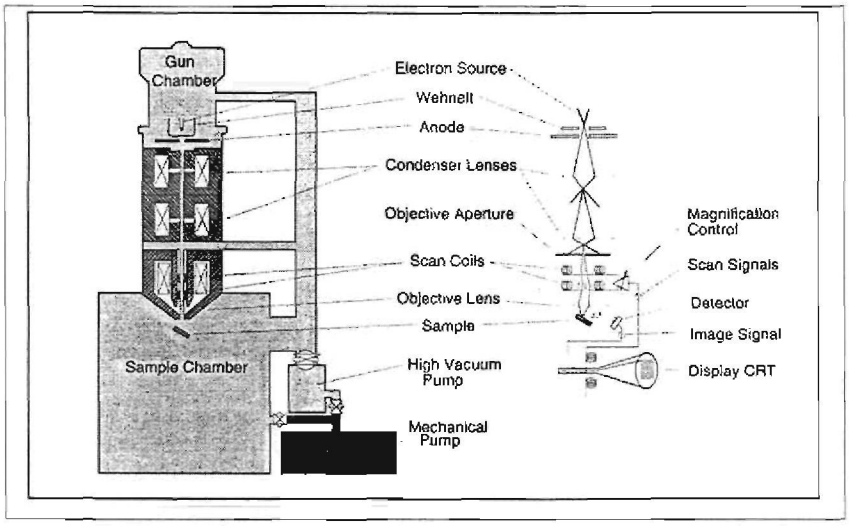


Figure 3.1: Schematic illustration of a SEM apparatus (Skoog *et al.*, 1998)

3.6 AFT analysis

Originally AFT tests were developed to evaluate the likeliness of a coal source to produce clinkers during operation in stoke – fired furnaces (Reifenstein *et al.*, 1999). Presently, however, AFT tests are employed to assess the slagging potential of a coal source during combustion processes (Jak, 2002; Reifenstein *et al.*, 1999; Wall *et al.*, 1996). AFT analyses are, strictly speaking, not measurements, but rather observations made by an observer when a coal sample is heated through a temperature range (Wall *et al.*, 1996). Huggins (as quoted by Govender, 2005) defines an AFT analysis as a documented observation of the melting process that occurs when a coal ash sample, in a pyramidal shape, is placed in a furnace and heated through a temperature range.

The temperature range to determine the AFT of a coal sample lies between 1000 and 1600°C. During the heating process the observer should be aware of the four different temperatures "measured" or observed in standard AFT tests. These four temperatures are:

- Initial deformation temperature (IDT)
- Softening temperature (ST)
- Hemispherical temperature (HT)
- Flow temperature (FT)

The temperature at which the tip of the pyramidal coal ash sample deforms and the rounding of the apex takes place is known as the **deformation temperature**. This temperature is also known as the initiation of the ash melting process. The second temperature, or **softening temperature**, is reached when the width of the heated pyramidal coal sample, is equal to its height. At this point the critical viscosity is reached. The **hemispherical temperature** is the next temperature and can be identified by the shape of the sample deformed up to a point where the height of the sample is half of its width. The last temperature is the **flow temperature** and at this point the ash is supposed to be completely molten and freely fluid. The height of the sample is more or less 1/16th of its width (Govender, 2005; Wall *et al.*, 1996).

These four temperatures, at which the different changes in the pyramid occur, are schematically illustrated in Figure 3.2.

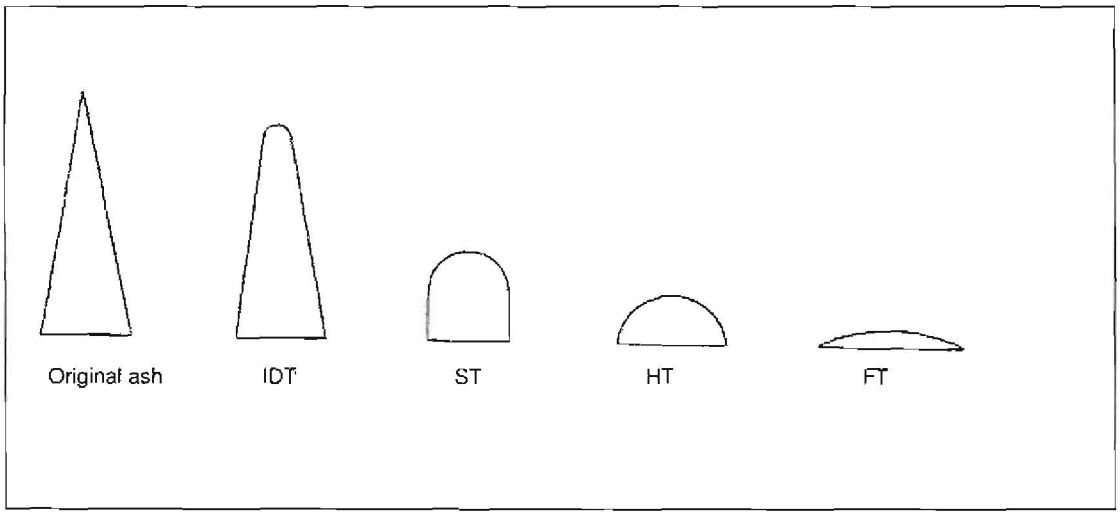


Figure 3.2: Schematic illustration of the four observed changes during a standard AFT test (Slegeir *et al.*, 1988)

The coal sources used by Sasol's plants for gasification processes typically have a flow temperature of greater than 1300°C and an initial deformation temperature of less than 1250°C (Govender, 2005; Van Dyk, 2006). During an AFT test the atmosphere in the furnace is controlled and can be either oxidizing (for example air) or reducing (for example CO) and this fact is important due to the oxidation behaviour of iron during heating (Govender, 2005). The whole AFT analysis is set out in standard ISO 540 and ASTM D1857 (ASTM D1857, 2004; Govender, 2005; Van Dyk, 2006; SABS, 1996).

Although AFT analyses have numerous advantages, like the inexpensive manner in which it can be conducted, the wide employment of the standard procedure, etc., there still exist a few doubts regarding this test. The main concerns center around the reasonable doubt there is regarding the reproducibility and repeatability of this analysis. Due to the fact that this analysis is based on observation rather than on measurement, makes it virtually impossible to obtain objective values. This necessitated the allowance for a large experimental error (± 30 °C) in the standard procedure as set out in standard ISO 540 (SABS, 1996). Also, AFT analysis cannot indicate the exact temperature at which the ash first starts to fuse/melt due to the transformation of the mineral matter. Normal AFT analysis basically provides an average flow property for the coal ash (Bunt, 2006; Reifenstein *et al.*, 1999; Van Dyk, 2006).

3.7 Mössbauer spectroscopy

Mineral matter transformation, especially iron-containing minerals, can be studied by means of Mössbauer spectroscopy. In this project Mössbauer spectroscopy was utilized to study the transformation of the iron-containing minerals within the coal samples, as well as the added pure elemental iron.

The Mössbauer apparatus used for this project is a Halder Mössbauer spectrometer that is capable of operating in conventional constant acceleration mode, in conjunction with a proportional counter filled with Xe gas at a pressure of 2 atm. Before any experimental work was conducted the Mössbauer apparatus was calibrated using α-iron as reference material.

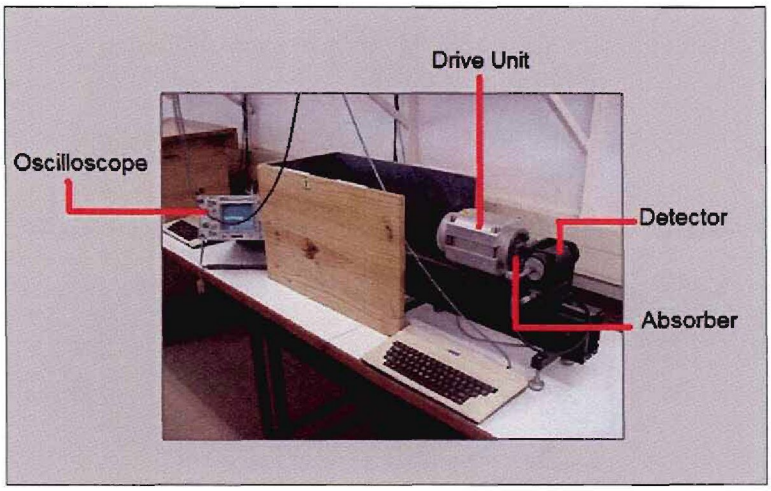


Figure 3.3: The Halder Mössbauer apparatus used for experimental purposes

3.7.1 Introduction to Mössbauer spectroscopy

Mössbauer spectroscopy was first used by Rudolf L. Mössbauer in 1958 and is defined as a technique of studying the absorption of γ–rays by the nuclei of the different atoms. A more detailed definition entails the recoilless absorption and emission of γ–rays by specific nuclei within a solid, and it provides an opportunity to study the local atomic environment around the nuclei, thus providing information about mineral transformation on a microscopic level (Cohen, 1976). The γ–rays mentioned in the previous paragraph are basically electromagnetic radiation and its properties are very similar to that of x–rays. The γ–rays have no electric charge and they can be deflected by neither an electric nor a magnetic field. When γ–rays pass through a sample they are either absorbed or scattered, mainly due to the random collisions with electrons. A beam consisting of γ–rays looses its intensity once some of the rays have been absorbed; however, the rays that are not absorbed or scattered out of the beam continue to proceed with the original intensity and energy (Cohen, 1976).

The Mössbauer effect is based on the emission of γ–rays by radioactive nuclei, as well as the absorption of the γ–rays by other nuclei of the same type. The type of solid, in which the nuclei are found, affects the nuclear emission and absorption energies (Cohen, 1976). The events that occur in Mössbauer spectroscopy is illustrated in Figure 3.4.

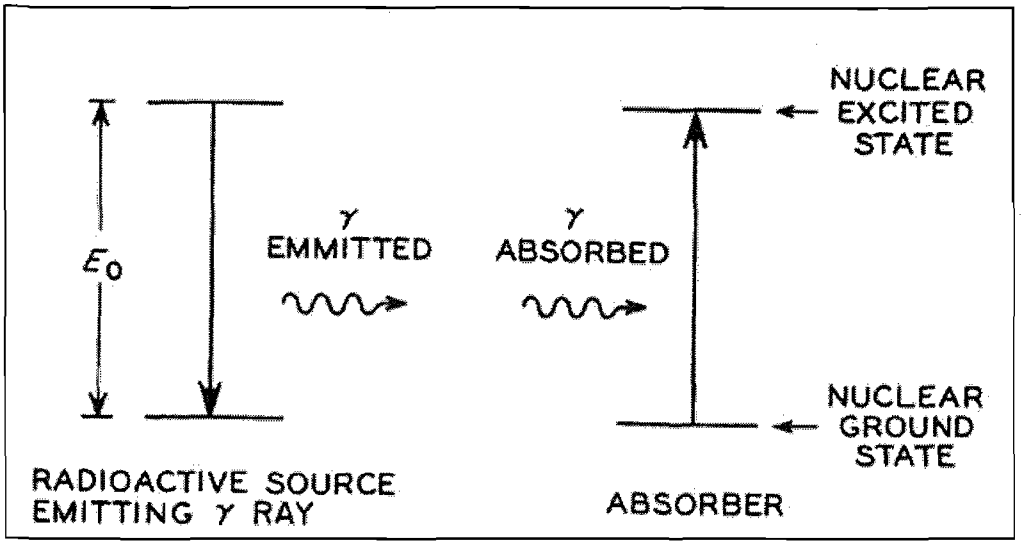


Figure 3.4: Events occurring in Mössbauer spectroscopy (Cohen, 1976)

In Figure 3.4 the four horizontal lines represent nuclear states.

In the left-hand side of the figure the nuclear state of the radioactive source changes from an excited state to a ground state with the result that a γ–ray is emitted. The emitted γ–ray is absorbed by the absorber on the right-hand side of the figure, resulting in an increase in the nuclear state of the absorber, i.e. from ground state to excited state (Cohen, 1976).

The Mössbauer spectrum that is studied and analyzed is produced by varying the γ–ray energy of the source and then measuring the resonance absorption as a function of the γ-ray energy. The γ–ray energies that equal the possible excitation energy of the nuclei in the absorber, resulting in nuclear resonance which leads to an increase in absorption and an absorption line will emerge (Cohen, 1976). According to Cohen the Mössbauer spectrum is made up of so-called dips or series of dips. This spectrum is usually displayed as a % transmission *versus* γ–ray energy shift spectrum. Analysis of this data is carried out by means of least squares fitting with the aid of a computer (Cohen, 1976).

The Mössbauer spectrum can effectively provide two types of information, the first being the relative and absolute line energies that are determined by electronic effects. The second type of information is the nuclear energy levels. These effects are grouped together and termed hyperfine parameters which can be subdivided into isomer shift, quadrupole interaction and dipole hf interaction (Cohen, 1976).

The Mössbauer apparatus can be divided into three parts, i.e. the source, absorber and detector. The source of this apparatus is usually a radioactive parent of the Mössbauer isotope. The γ–rays are produced in the source through nuclear decay. In transmission studies a linear arrangement is required where the detector is located behind the source and the absorber. The absorber receives the information and displays a spectrum as discussed in the previous paragraphs. (McCammon, 2000).

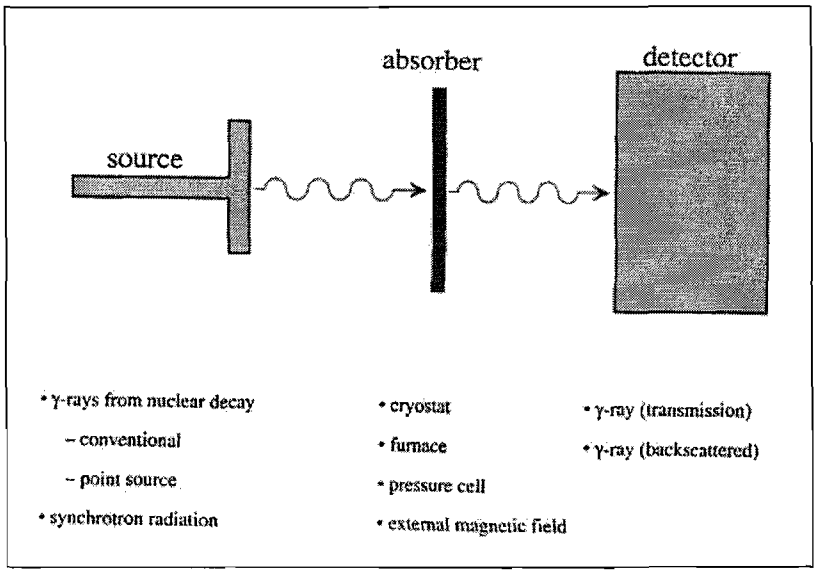


Figure 3.5: Schematic illustration of a Mössbauer apparatus (McCammon, 2000)

In the Halder Mössbauer apparatus the samples are placed between Perspex plates before being irradiated with γ–rays from a 50mCi^{57}Co(Rh) radioactive source at room temperature, in order to obtain a spectrum. The data are then collected by a multi–channel analyser which produces a spectrum of count rate *versus* source velocity. A least squares program was used for the analysis of the data. The three different hyperfine parameters, i.e. isomer shift, quadrupole splitting and hyperfine magnetic splitting are now discussed.

Isomer shift

An isomer shift (also known as the chemical shift) occurs due to the interaction energy of the part of the electron cloud, within the volume of the nucleus, and the nuclear charge (Cohen, 1976). McCammon (2000) defines an isomer shift as the result of interaction between the positive nuclear charge and the electric field of the surrounding electrons. Due to this interaction a shift in the nuclear energy levels compared to that of the undisturbed nucleus occurs. The extent of the shift is a function of the difference in the s-electrons densities in the source and absorber, respectively (McCammon, 2000). Thus, an isomer shift produces information regarding the electron density at the nucleus directly, which can then be interpreted in order to gain unambiguous information about the valence state of the ion being studied (Cohen, 1976).

Furthermore, it is also a measure of the electron density present in the annular shell which in turn makes up the difference that exists between the volumes of the nuclear states (Dickson & Berry, 1986; Murad & Cashion, 2004).

A typical isomer shift observation found in a Mössbauer spectrum, is illustrated in Figure 3.6.

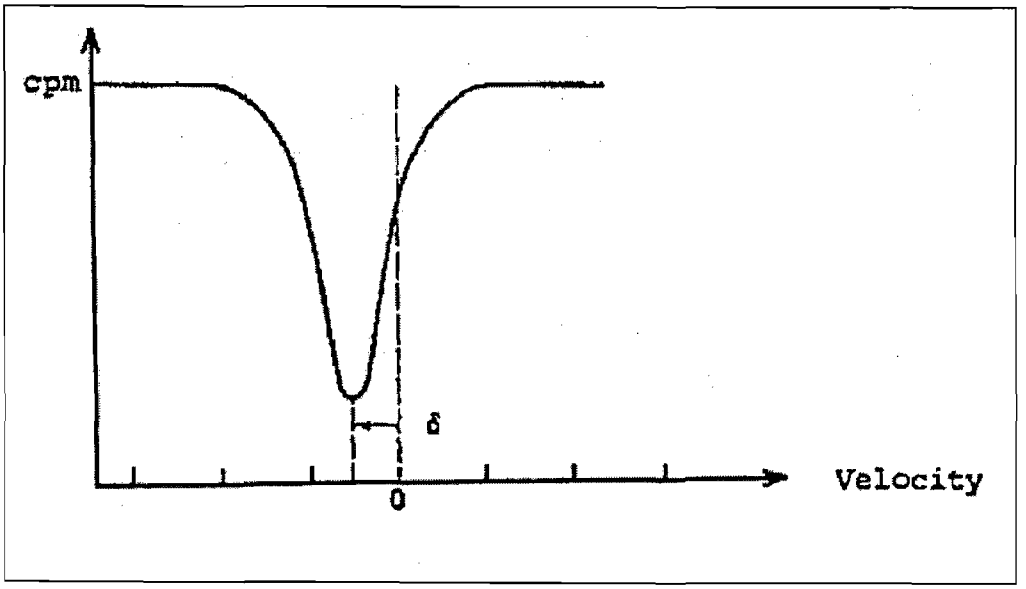


Figure 3.6: Schematic representation of the isomer shift observed in a Mössbauer spectrum (Cohen, 1976)

Quadropole interactions

Cohen (1976) states that quadrupole coupling occurs due to the geometry of the nucleus. It may be possible that the nucleus is not a perfect sphere but rather an ellipsoid that is either elongated or flattened (Cohen, 1976). Quadrupole splitting, on the other hand, occurs as a result of a quadrupole interaction between the electric field gradient at the nucleus and the nuclear quadrupolar moment. This interaction is forced by the presence of the surrounding electrons, resulting in a splitting of the nuclear energy states. When observing the behaviour of ^{57}Fe it is noted that the excited state is split into two different levels with the result that a doublet is formed (McCammon, 2000). The quadrupole split provides information regarding the bonding environments and the structure that can be found near the Mössbauer atom (Dickson & Berry, 1986).

Quadrupole splitting depends on various factors such as the valence and the spin state of the atoms located within the absorber. Another important factor is the coordination and degree of distortion of the crystallographic site (McCammon, 2000).

Figure 3.7 illustrates a quadrupole splitting as observed in a Mössbauer spectrum.

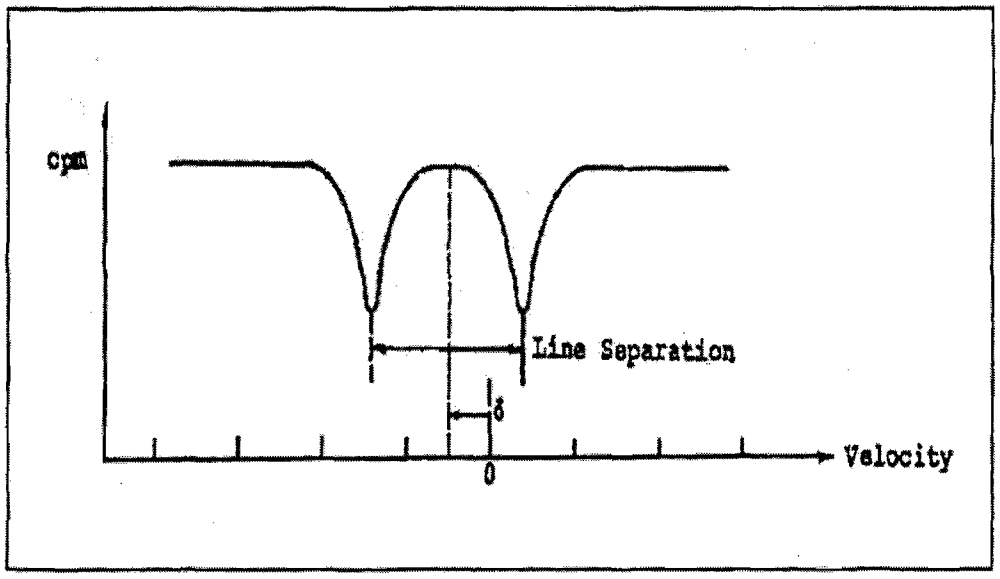


Figure 3.7: Schematic representation of a qaudrupole splitting observed in a Mössbauer spectrum (Cohen, 1976)

Hyperfine magnetic interactions

Hyperfine magnetic interactions (also known as Zeeman splitting) occur due to the coupling between the nuclear magnetic moment and the effective magnetic fields located at the nucleus. This coupling leads to the splitting of the nuclear ground and excited states if they exhibit a nuclear spin $I > 0$ (Cohen, 1976; Dickson & Berry, 1986). McCammon (2000) defines hyperfine magnetic splitting as a dipole interaction occurring between the nuclear magnetic dipole moment and a hyperfine magnetic field located within the nucleus. As a result of this interaction a splitting of the nuclear energy states occurs. Splitting of the spectral line, as observed in a Mössbauer spectrum, is directly related to the magnetic field experienced by the particular nucleus (Dickson & Berry, 1986).

When, again taking ^{57}Fe as an example, it is observed that the excited state is split into four different levels and the ground level in two levels. Thus, six possible transitions are possible resulting in a sextet (McCammon, 2000).

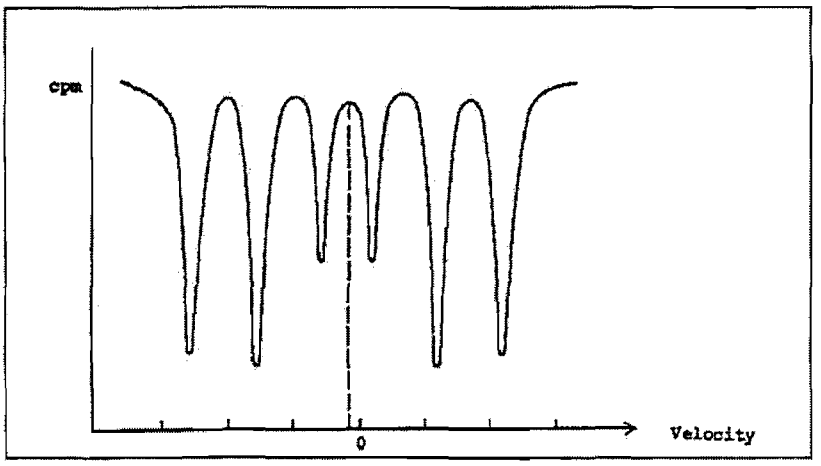


Figure 3.8: Schematic representation of a typical hyperfine magnetic splitting as observed in a Mössbauer spectrum (Cohen, 1976)

3.8 FactSage modelling

FactSage is a thermo-equilibrium computer simulation package that enables the user to perform simulations on coal behaviour, in order to predict characteristics such as mineral transformations and slagging behaviour. This simulation package has its origin in the fusion of two simulation packages that specialize in computational thermochemistry, namely Fact–Win and ChemSage (Bale *et al.*, 2002). One of the main advantages of FactSage is that it is able to perform complex chemical equilibrium manipulations and calculations. It is also able to calculate and manipulate phase diagrams. The other advantage of this package that stands out is the fact that it can take carbon reactions with the minerals into account and it is also possible to vary the gas composition, as well as the atmosphere (Hack, 2005).

FactSage was developed to run on a computer under the Microsoft Windows® operating system. This simulation package consists of a series of information, database, calculation and manipulation modules that make it possible for the user to manipulate the databases containing pure substances and solutions. FactSage, as a 32 bit application, consists of Visual–Basic (45%), Delphi (20%), C++ (10%) and forton – 90 (25%) (FactSage, 2008).

Two of the mostly used modules in FactSage are the equilib and phase diagram modules. With the equilib module the concentrations of mineral species, imbedded in the coal, can be calculated when certain elements or compounds react or partially react to reach a state where there is chemical equilibrium. The phase diagram module can be defined as a module which enables the user to calculate, plot and edit phase diagram sections where there are one, two, three, four or multi components present. The axes of these phase diagrams can be various combinations of T, P, V, composition, activity, chemical potential, etc. (Bale *et al.*, 2002; Hack, 2005).

For this project FactSage will be mainly implemented to predict mineral transformation, as well as slagging potential in order to construct a viscosity model. The results from these simulations will also be compared to experimental results.

4.1 Introduction

The results obtained from the experimental work are presented and discussed in this chapter. Characteristic analysis were performed before the rest of the experimental work in order to establish whether the properties of the coal samples falls within the range of values of the coal Sasol uses for commercial purposes.

4.2 Characteristics of coal samples

The general characteristics analyses, i.e. proximate and ultimate analysis, as well as ash composition, were carried out on all three the coal samples.

4.2.1 Proximate analysis

In the proximate analysis the moisture content, volatiles and ash content were determined by the standard procedures ISO 1171 and ISO 562 (ISO 562, 1998; ISO 1171, 1997). The fixed carbon content was determined by difference. The result of the proximate analysis on the three samples is shown in Table 4.1.

Table 4.1: Proximate analysis for the three coal samples received (on a mass percentage basis)

Sample	Moisture	Volatiles	Fixed Carbon	Ash	Total
Sample A	2.9	22.1	41.8	33.2	100
Sample B	3.6	20.7	46.7	29	100
Sample C	3.8	20.9	49.2	26.2	100

4.2.2 Ultimate analysis

An ultimate analysis expresses the constituents of the coal samples in terms of the principal chemical elements carbon (C), hydrogen (H), nitrogen (N), and oxygen (O). The C, H and N contents were determined by the standards ASTM D4239 and ASTM D5373 (ASTM D4239, 2005; ASTM D5373; 2002).

Oxygen was determined by difference. The result of the ultimate analysis is shown in Table 4.2

Table 4.2: Ultimate analysis for the three coal samples received

Element	Mass percentage
Sample A	
Carbon	78.6
Hydrogen	4.4
Nitrogen	2.0
Sulphur	1.9
Oxygen	13.1
Total	100
Sample B	
Carbon	78.8
Hydrogen	4.1
Nitrogen	2.1
Sulphur	2.0
Oxygen	13.0
Total	100
Sample C	
Carbon	78.8
Hydrogen	4.1
Nitrogen	2.1
Sulphur	2.0
Oxygen	13.0
Total	100

4.2.3 Ash composition analysis

The composition of the ash is an important parameter to determine, since the minerals present in the ash will give an indication of the likeliness of a coal source to slag. The ash composition was determined in terms of the oxides of the different elements according to the procedure set out in standard ASTM D3682 (ASTM D3682, 2001). The result of the ash composition analysis is shown in Table 4.3.

Table 4.3: Ash composition analysis for the three coal samples received

Element	Mass percentage
Sample A	
SiO_2	50.2
Al_2O_3	25.0
Fe_2O_3	5.9
P_2O_5	0.8
TiO_2	1.3
CaO	7.8
MgO	2.0
K_2O	1.0
Na_2O	0.5
SO_3	5.5
Total	100
Sample B	
SiO_2	50.1
Al_2O_3	23.3
Fe_2O_3	6.4
P_2O_5	0.7
TiO_2	1.0
CaO	8.3
MgO	2.7
K_2O	0.8
Na_2O	0.6
SO_3	6.1
Total	100
Sample C	
SiO_2	50.1
Al_2O_3	23.3
Fe_2O_3	6.4
P_2O_5	0.7
TiO_2	1.0
CaO	8.3
MgO	2.7
K_2O	0.8
Na_2O	0.6
SO_3	6.1
Total	100

4.2.4 SEM results

Results obtained from the SEM analysis in terms of the elemental, as well as oxide compositions, are provided in the Appendix in Tables A.1 and A.2. Microphotographs were taken from the coal, as well as the iron-added ash samples and shown in Figures 4.1-4.3.

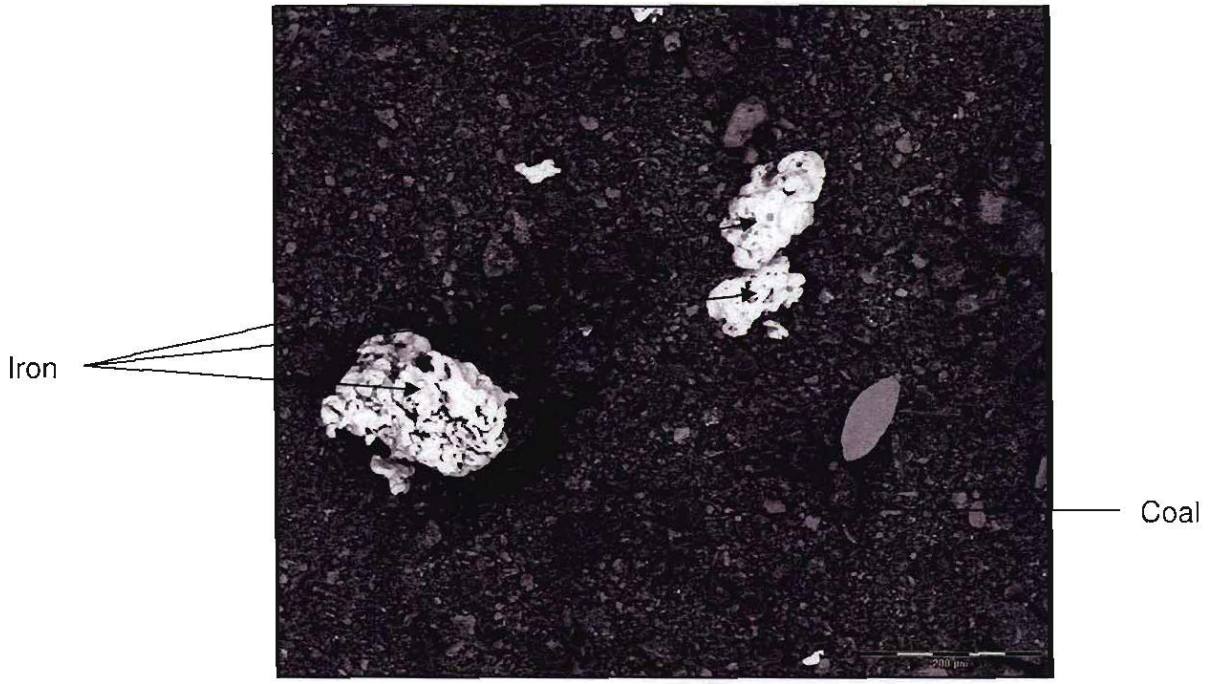


Figure 4.1: SEM image of Sample C with 15 mass percentage iron addition



Figure 4.2: SEM image of sample B with 20 mass percentage iron addition

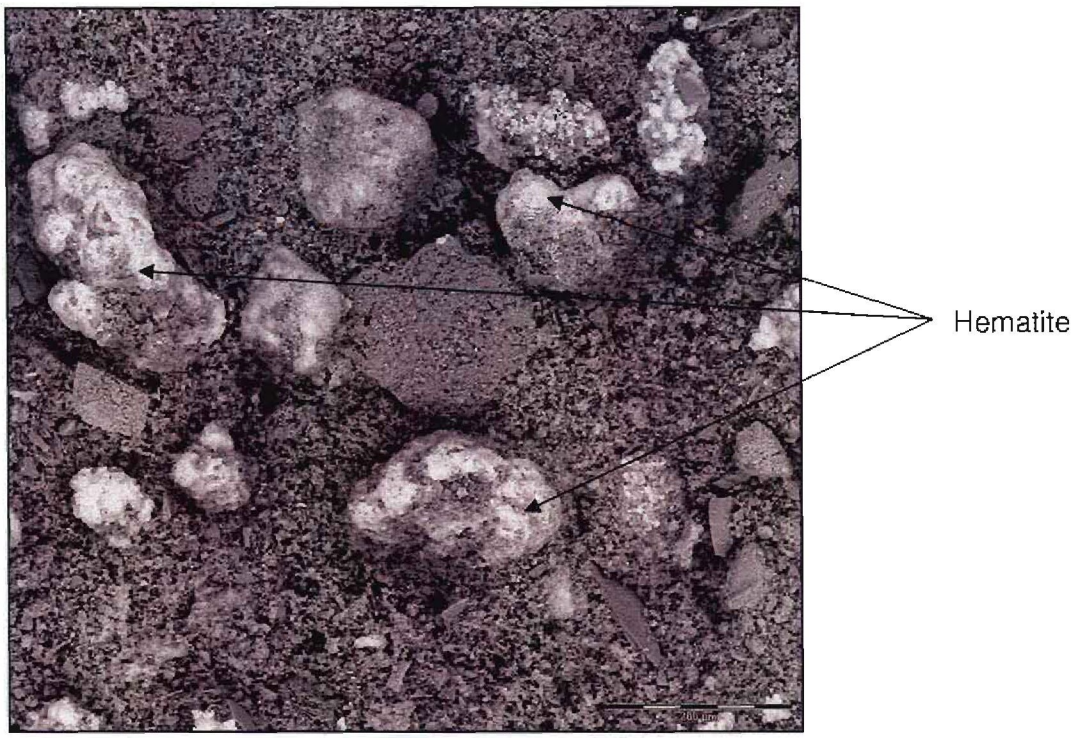


Figure 4.3: SEM image of Sample C ash with 15 mass percentage iron addition

In Figures 4.1 and 4.2 the lighter, shiny particles observed is the iron added to the coal samples. The ash sample in Figure 4.3 illustrates the presence of hematite which can clearly be identified as the large, grey particles.

4.3 AFT analysis

AFT analyses obtained *via* the standard procedures ISO 540 and ASTM D1857 are discussed in this section (ASTM D1857, 2004; SABS, 1996).

4.3.1 Analysis of original samples

The AFT analysis provides an understanding in which manner, and by how much, the iron affects the slagging properties of a coal source. As mentioned in Chapter 3 the AFT tests were carried out under oxidizing and reducing conditions.

Firstly, the results of the AFT analysis on the three main samples are given in Tables 4.4 and 4.5. The results for the 15 sub-samples, under reducing and oxidizing conditions, are shown in the rest of this section.

Table 4.4: AFT results of the original samples under oxidizing conditions

Sample	IDT (°C)	HT (°C)	ST (°C)	FT (°C)
Sample A	1280	1435	1450	1470
Sample B	1260	1325	1345	1360
Sample C	1260	1325	1345	1360

Table 4.5: AFT results of the original samples under reducing conditions

Sample	IDT (°C)	HT (°C)	ST (°C)	FT (°C)
Sample A	1230	1310	1340	1390
Sample B	1290	1325	1340	1370
Sample C	1265	1370	1400	1425

The analysis of the original coal samples and that of the sub-samples were done in two different laboratories. This explains the larger than expected experimental error between the sets of data.

4.3.2 Results for AFT experiments on iron addition samples under oxidizing conditions

The results obtained from the AFT analysis on the iron addition samples under oxidizing conditions are shown in Figures 4.4 to 4.6. All of these experiments were carried out according to the procedures of standard ISO 540 (SABS, 1996). According to this standard the maximum acceptable experimental error in the flow temperature (FT) must be of the order of ±50°C (SABS, 1996). The detailed tabulated data is provided in the Appendix in Tables A.3-A.12.

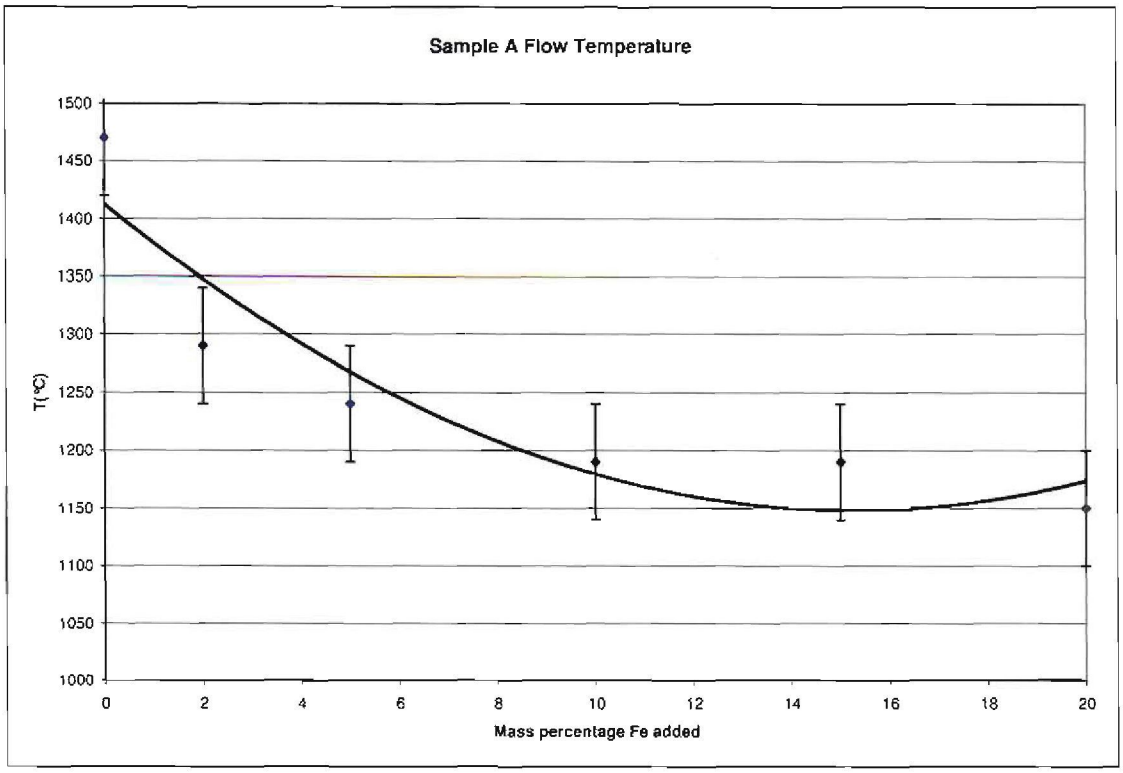


Figure 4.4: AFT results of Sample A and those to which different amounts of iron were added under oxidizing conditions

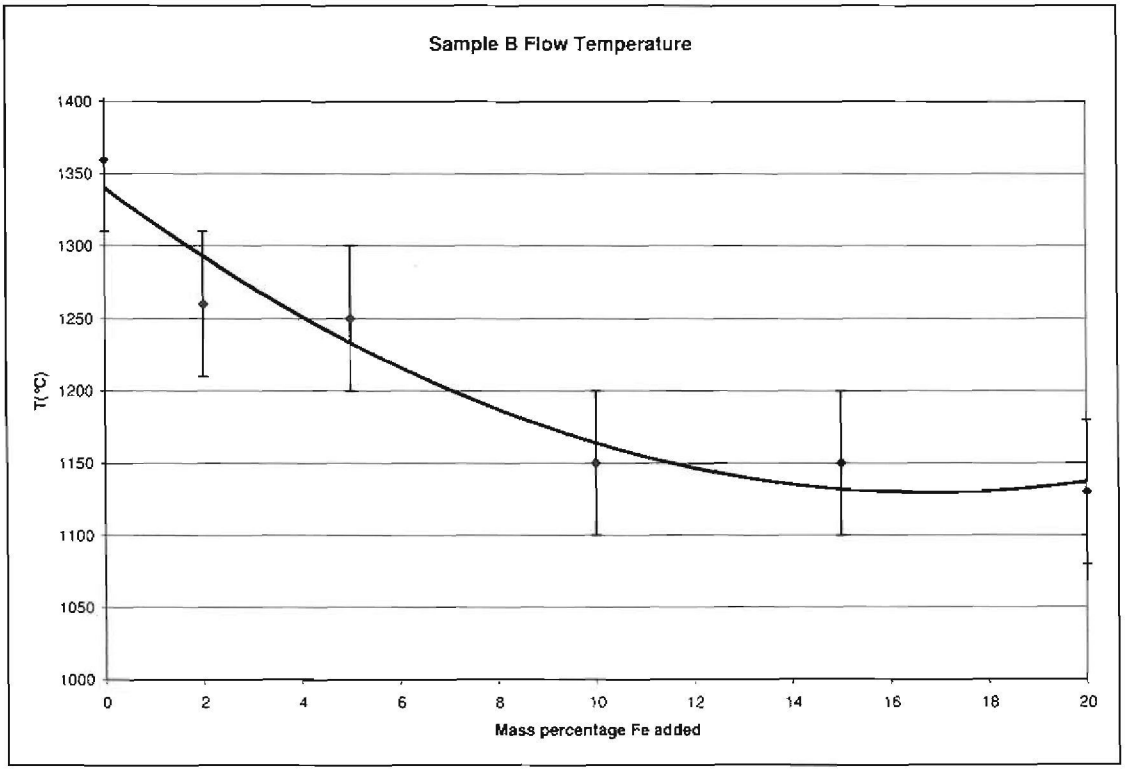


Figure 4.5: AFT results of Sample B and those to which different amounts of iron were added under oxidizing conditions

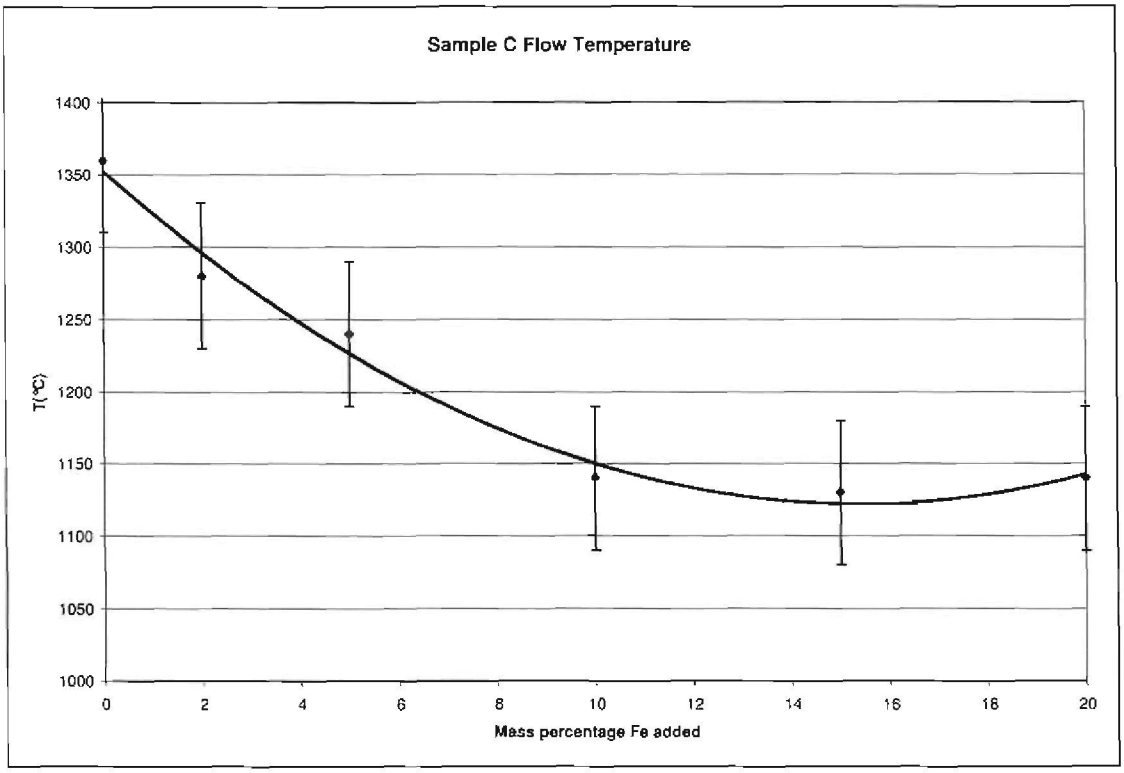


Figure 4.6: AFT results of Sample C and those to which different amounts of iron were added under oxidizing conditions

In Figures 4.7 to 4.9 the trend of all four deformation temperatures with an increase in iron, under oxidizing conditions, are shown for all three samples.

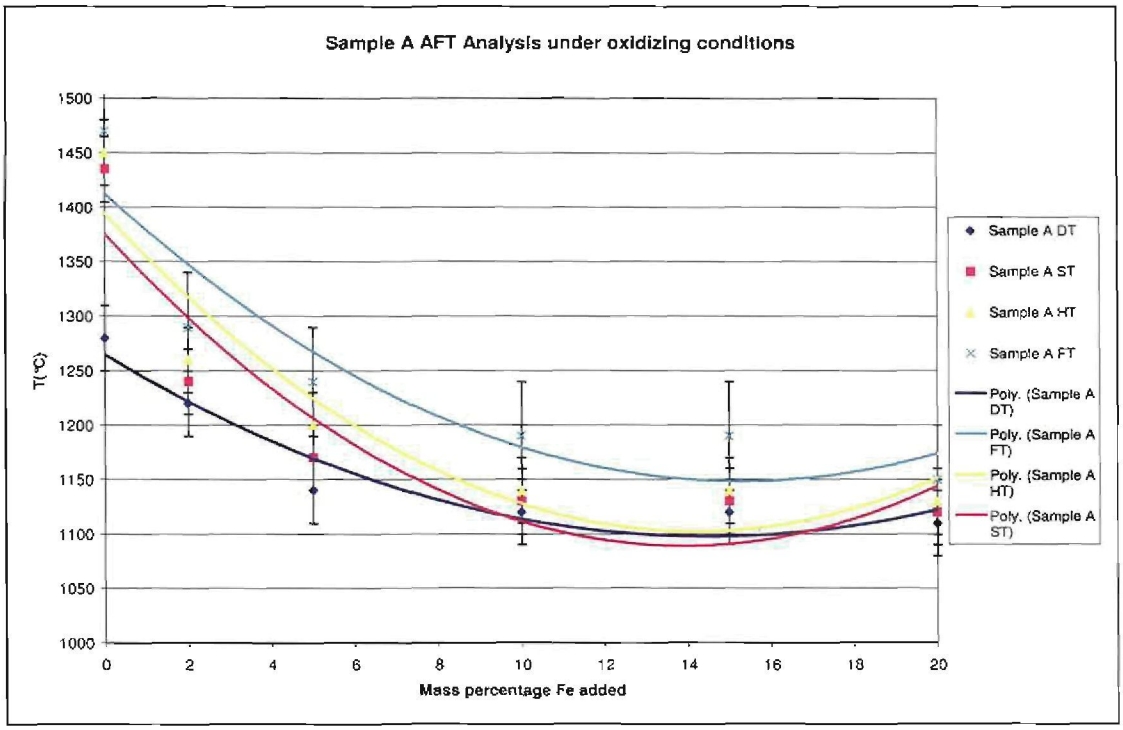


Figure 4.7: Complete AFT results of Sample A showing all four deformation temperatures under oxidizing conditions

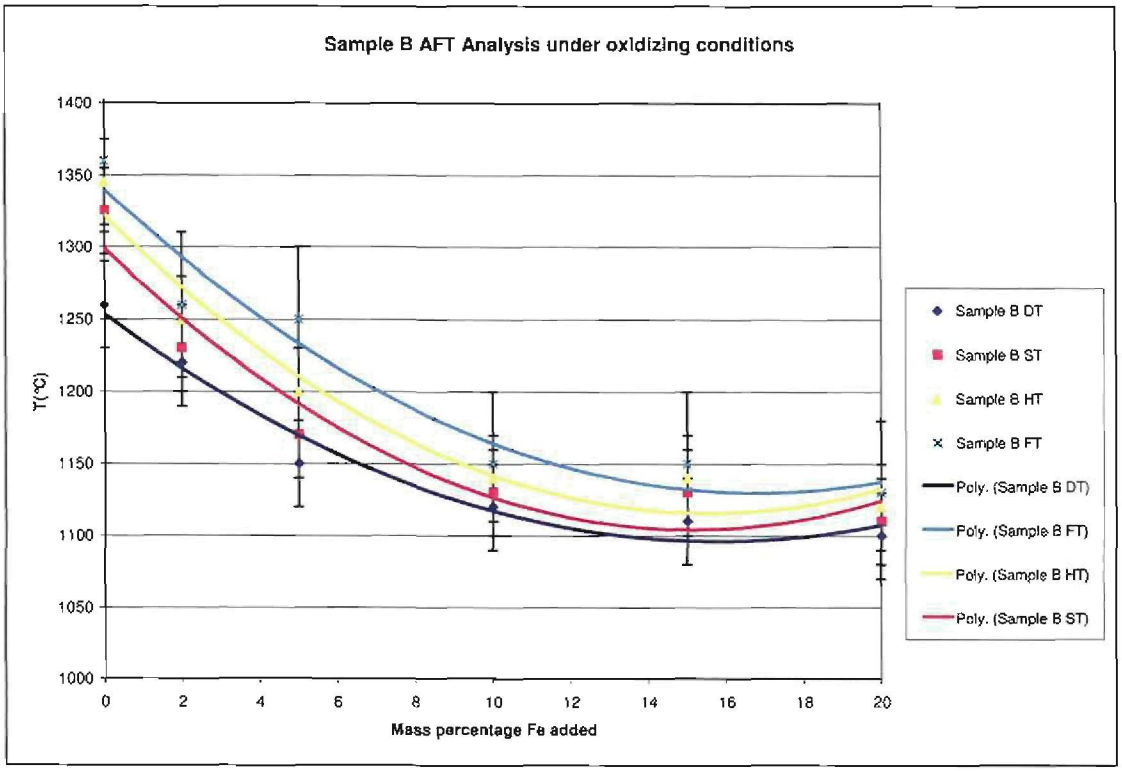


Figure 4.8: Complete AFT results of Sample B showing all four deformation temperatures under oxidizing conditions

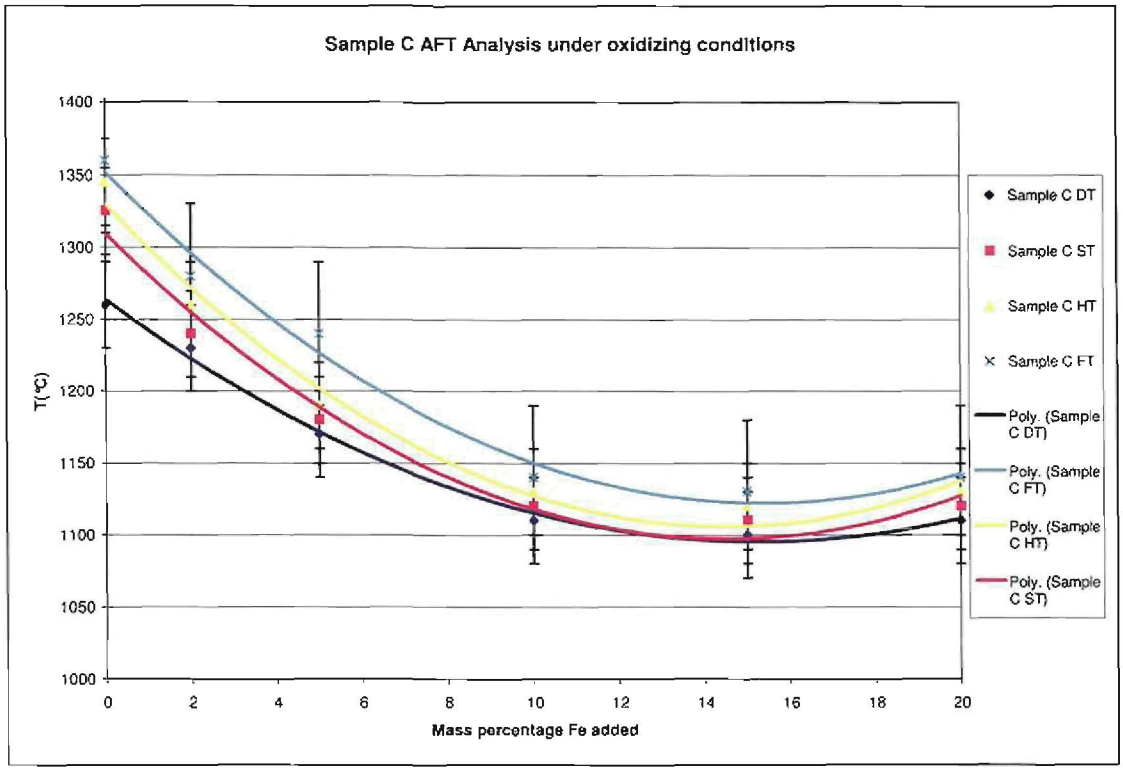


Figure 4.9: Complete AFT results of Sample C showing all four deformation temperatures under oxidizing conditions

4.3.3 Results of the AFT experiments conducted on the iron addition samples, under reducing conditions

The AFT experiments conducted under a reducing atmosphere were also compliant with the procedures set out in the ISO 540 standard (SABS, 1996). Results of the experiments under reducing conditions are shown in Figures 4.10 to 4.12.

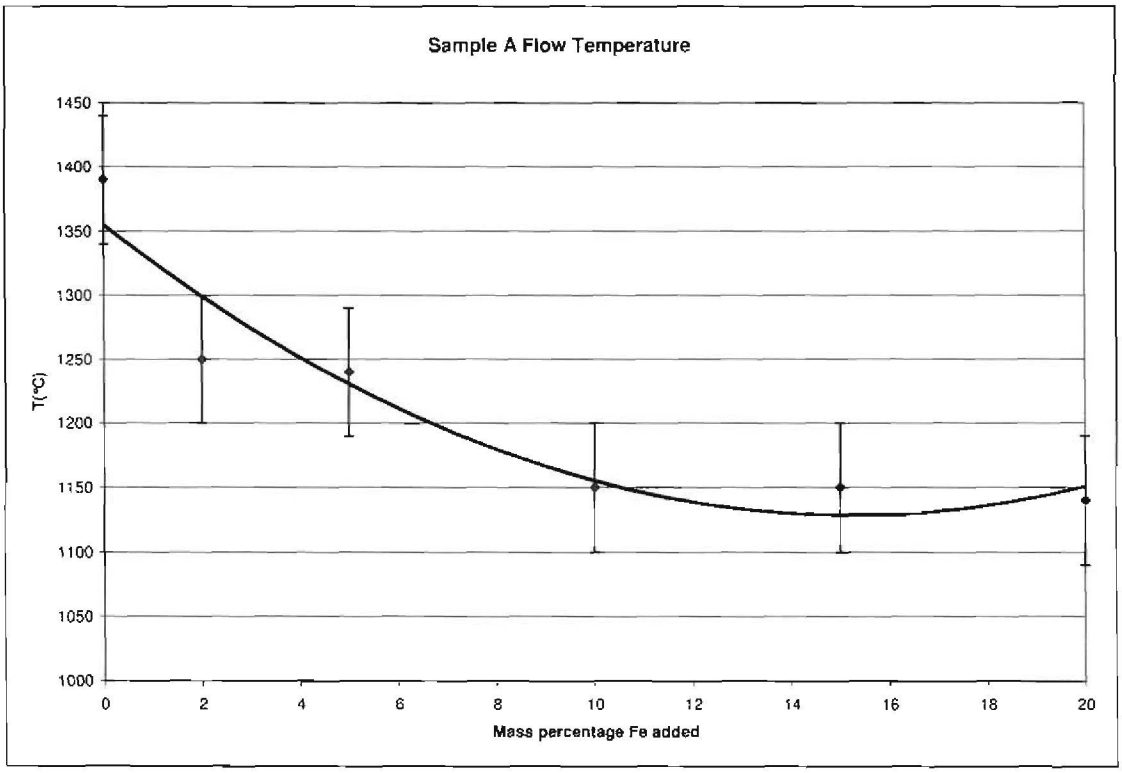


Figure 4.10: AFT results of Sample A and those to which different amounts of iron were added under reducing conditions

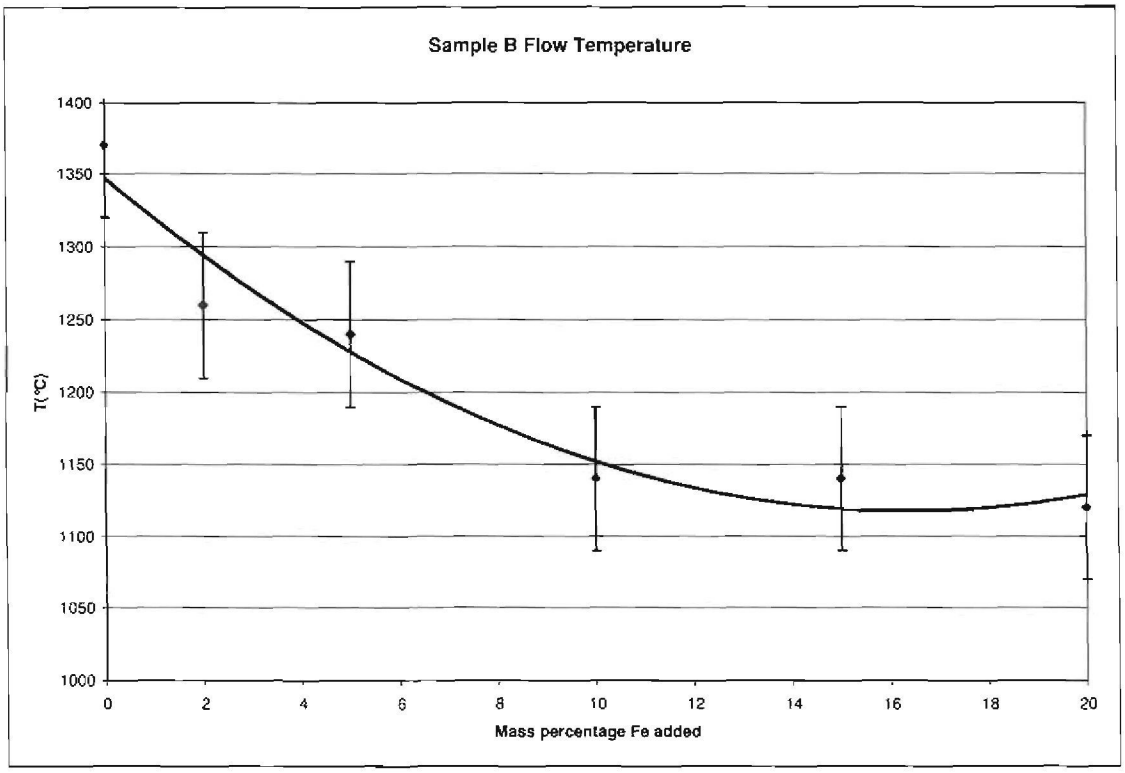


Figure 4.11: AFT results of Sample B and those to which different amounts of iron were added under reducing conditions

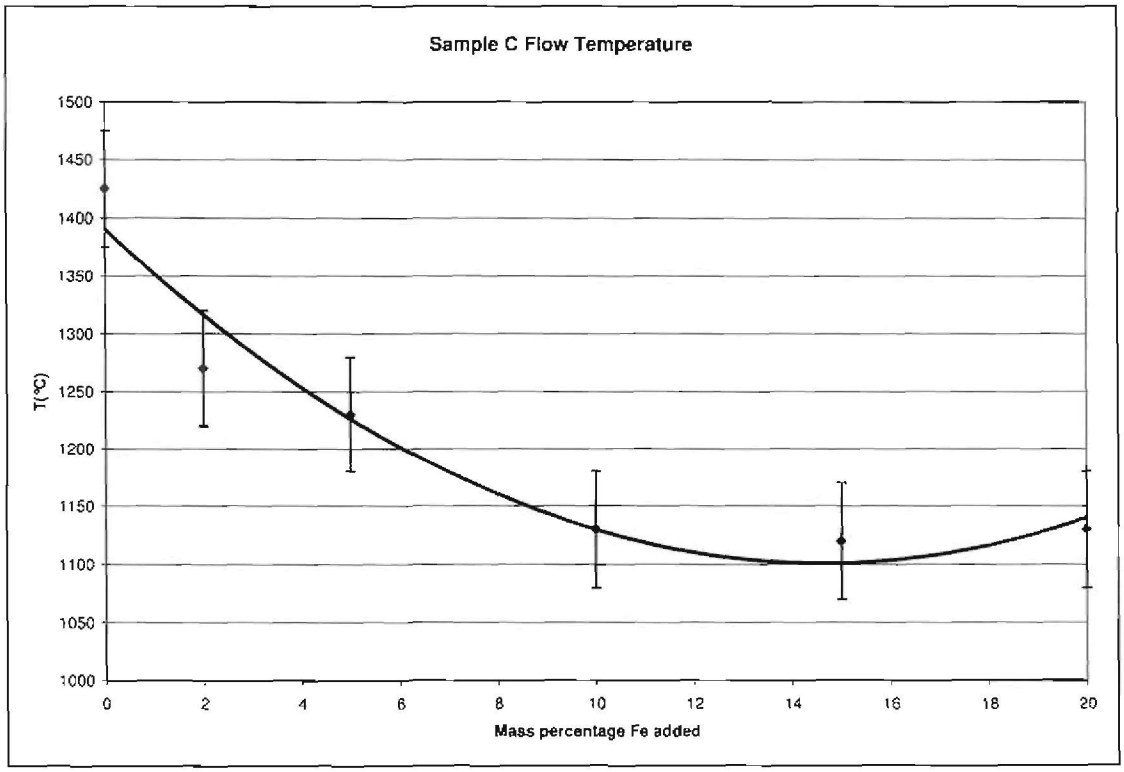


Figure 4.12: AFT results of Sample C and those to which different amounts of iron were added under reducing conditions

Figures 4.13 to 4.15 show the trend of the four deformation temperatures with an increase in iron content under reducing conditions.

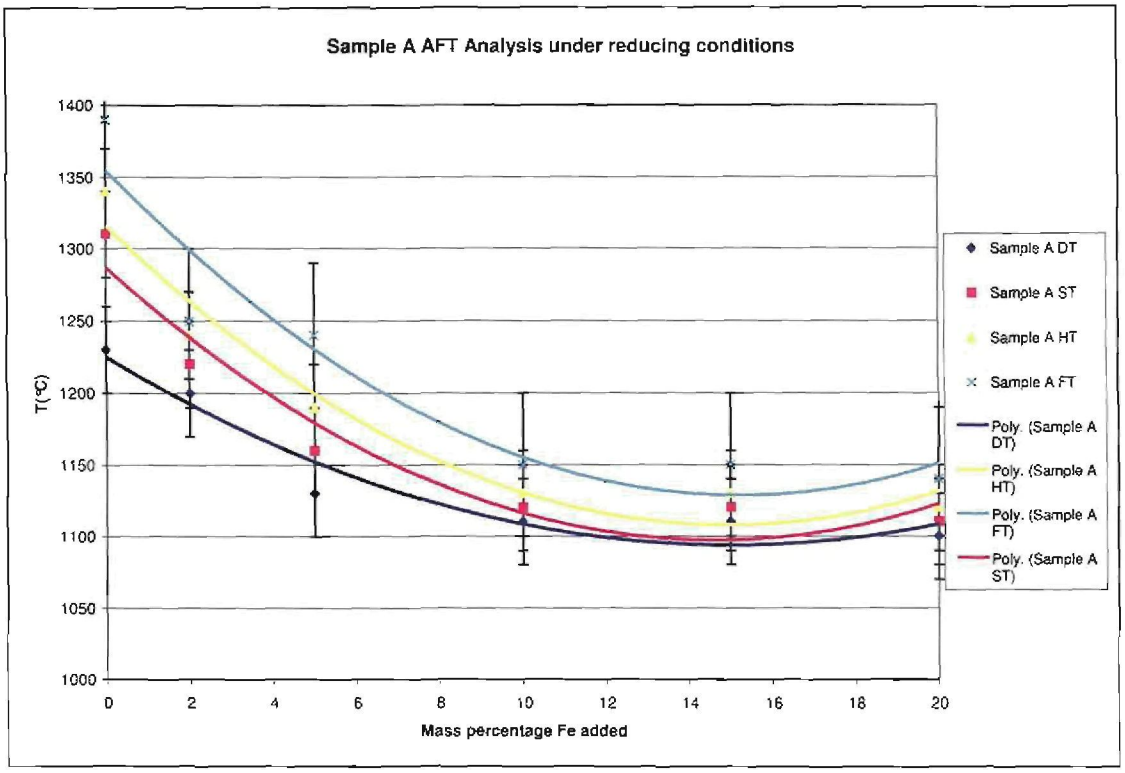


Figure 4.13: Complete AFT results of Sample A showing all four deformation temperatures under reducing conditions

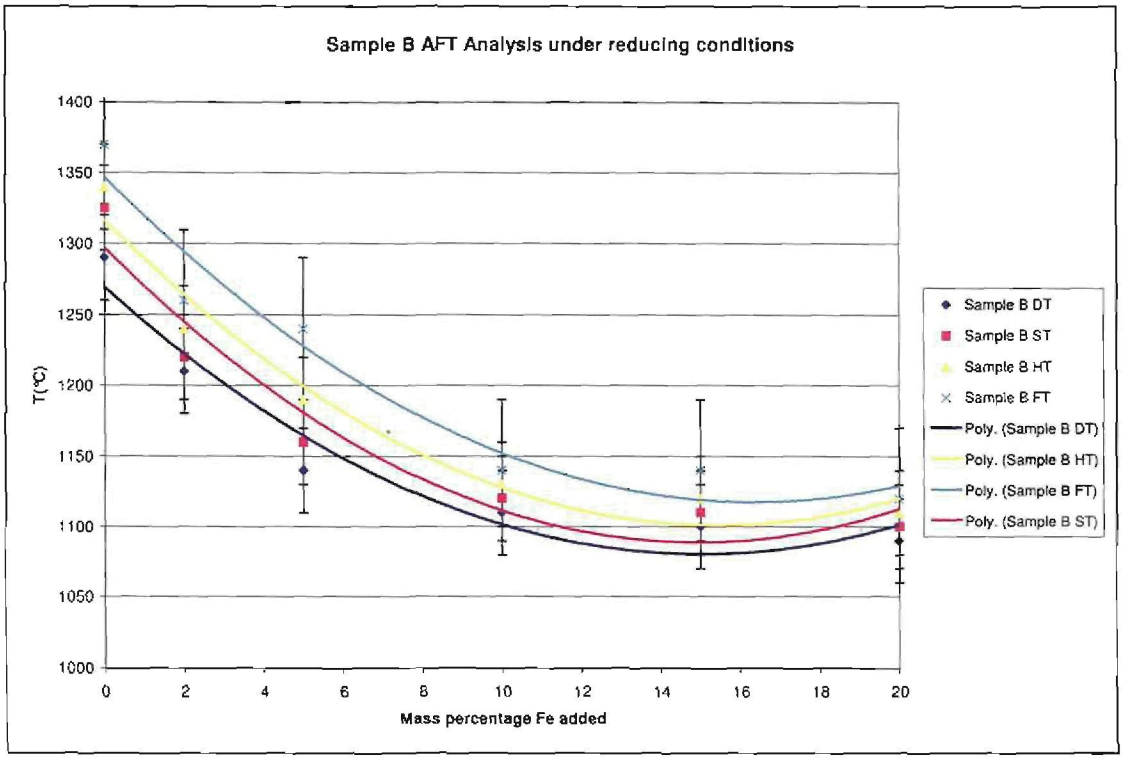


Figure 4.14: Complete AFT results of Sample B showing all four deformation temperatures under reducing conditions

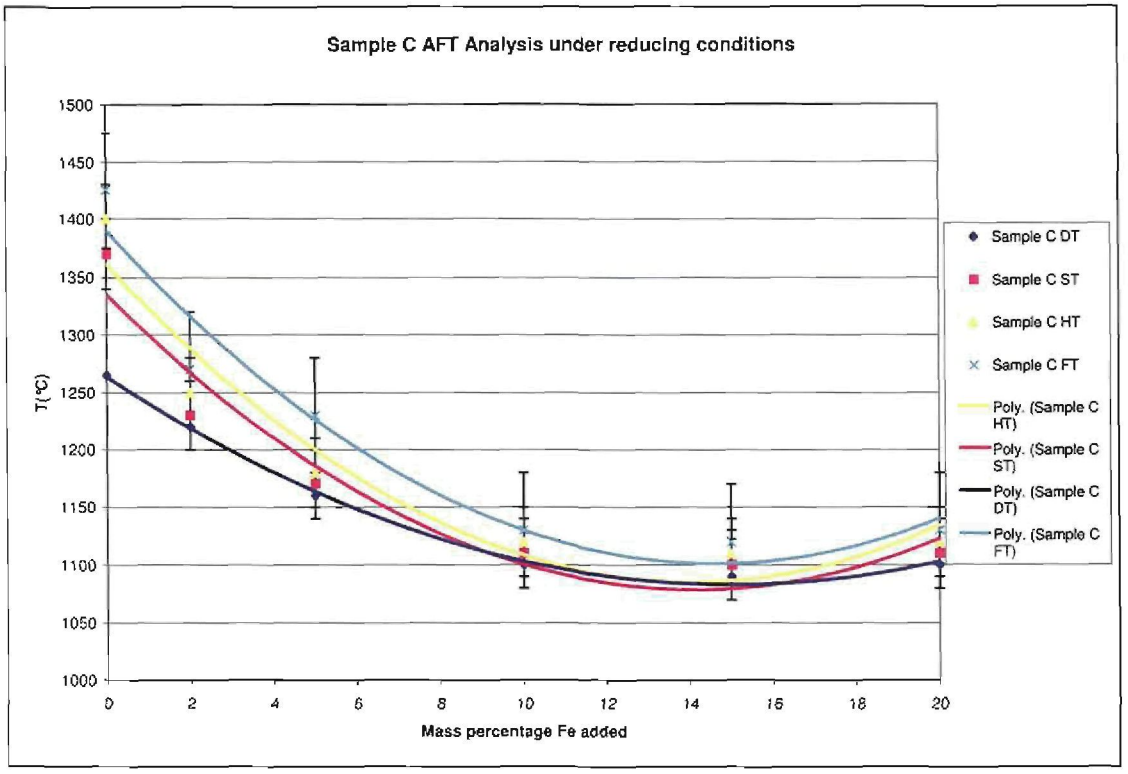


Figure 4.15: Complete AFT results of Sample C showing all four deformation temperatures under reducing conditions

4.3.4 Discussion of the AFT results

The flow temperatures in Figures 4.4 to 4.7 and 4.11 to 4.13 were plotted, since this temperature is generally used to give the final AFT value.

The most evident aspect evident in Figures 4.4 to 4.15 is a clear decrease in the AFT of all three coal sources, with an increase in the amount of iron added. Beyond 10 mass percentage iron addition, however, the AFT stays constant in all the samples. These trends are observed in both oxidizing and reducing conditions. The percentages by which the iron addition lowers the AFT of the coal sources can be seen in Table 4.6. This percentage difference was calculated, based on the maximum amount by which the iron addition lowers the AFT of that particular sample.

Table 4.6: Percentage difference in AFT induced by iron addition

	Percentage difference in AFT	
Sample	**Oxidizing conditions**	**Reducing conditions**
Sample A	22	18
Sample B	17	18
Sample C	17	21

In Table 4.6 it can be seen that there is a difference in the percentages obtained for Sample A and C under reducing and oxidizing conditions. This difference is, however, still within the ±50°C error bands and it can be seen that an average lowering of 20% in the AFT occurs under both oxidizing and reducing conditions.

The trends illustrated in Figures 4.4 to 4.15 were expected, as stated in the hypothesis in Chapter 1. In the literature various studies point out the fluxing properties of the iron-containing species found in coal (Huggins *et al.*, 1981; Patterson & Hurst, 2005; Renton, 1982; Van Dyk *et al.*, 2005; Vassilev *et al.*, 1995). Huggins *et al.* (1981) noticed that the AFT of a coal source tended to decrease with the addition of Fe_2O_3, as illustrated in Figure 4.16.

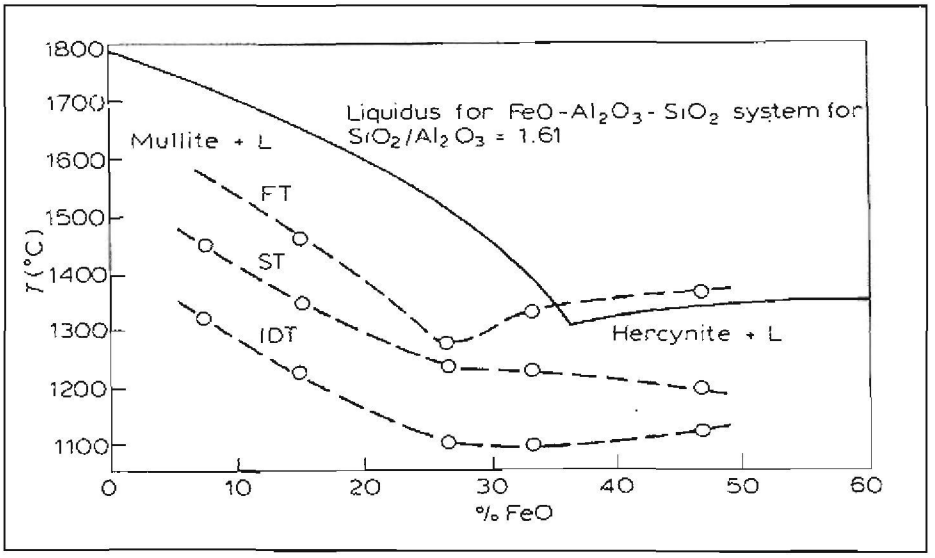


Figure 4.16: AFT results for an ash sample with added Fe_2O_3 (Huggins *et al.*, 1981)

In Figure 4.16 the liquidus (temperature at which melting is complete) line is indicated showing the large temperature difference of about 200°C from the flow temperature (FT) of the sample with the smallest addition of FeO to the liquidus. It is also clear that, as the amount of FeO was increased, the flow temperature became even higher than the liquidus temperature. The increase observed in the flow temperature at around 28% FeO in Figure 4.16 can be ascribed to an increase in the amount of unreacted solids (Huggins *et al.*, 1981). In this case the ability of the liquid phase to flow is counteracted by the structure provided by the solids. Thus, a higher temperature is needed for a new liquid phase to be produced (EPRI, 1980). In the present investigation a maximum of 20 mass percentage iron was added and only the start of the flattening out of the FT *vs.* %FeO added, was observed (Figure 4.16). The coal used by Huggins *et al.*, (1981) had a SiO_2/Al_2O_3 ratio of 1.61 which correlates very well with the coal samples used in this study (ratio of more or less

1.60). Thus, it can be concluded that the AFT of the coal sources will increase with more than 20 mass percentage iron addition as shown in Figure 4.16. Such a large addition of iron will not be economically viable and was, therefore, not considered in this study.

The fluxing effect of iron-containing species is best illustrated by the use of ternary phase diagrams. This approach was followed by Huggins *et al.* (1981), as well as Van Dyk (2006) with a phase diagram (for the Al_2O_3-FeO-SiO_2 system) such as the one shown in Figure 4.17.

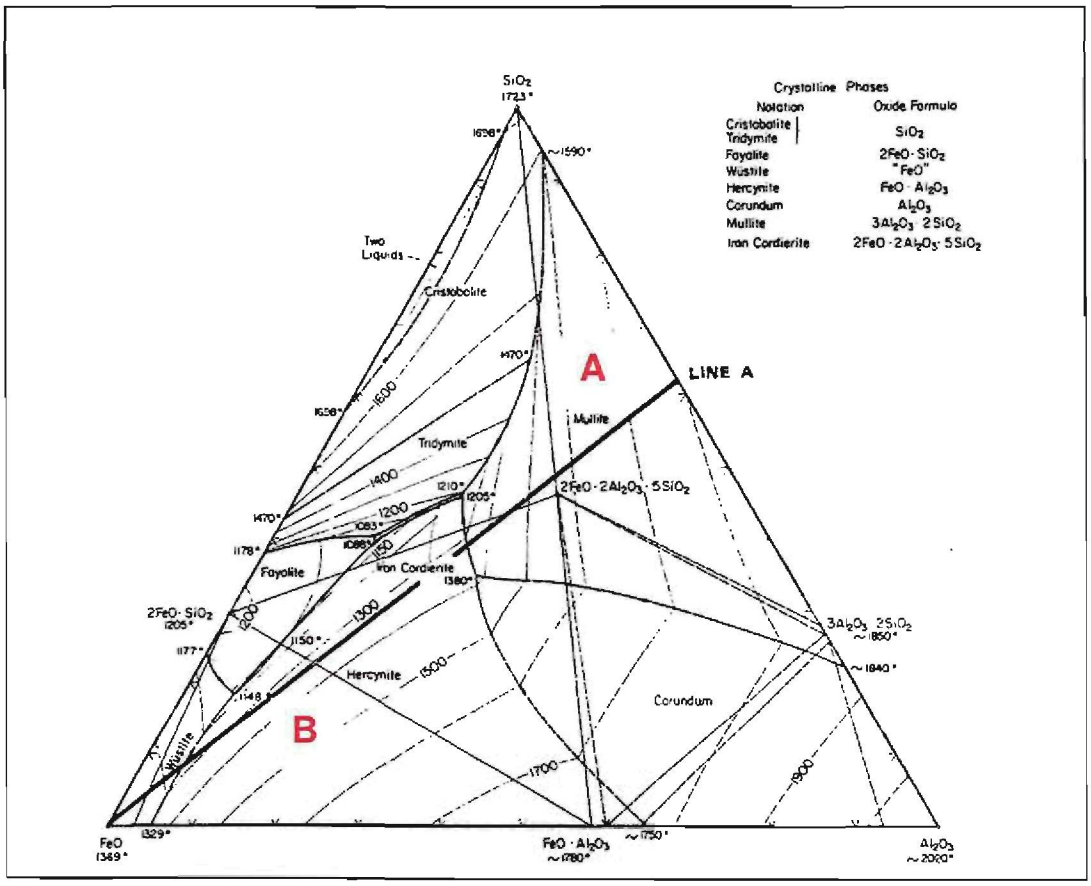


Figure 4.17: The ternary phase diagram for the three component system Al_2O_3-FeO-SiO_2 (Huggins *et al.*, 1981)

On Figure 4.17 Line A is indicated. If there is an increase in the iron content, moving from point A to B on the diagram, it becomes evident that the AFT of the coal source decreases. Point A on the diagram is located on the 1700°C isotherm whereas point B is very close to 1300°C. Thus, a decrease of more or less 400°C occurs with a relative large increase in the iron content.

According to the study by Huggins *et al.* (1981) the main parameters governing the AFT behaviour are the SiO_2/Al_2O_3 ratio and the percentage base components (CaO, FeO, etc.) present. However, these parameters are only valid if the amount of Al_2O_3 and SiO_2 exceeds 70%. This implies that coals in which mullite is expected, will be in the subliquidus phase (Huggins *et al.*, 1981). For the three coal sources used in this study, this condition is valid for all of them. For Sample B and C the sum of Al_2O_3 and SiO_2 is 73.4%, while for Sample A it is 75.1%.

Van Dyk (2006) generated a ternary phase diagram with the FactSage simulation package for the Al_2O_3-Fe_2O_3-SiO_2 system. This diagram, with 8 mass percentage Fe_2O_3 content, is shown in Figure 4.18.

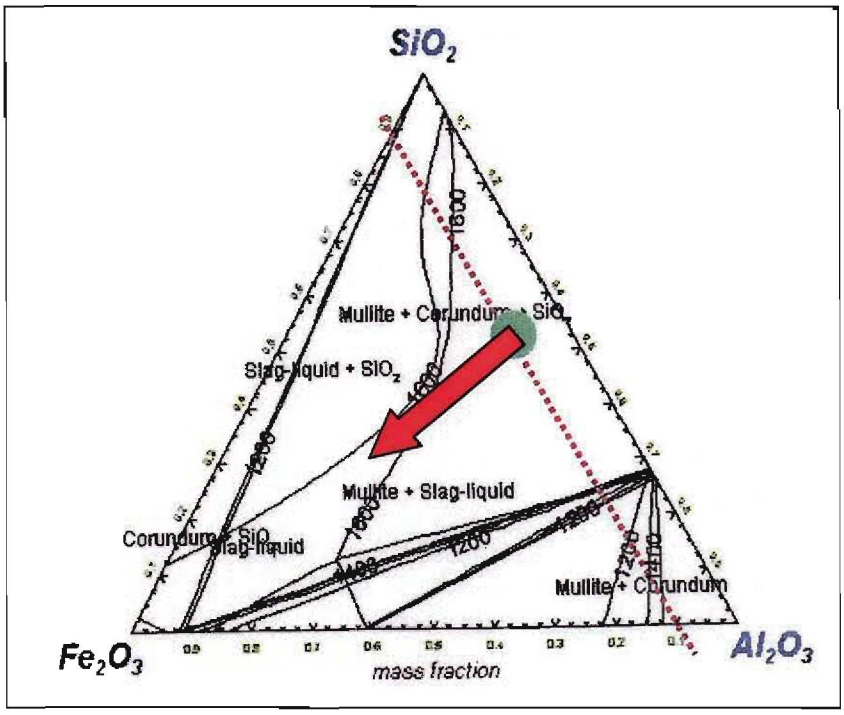


Figure 4.18: A ternary phase diagram for the three component system Al_2O_3-Fe_2O_3-SiO_2 (Van Dyk, 2006)

Figure 4.18 shows a green dot which is related to relatively low iron content (8% Fe_2O_3). The area, in which this dot is located, is where mullite is known to form. It is also clear from the figure that the dot is located above the 1600°C isotherm. When the iron content of the particular coal source increases, thus moving the dot to the bottom left hand corner as indicated by the arrow, it is clear that the fusion temperature will decrease. The area changes from the mullite forming area to an area where slag-liquid prevails (Van Dyk, 2006). Thus, the increase of iron forces the flow temperature below the 1600°C isotherm and is responsible for the transformation to a slag-liquid state (Van Dyk, 2006).

The results from the study by Van Dyk (2006) indicate that the increase of iron in the coal results in iron-containing phases with a markedly lower melting temperature, which explains the decrease in the flow temperature. From the phase diagrams it can be concluded that an increase in iron content in the coal will lower the flow temperature of a coal source, mainly due to the increasing presence of lower melting iron-containing phases.

Another possible explanation for the decrease observed can be found in the study by Kalmanovitch and Frank (1988). As was mentioned previously, these two authors divide oxides into three groups, i.e. network formers, network modifiers and amphoterics. The two iron oxides, FeO (Fe^{2+}) and Fe_2O_3 (Fe^{3+}), are located in the network modifier and amphoteric groups, respectively. A network modifier (FeO) is responsible for the destabilization of the network when it forces the bridging of oxygen bonds located in the network former. This ultimately results in the lowering of the viscosity, which implies that more liquid slag will be present. The amphoteric oxides can have the characteristics of both of the other two groups with the composition of the melt the deciding factor on which of the two will be dominant. From the results obtained by this study it is clear that the hematite (Fe_2O_3), that form from the iron added, adopt the characteristics of the network modifier group. The effect of the two iron oxides will have an adverse effect on the viscosity, forcing it lower to obtain a more viscous slag (Kalmanovitch & Frank, 1988). Thus, an increase in the presence of the iron-oxides will ensure that the network is destabilized, reducing the strength of the bonds which will lead to slag forming at lower temperatures as would have been the case without these oxides.

To conclude this section, the results from the AFT experiments confirm the hypothesis, as well as the results published in literature sources, on the effect of iron on the slagging behaviour of coal. The decrease of the AFT due to the increasing iron content can thus be ascribed to:

- Formation of lower melting point iron-containing phases
- Bridging of oxygen bonds by FeO and Fe_2O_3
- Lowering of the viscosity by the iron-oxides

4.4 Mössbauer spectroscopy

In Chapter 3 it is mentioned that three interactions (isomer shift (δ), quadrupole split (Δ) and/or hyperfine magnetic field (H)) were measured during an experimental run on the Halder Mössbauer Spectrometer. The measured values for these interactions are provided in Table 4.7 for the iron added coal samples and Table 4.8 for the ash samples. In both tables the percentages indicates the mass percentage iron present.

Table 4.7: Room temperature Mössbauer parameters of the various Fe species present in the coal

Sample	Mineral	δ (mm/s) ± 0.01	Δ (mm/s) ±0.01	H (T)	Relative area (%)
Sample A original	Pyrite	0.205	0.632	-	100
Sample A 2% iron	Pyrite Fe	0.280 -0.051	0.596 -0.017	- 32.557	46 54
Sample A 5% iron	Fe	-0.023	0.006	32.726	100
Sample A 10% iron	Fe	-0.020	0.024	32.920	100
Sample A 15% iron	**No result available**				
Sample A 20% iron	Fe	-0.017	0.020	32.963	100
Sample B Original	Pyrite	0.268	0.494	-	100
Sample B 2% iron	Pyrite Fe	0.290 -0.013	0.554 0.016	- 32.218	40 60
Sample B 5% iron	Fe	-0.016	0.002	32.791	100
Sample B 10% iron	Fe	-0.024	0.011	32.837	100
Sample B 15% iron	Fe	-0.032	0.014	32.791	100
Sample B 20% iron	Fe	-0.020	0.009	32.785	100
Sample C original	Pyrite	0.223	0.589	-	100
Sample C 2% iron	**No result available**				
Sample C 5% iron	Fe	-0.016	0.001	32.790	100
Sample C 10% iron	Fe	-0.015	0.038	32.921	100
Sample C 15% iron	Fe	-0.026	0.026	32.782	100
Sample C 20% iron	Fe	-0.016	0.001	32.790	100

Table 4.8: Room temperature Mössbauer parameters of the various Fe species present in the coal ash

Sample	Mineral	δ (mm/s) ± 0.01	Δ (mm/s) ±0.01	H (T)	Relative area (%)
Sample A original	Fe^{2+}	1.065	1.502	-	4
	Fe^{3+}	0.406	0.822	-	16
	Hematite	0.363	-0.198	51.411	80
Sample A 2% iron	Hematite	0.359	-0.171	51.019	100
Sample A 5% iron	Fe^{2+}	1.183	0.954	-	2
	Fe^{3+}	0.541	0.938	-	8
	Hematite	0.348	-0.181	51.156	90
Sample A 10% iron	Hematite	0.347	-0.165	51.188	100
Sample A 15% iron	Hematite	0.356	-0.180	51.537	100
Sample A 20% iron	Hematite	0.354	-0.170	51.263	100
Sample B original	Fe^{2+}	0.863	2.027	-	42
	Fe^{3+}	0.694	0.335	-	19
	Hematite	0.353	-0.179	50.954	39
Sample B 2% iron	Hematite	0.360	-0.193	51.347	100
SSF slurry 5% iron	Hematite	0.361	-0.181	51.440	100
Sample B 10% iron	Hematite	0.356	-0.190	51.382	100
Sample B 15% iron	Hematite	0.358	-0.195	51.435	100
Sample B 20% iron	Fe^{3+}	0.323	0.570	-	2
	Hematite	0.361	-0.186	51.496	98
Sample C original	Fe^{2+}	0.845	1.878	-	20
	Fe^{3+}	0.573	0.250	-	8
	Hematite	0.356	-0.155	51.474	72
Sample C 2% iron	Fe^{3+}	0.323	0.570	-	8
	Hematite	0.360	-0.188	51.444	92
Sample C 5% iron	Fe^{3+}	0.323	0.570	-	5
	Hematite	0.361	-0.198	51.482	95
Sample C 10% iron	Fe^{3+}	0.323	0.570	-	4
	Hematite	0.358	-0.186	51.490	96
Sample C 15% iron	Fe^{3+}	0.323	0.570	-	3
	Hematite	0.359	-0.182	51.428	97
Sample C 20% iron	Fe^{3+}	0.323	0.570	-	2
	Hematite	0.356	-0.183	51.374	98

All the values obtained by Mössbauer spectroscopy, shown in Tables 4.7 and 4.8, are in accordance with those found in the literature (Stevens *et al.*, 1998).

The discussion of the Mössbauer results will be done with reference to the spectra obtained of the original sample, as well as the sample with 20 mass percentage iron addition for all three samples. This will include the ashed samples, as well as the normal coal samples. The remainder of the spectra is shown in the Appendix.

4.4.1 Sample A

The Mössbauer spectra for the normal coal samples with 0 (original coal sample) and 20 mass percentage iron addition, respectively, are shown in Figures 4.19 and 4.20.

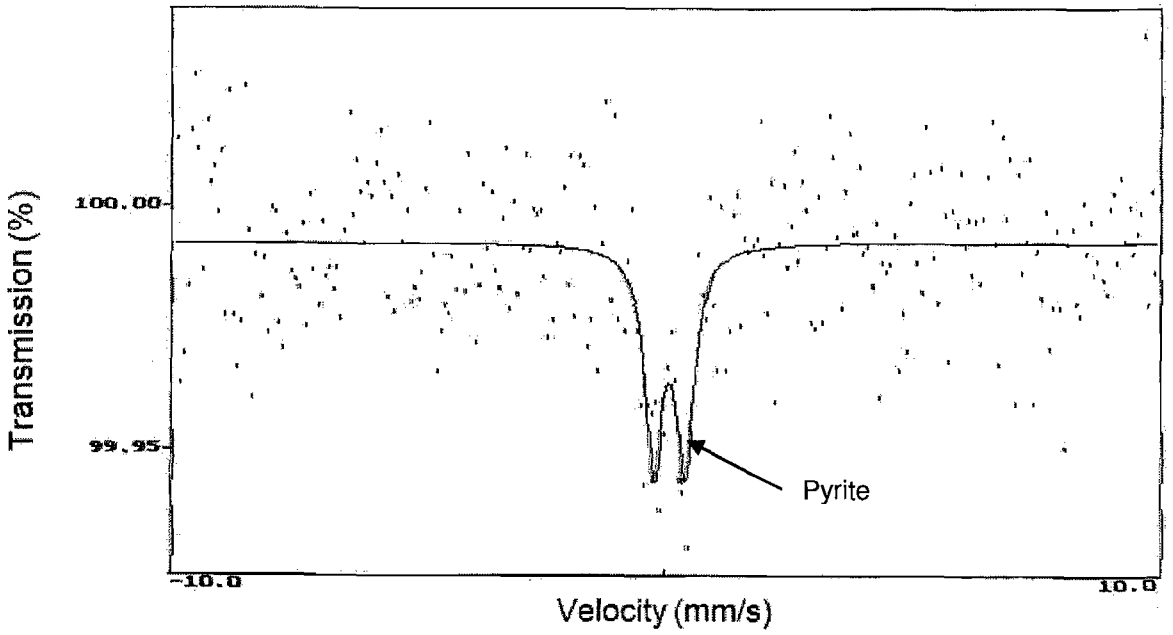


Figure 4.19: The Mössbauer spectrum of Sample A coal (0 mass percent Fe added)

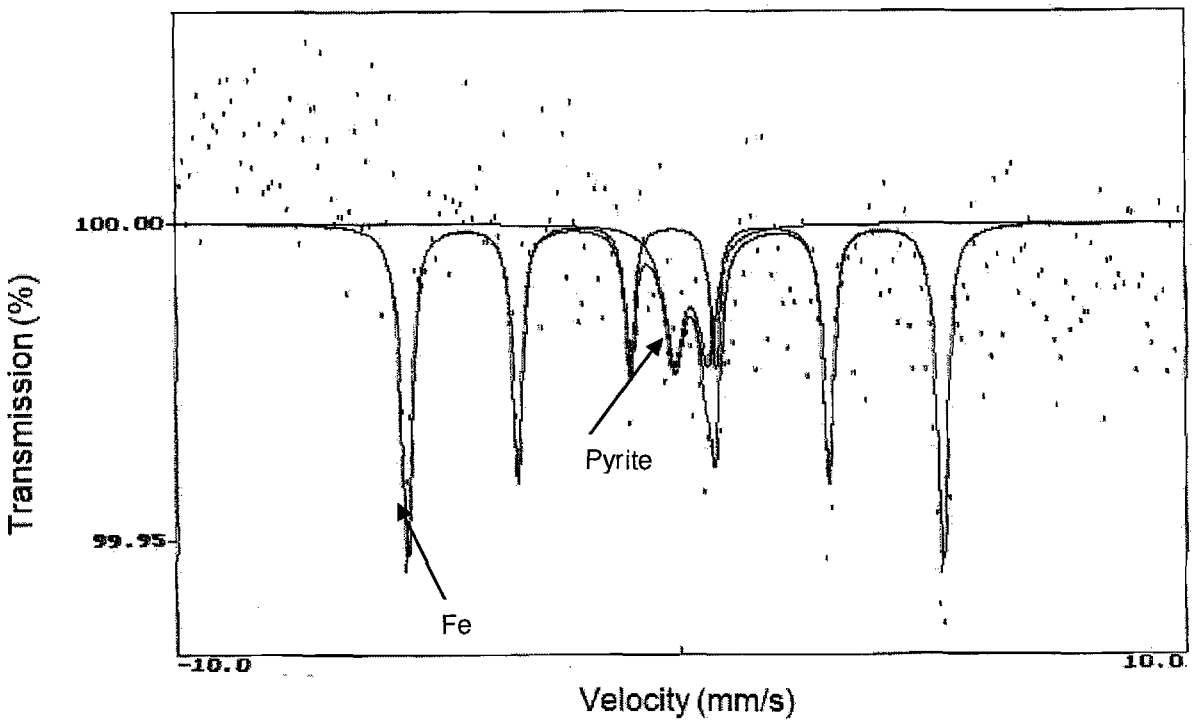


Figure 4.20: The Mössbauer spectrum of Sample A coal
(20 mass percentage Fe added)

In Figure 4.19 it can be seen that the main iron-containing mineral in the original sample is pyrite. This is to be expected since pyrite is one of the most common iron-containing minerals present in South African, as well as other, coal sources (Vassilev & Vassileva, 1996; Van Dyk, 2006). In Figure 4.20 mostly iron is visible, which can be ascribed to the fact that such a large amount of iron is added that the pyrite will be totally overshadowed by the iron and thus not observed.

The Mössbauer spectra of the ashed original, as well as the 20 mass percentage iron-added samples, give a good indication of the effect of the added iron on the coal properties. Figures 4.21 and 4.22 show the spectra of the ashed samples.

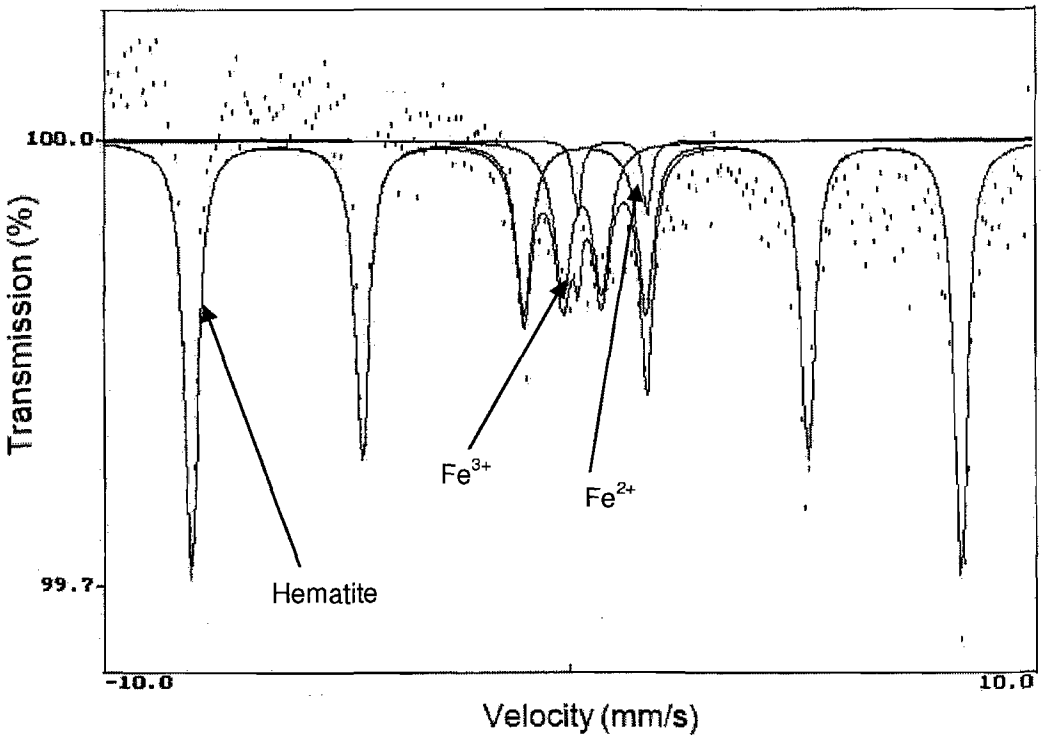


Figure 4.21: The Mössbauer spectrum of Sample A ash
(0 mass percentage Fe added)

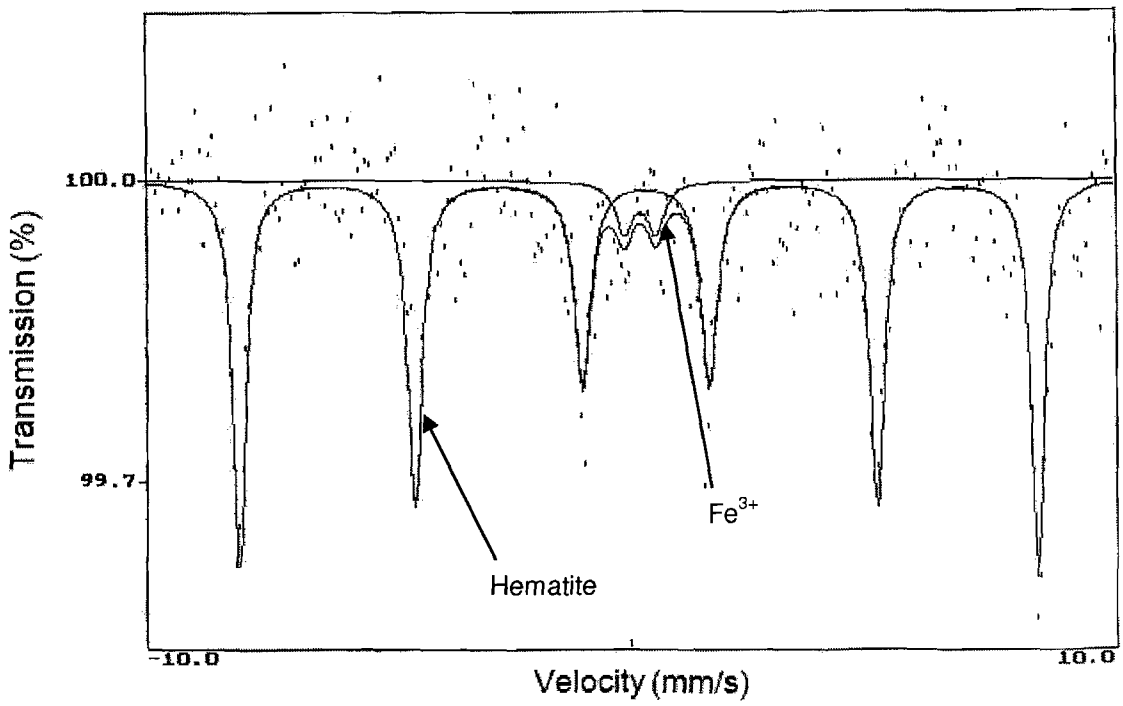


Figure 4.22: The Mössbauer spectrum of Sample A ash
(20 mass percentage Fe added)

Figure 4.21 is the spectrum of the ash from Sample A with no iron addition and will thus be a good representation of the transformation of the iron-containing minerals during gasification. It is clearly observed that two main components arise from the transformation of the pyrite observed in Figure 4.19. The first doublet indicates the formation of a (Fe^{2+}, Fe^{3+}) glass, which is represented in the ash of Sample A, as can be seen in Figure 4.21. Hematite is the other observable component due to the pyrite decomposition, as well as oxidation, which starts to play a significant role as the temperature increases. According to Waanders and Bunt (2007) the decomposition of pyrite ends in hematite with pyrrhotite being an intermediate phase. The transition of pyrite to pyrrhotite is, however, fairly quick and was not observed in the Mössbauer spectrum. The transformation of pyrite to hematite and glass occurs in conjunction with SiO_2 and Al_2O_3 present in the coal (Waanders & Bunt, 2007).

In previous experiments under combustion conditions conducted by Waanders and Bunt (2007), the pure iron transformed to hematite. In Figure 4.22 it can clearly be seen that the hematite that formed totally dominates the spectrum. The large amount of iron added, transformed to hematite with only a small amount of glass visible.

4.4.2 Sample B

The Mössbauer spectra for the Sample B coal samples with 0 (original coal sample) and 20 mass percentage iron addition, respectively, are shown in Figures 4.23 and 4.24.

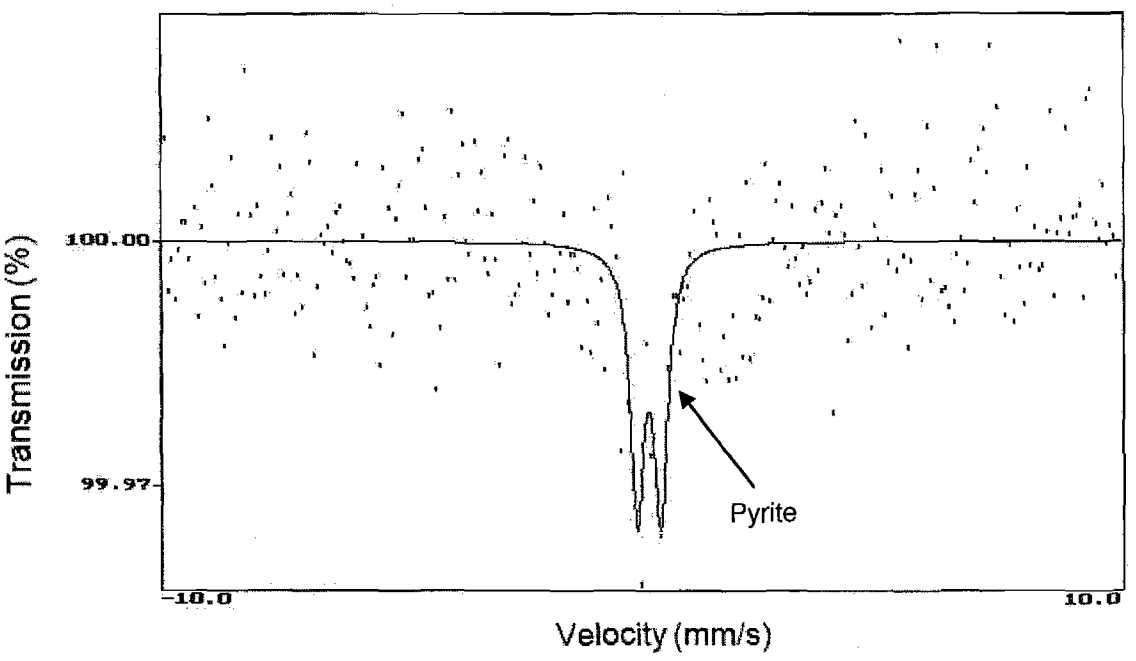


Figure 4.23: The Mössbauer spectrum of Sample B coal
(0 mass percentage Fe added)

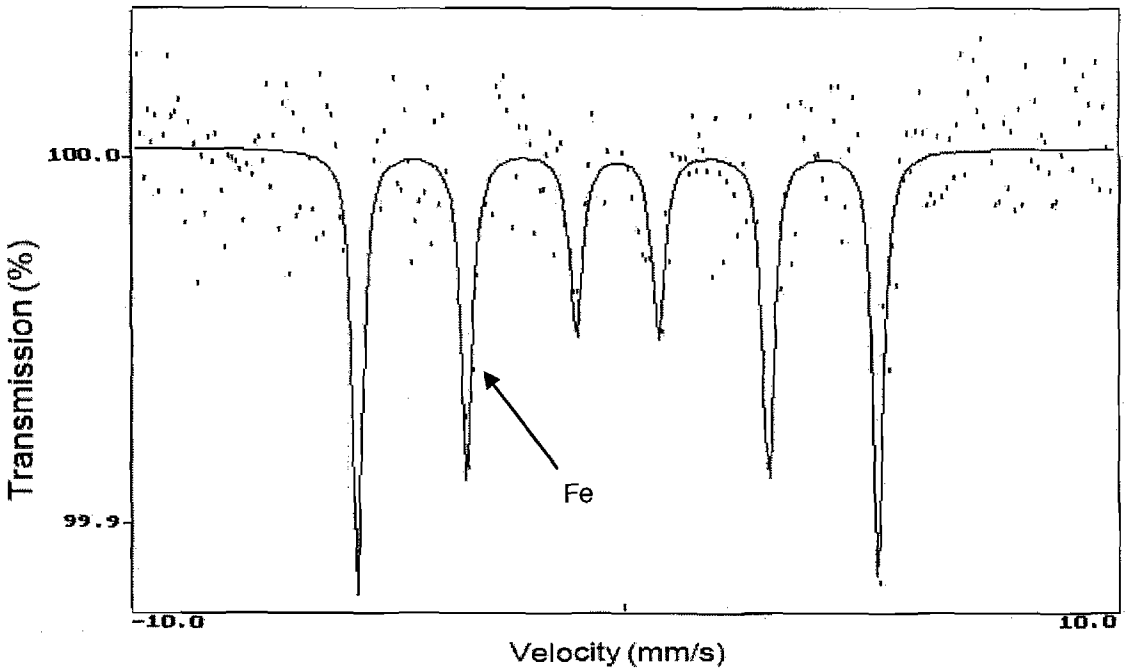


Figure 4.24: The Mössbauer spectrum of Sample B coal
(20 mass percentage Fe added)

Sample B, with no iron addition (original sample), also contains pyrite as the only iron-bearing mineral. In Figure 4.24, however, no pyrite is visible such as in Figure 4.20. This result illustrates the dominance of the iron added to the coal to such an extent that the original iron-mineral (pyrite) is not visible.

The Mössbauer spectra of the Sample B ash with 0 and 20 mass percentage iron added are shown in Figures 4.25 and 4.26, respectively. Figure 4.25 shows that the original ash sample also contains two main components: hematite and an iron-containing (Fe^{2+}, Fe^{3+}) glass, although the hematite is less prominent in Figure 4.25 as it is in Figure 4.21. In Figure 4.26 the hematite dominates the spectrum, as expected, due to the large amount of iron added. The spectrum in Figure 4.26 correlates well with Figure 4.22, illustrating that the result of iron addition to the coal leads to an increase in the amount of hematite in the coal.

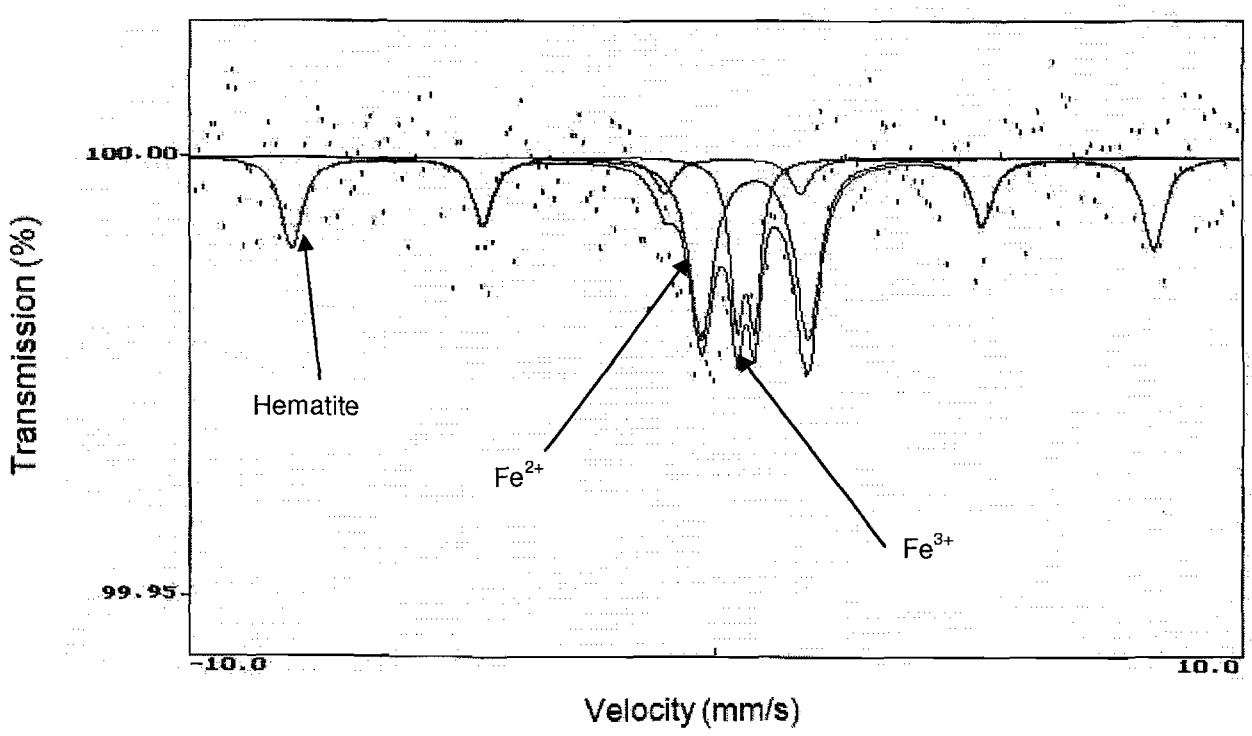


Figure 4.25: The Mössbauer spectrum of Sample B ash
(0 mass percentage Fe added)

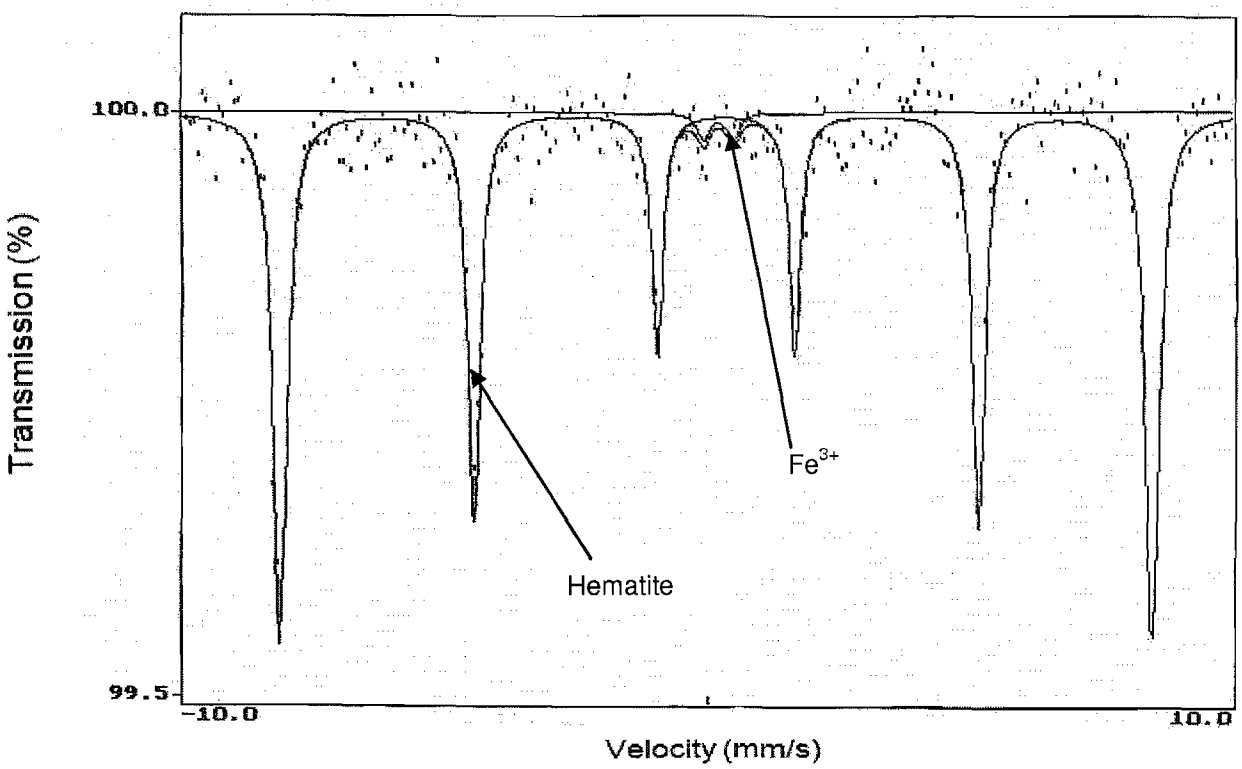


Figure 4.26: The Mössbauer spectrum of Sample B ash
(20 mass percentage Fe added)

4.4.3 Sample C

The Mössbauer spectra of Sample C with 0 and 20 mass percentage iron addition are shown in Figures 4.27 and 4.28, respectively.

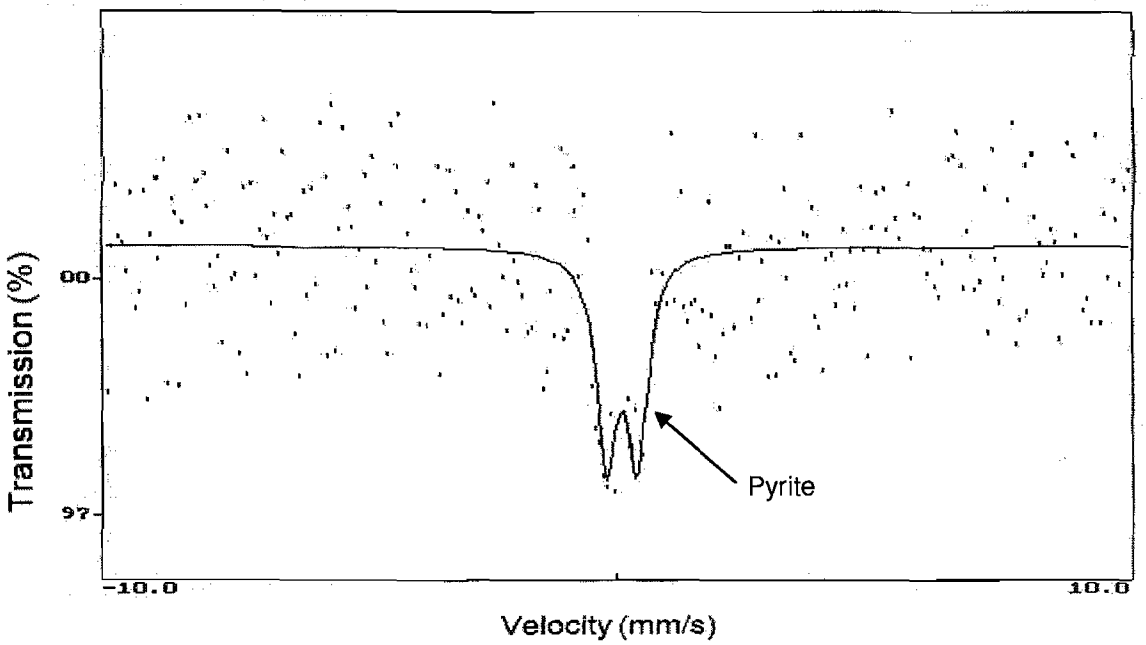


Figure 4.27: The Mössbauer spectrum of Sample C coal
(0 mass percentage Fe added)

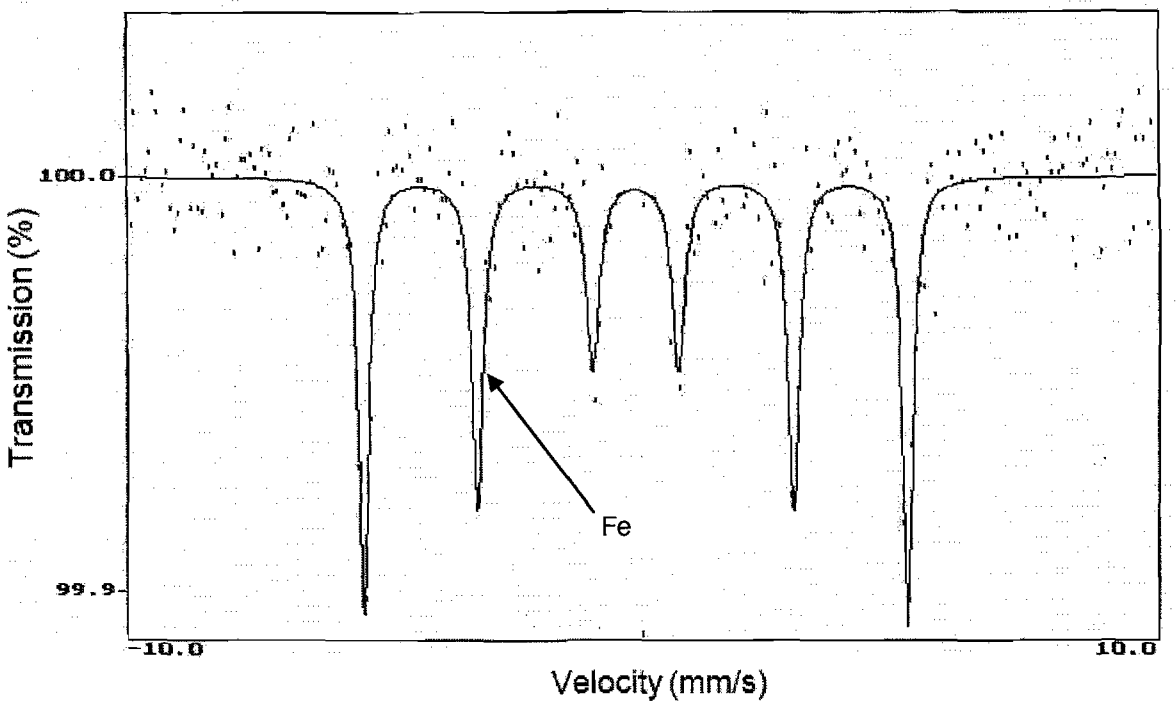


Figure 4.28: The Mössbauer spectrum of Sample C coal
(20 mass percentage Fe added)

The Mössbauer spectra of the ashed samples containing 0 and 20 mass percentage elemental iron are shown in Figures 4.29 and 4.30.

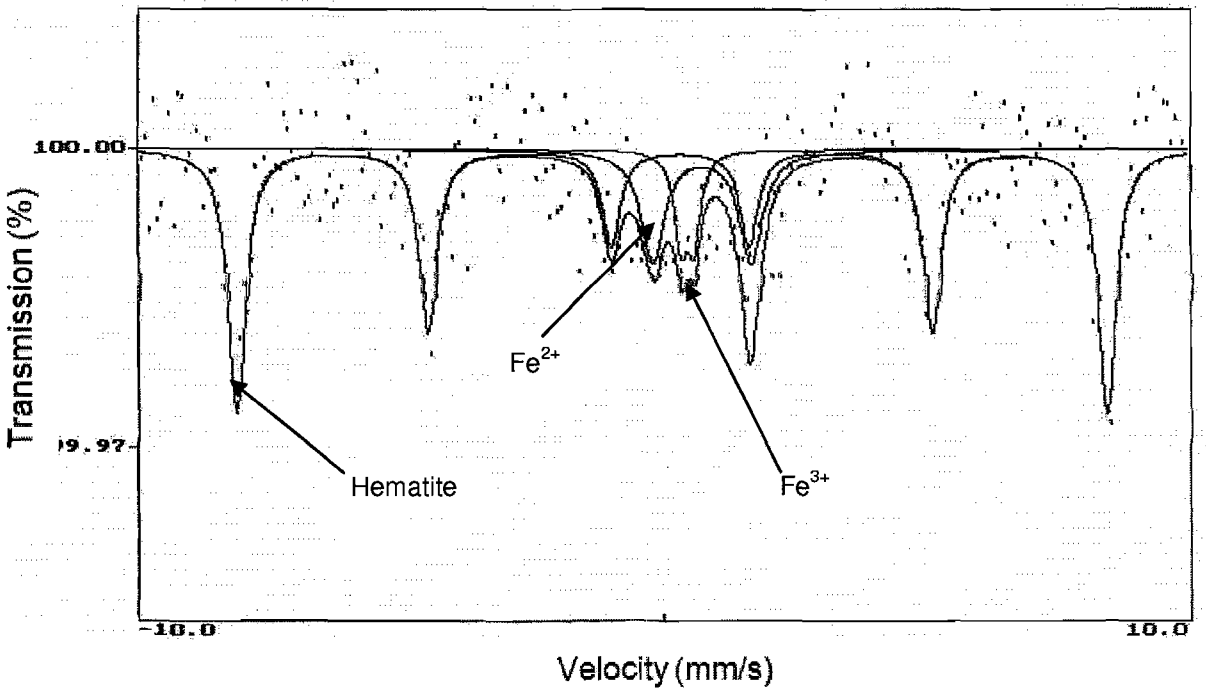


Figure 4.29: The Mössbauer spectrum of Sample C ash
(0 mass percentage Fe added)

Figure 4.27 again indicates the presence of pyrite as the only iron-containing mineral. This confirms the literature that states that pyrite is the main iron-containing mineral in South-African coal (Van Dyk, 2006). The spectrum in Figure 4.28 again illustrates the dominance of the added iron, as is also seen in Figure 4.24.

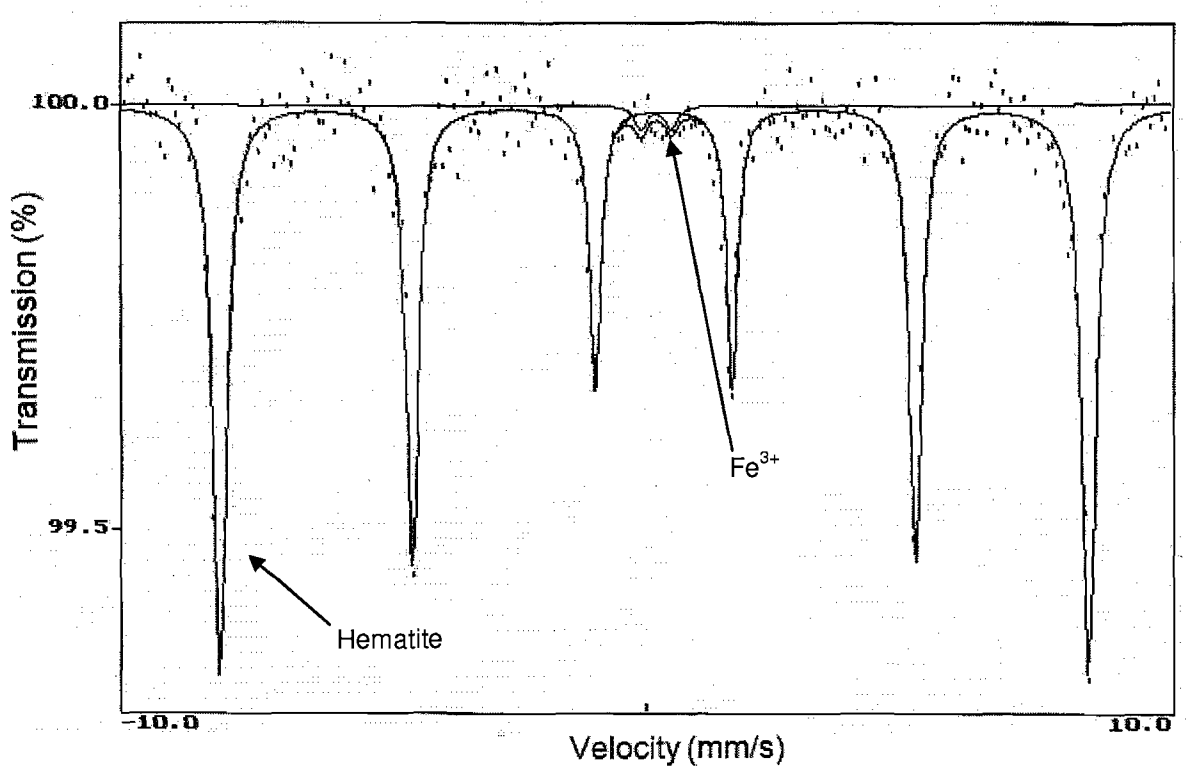


Figure 4.30: The Mössbauer spectrum of Sample C ash
(20 mass percentage Fe added)

The discussion in 4.4.1 and 4.4.2 also applies here, since the iron (Fe^{2+}, Fe^{3+}) glass and hematite were observed in the original coal sample with an increase in hematite, as the amount of iron added to the coal was increased. Thus it can be concluded that an increase in iron content will lead to an increase in the amount of hematite and, according to the discussion in 4.3.4, will make a significant contribution to a decrease in the AFT of the coal sources.

4.5 FactSage modelling

The FactSage simulation package was used mainly to verify the results obtained from the Mössbauer analysis with regard to the transformation of the iron-containing minerals (mainly pyrite), as well as the added elemental iron.

A phase diagram, Figure 4.31, was constructed with the simulation package, in order to establish the possible phases that might form if pyrite is subjected to combustion conditions.

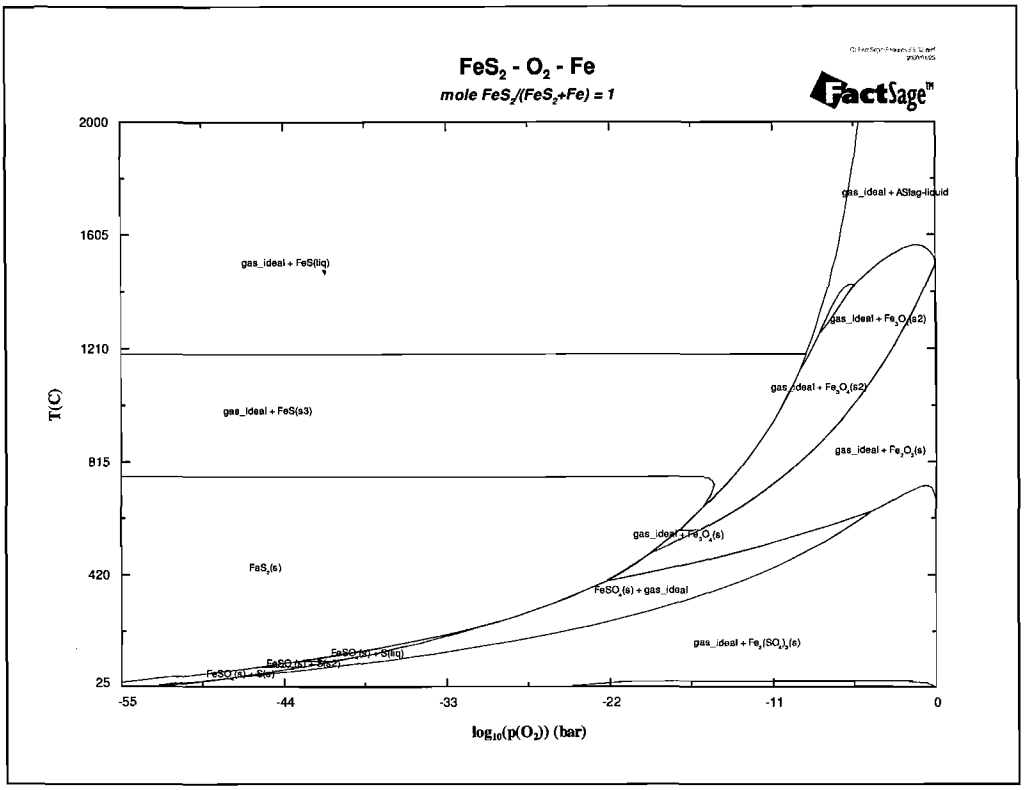


Figure 4.31: Phase diagram depicting possible phases as the result of pyrite subjected to combustion conditions

In Figure 4.31 it can be seen that the x-axis represents the partial pressure of the oxygen which is one of the reagents in a gasifier. It is evident from Figure 4.31 that the partial oxygen pressure plays an important role in the decomposition of the pyrite. By using the phase diagram, for example, it can be established that the partial oxygen pressure should be $\log_{10}(pO_2) \approx -22$ bar (10^{-22} bar) at 420°C to ensure that pyrite transforms to hematite. What this implies is that the pyrite in the coal transforms into hematite since the partial oxygen pressure in a commercial gasifier is significant larger than the value stated in the previous sentence.

In the case of a constant partial oxygen pressure, which would be more or less the case in gasifiers, it is observed that pyrite transforms into pyrrhotite at a temperature of more or less 300°C as shown in Figure 4.32. This phase stays stable up to a temperature of 1200°C from where it can lead to formation of a Fe-slag.

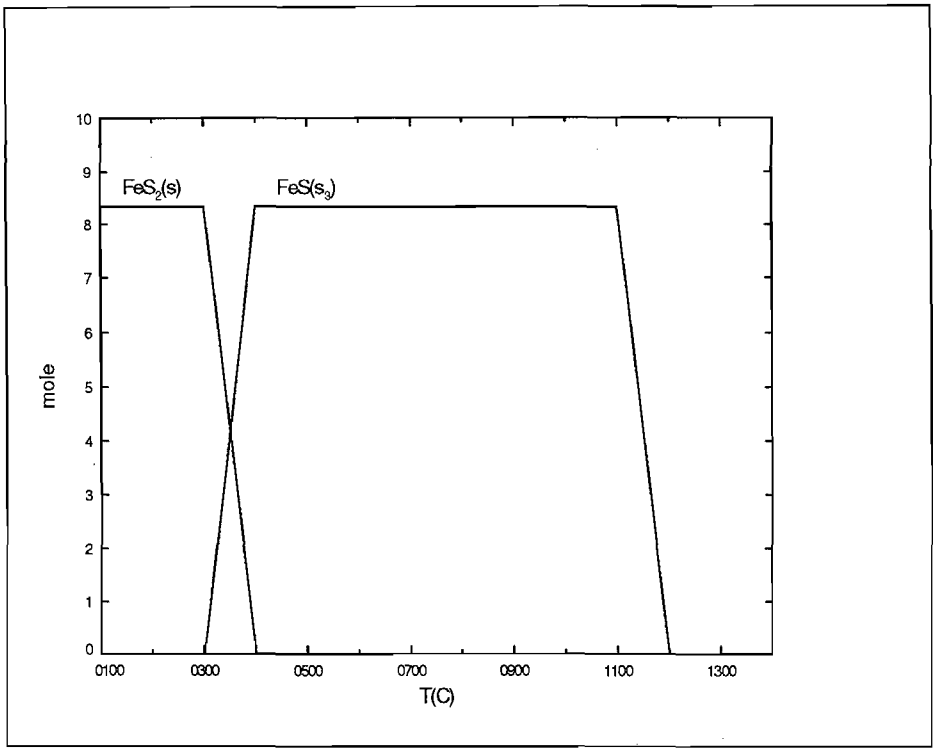


Figure 4.32: FactSage diagram illustrating the transformation of pyrite to pyrrhotite at a constant oxygen partial pressure

Since the pyrrhotite formation was not observed in the present investigation, a more oxidizing atmosphere has to be inferred. In the presence of more oxidizing combustion conditions, it is suggested that the transformation of pyrite to hematite occurs at around 600℃ (see Figure 4.32) which is higher than the literature values of 430℃ to 540℃ (Tomeczek & Palugniok, 2002; Van Dyk, 2006). The higher temperature result was expected, since the simulation was done with the pyrite alone and not as a mineral in the coal.

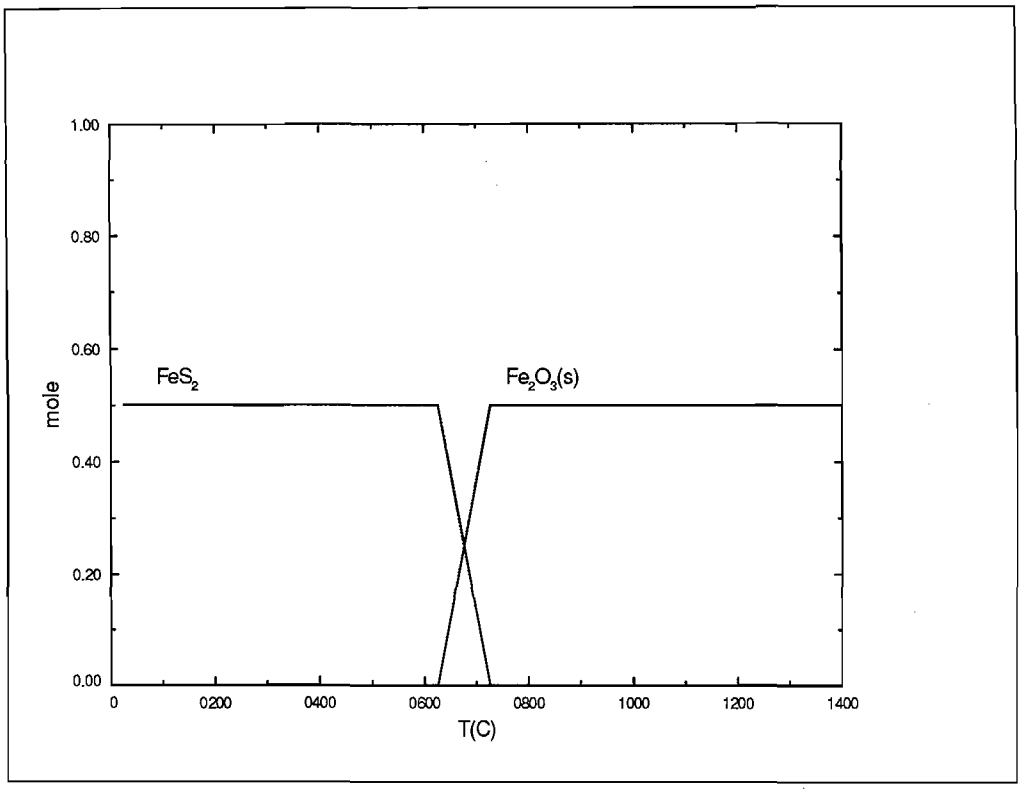


Figure 4.33: FactSage diagram illustrating the transformation of pyrite to hematite at a constant oxygen partial pressure

When elemental iron was incorporated into the simulation, several possible iron species could be produced by an increase in temperature (see Figure 4.31). However, the Mössbauer analysis clearly indicated that the elemental iron only transformed to hematite and, when added in larger quantities, only succeeded in masking the iron-containing glass.

A recent study conducted by Bunt *et al.* (2008) in which FactSage modelling was conducted, it was found that iron in the feed coal to a gasifier (in the form of solid pyrite) transformed at 225°C to pyrrhotite. The pyrrhotite phase continued to be stable up to a temperature of 525°C from where it transformed into iron meta-titanate and iron ortho-titanate. A small quantity of the iron meta-titanate transformed into iron cordierite at a temperature of 625°C. At a temperature of 725°C the stable iron-containing species present were iron cordierite, iron ortho-titanate and iron meta-titanate. The concentration of these three solid iron-containing species remained constant up to a temperature of 1025°C. A further increase in temperature resulted in a sharp decrease in the concentration of the solid iron-containing species, due to the melting of these species (Bunt *et al.*, 2008)

At a temperature of 1316°C all of iron in the gasifier is in the form of a liquid slag with trace quantities of gaseous Fe, $Fe(OH)_2$, $Fe(CO)_5$, FeS present, as well as a liquid FeS phase. This process is shown schematically in the FactSage diagram shown in Figure 4.34.

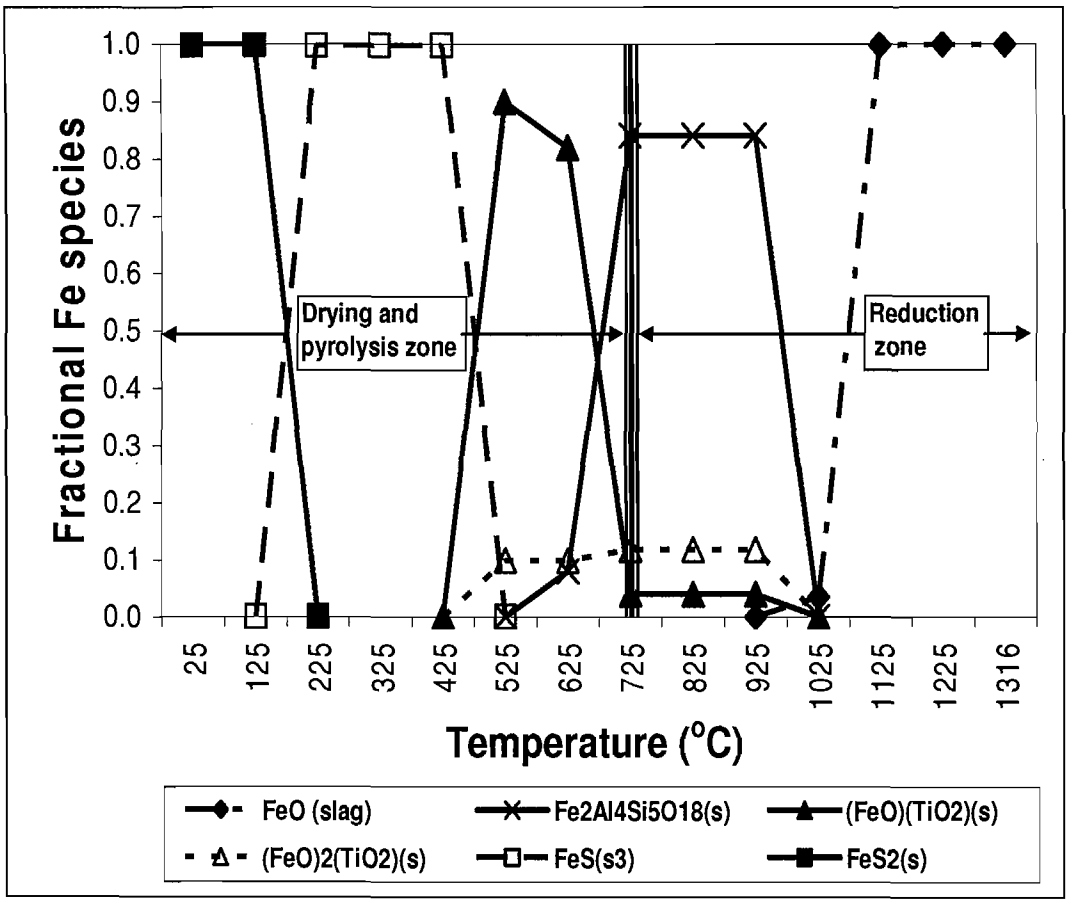


Figure 4.34: FacSage diagram depicting iron transformation during gasification (Bunt *et al.*, 2008)

In Section 4.3 it is mentioned that hematite could take on the characteristics of a network modifier which is responsible for the destabilization of the coal and the reduction of bond strength. After an evaluation of the Mössbauer and FactSage results it is clear that the transformation of the elemental iron to hematite is responsible for the reduction in the AFT of the coal sources. An increase in the amount of iron added leads to an increase in the amount of hematite that forms, which in turn results in more strain on the bond strengths. Thus, the lower AFT values obtained are the result of an increasing presence of iron.

CHAPTER 5 SUMMARY & CONCLUSIONS

At the beginning of this dissertation it is stated that the main motivation for this study originated from the desire to know the effect of iron addition on the characteristics of a coal source when subjected to a gasifying environment. Three coal sources were chosen in order to establish the effect of pure iron addition.

All three samples were taken from Sasol's operations at their South African plants. No pre-treatment of any kind was done on these samples. Various amounts of elemental iron were added to the finely crushed samples, so that the effect of the iron additions could be established, as well as to investigate whether an optimum amount of iron addition could be found. The amounts added were: 2, 5, 10, 15 and 20 mass percentage.

The proximate analysis, ultimate analysis and ash composition were carried out on all three the coal samples and it was found that they were within the range of values for Sasol coals.

The AFT analysis, Mössbauer spectroscopy and FactSage modelling were conducted on the original coal samples and those with the various amounts of iron added.

5.1 AFT analysis

The AFT analyses for all the samples were carried out in both an oxidizing and reducing atmosphere.

The AFT analyses on all of the samples indicated that the iron addition led to a 20% decrease in the AFT of the particular coal source. Results indicated that in the case of Sample B the reduction was slightly more in the reducing atmosphere. Samples A and C experienced a bigger decrease in AFT in an oxidizing environment. A slight increase in the AFT of Sample C was observed with 20 mass percentage iron addition. The results obtained from the AFT analysis suggest that the amphoteric group adopted the characteristics of the network modifier group.

This resulted in an increase in the strain experienced by the bonds, which ultimately led to the formation of slag at a lower temperature. It was noted, however, that there is virtually no further decrease observed with more than 10 mass percentage iron addition. Thus, should this project be implemented it is strongly recommended that 10 mass percentage iron addition should be considered as the limit.

5.2 Mössbauer spectroscopy

The parameters obtained from the Mössbauer spectroscopy experiments ((specific isomer shift (δ), quadrupole split (Δ) and/or hyperfine magnetic field (H)) were found to correspond well with values reported in the literature.

The Mössbauer spectra indicated that the only iron-bearing mineral present in all three of the original coal samples present was pyrite. In the case of Samples B and C an increase in the amount of iron resulted in the total overshadowing of the pyrite by the iron in the spectra and, thus, no pyrite could be observed with a large (20 mass percentage) iron addition. Sample A still showed pyrite with 20 mass percentage iron addition.

The three original ash samples showed two main components present, i.e. hematite and an iron (Fe^{2+}, Fe^{3+}) glass, both the result of pyrite transformation. When the spectra of all three samples with 20 mass percentage iron added were studied, it became evident that the glass component was still present but in a far lesser quantity and the hematite was dominant in the spectra. The dominance of the hematite in the spectra was mainly due to the transformation of the pure iron with a smaller contribution from the pyrite.

This increase in hematite with an increase in iron confirms the theory that an increase in hematite in the coal will lead to slagging at lower temperatures.

5.3 FactSage modelling

Initial simulations with the aid of this package were carried out and they indicated that the partial oxygen pressure played a significant role in the transformation of pyrite in particular. The simulation showed that with the addition of iron to the coal samples there was a whole range of possible iron species that might form.

Thus, when reviewing all of the results obtained from the various experiments it can be concluded that the addition of iron to a coal source will definitely lower the AFT of that coal. This implies that the hypothesis, stating that the addition of iron will lead to a decrease in AFT as well enhance slag formation, was proved correct by the experimental results. The hypothesis confirmation thus complements existing literature regarding the use of iron as possible fluxing agent during gasification.

The results of this study indicate that it is not desirable to add iron to the coal sources entering gasifiers, since the lowering of the AFT leads to operating problems.

REFERENCES

ALPERN, B., NAHUYS, J. MARTINEZ, L. 1983. *Mineral matter in ashy and non-washable coals – Its influence on chemical properties. (In* **Comunicaçoes dos Serviços Geológicos de Portugal.** Symposium on Gondwana coals: Papers read at the symposium held in Lisbon 1983. Lisbon. p. 299-317)

ASTM D1857. 2004. Standard Test Method For Fusibility of Coal and Coke Ash. ASTM International, West Conshohocken, PA, www.astm.org.

ASTM D3682. 2001. Standard Test Method for Major and Minor Elements in Combustion Residues from Coal Utilization Processes. ASTM International, West Conshohocken, PA, www.astm.org.

ASTM D4239. 2005. Standard Test Methods for Sulfur in the Analysis Sample of Coal and Coke Using High-Temperature Tube Furnace Combustion Method with Infrared Absorption. ASTM International, West Conshohocken, PA, www.astm.org.

ASTM D5373. 2002. Standard Test Methods for Instrumental Determination of Carbon, Hydrogen and Nitrogen in Laboratory Samples of Coal and Coke. ASTM International, West Conshohocken, PA, www.astm.org.

BALE, C.W., CHARTRAND, P., DEGTEROV, S.A., ERIKSSON, G., HACK, K., MAHFOUD, R.B., MELANCON, J., PELTON, A.D. & PETERSON, S. 2002. FactSage thermodynamical software and databases. *Calphad,* 26(2):189-228.

BENSON, S.A. 1987. Laboratory studies of ash deposit formation during the combustion of western U.S. coals. Pennsylvania State University. (D.Phil dissertation). 243 p.

BUNT, J.R. 2006. A new dissection methodology and investigation into coal property transformational behaviour impacting on a commercial – scale Sasol – Lurgi MK IV Fixed – bed gasifier. Potchefstroom(NWU). (Ph.D. thesis) 167p.

BUNT, J.R., WAANDERS, F.B. & SCHOBERT, H. 2008. The behaviour of some selected major elements in the Sasol-Lurgi MK IV FBDB gasifier. Article submitted to *Fuel.*

COHEN, R.L. 1976. Applications of Mössbauer spectroscopy. New York: Academic Press. 349p. (Applications of Mössbauer spectroscopy, vol.1.)

COLLOT, A.G. 2002. Matching gasifiers to coal. IEA Clean Coal Centre, CCC/65. 100p.

CRNOMARKOVIC, N., REPIC, B., MLADENOVIC, R., NESKOVIC, O. & VELJKOVIC, M. 2007. Experimental investigation of role of steam in entrained flow gasification. *Fuel*, 86(2007):194-202.

DICKSON, D.P.E. & BERRY, F.J. (*eds.*). 1986. Mössbauer spectroscopy. Cambridge: Press Syndicate of the University of Cambridge. 274p.

EPRI (Electric Power Research Institute). 1980. Electric Utility Use of Fireside Additives. EPRI Final Report, CS – 1318, Project 1035 -1, p. III4.3 – III4.5

FACTSAGE. 2008. Factsage 5.5. [Web:] www.factsage.com [Date of access: 12-15 Jan 2008].

FALCON, R.M.S. & SNYMAN, C.P. 1986. An introduction to Coal Petrography: Atlas of petrographic constituents of the bituminous coals of Southern Africa. 1st ed. Johannesburg: The Geological Society of South Africa. 27p

FALCON, L.M. & FALCON, R.M.S. 1987. The petrographic composition of Southern African coals in relation to friability, hardness and abrasive indices. *Journal of the South African Institute of Mining and Metallurgy,* 87(10):323-326.

FALCON, R. & HAM, A.J. 1988. The characteristics of Southern African coals. *Journal of the South African institute of mining and metallurgy,* 88(5):145-161.

GIBB, W.H. 1996. The UK collaborative research programme on slagging pulverised coal – fired boilers: Summary of findings. *Applications of Advanced Technology to Ash – Related Problems in Boilers.* Kluwer Academic Pub. p. 41 -65

GOVENDER, A. 2005. Determination and statistical evaluation of the effect of minerals and mineral associations in specific dense medium fractions on ash fusion temperature. Potchefstroom:NWU (Dissertation - MSc) 83p.

GUO, X., DAI, Z., GONG, X., CHEN, X., LIU, H., WANG, F. & YU, Z. 2007. Performance of an entrained – flow gasification technology of pulverized coal in pilot scale plant. *Fuel Processing Technology,* 88(2007): 451-459.

HACK, K. 2005. FactSage-Teach: A selftuition Package on Computational Thermochemistry. Herzogenrath: GTT-Technologies.

HUGGINS, F.E., KOSMACK, D.A. & HUFFMAN, G.P. 1981. Correlation between ash-fusion temperatures and ternary equilibrium phase diagrams. *Fuel,* 60:577-587, Jul.

HUGGINS, F.E. 2002. Overview of analytical methods for inorganic constituents in coal. *International journal of Coal Geology,* 50:169-214.

ISO 562. 1998. Hard coal and coke – Determination of volatile matter. International Organisation for Standardisation – ISO, Geneva, P.A., www.iso.org.

ISO 1171. 1997.Solid mineral – Determination of ash. International Organisation for Standardisation – ISO, Geneva, P.A., www.iso.org

JAK, E. 2002. Prediction of coal ash fusion temperatures with the F*A*C*T thermodynamic computer package. *Fuel,* 81(13):1655-1668.

KALMANOVITCH, D.P. & FRANK, M. 1988. An effective model of viscosity for ash deposition phenomena. (*In* Bryers, R.W. & Vorres, K.S., *eds.* Mineral matter and ash deposition from coal: 1988 Conference organised by Engineering Foundation Conferences, Santa Barbara, California. p. 89-101.)

KAMER, F.R., ZYGARLICKE, C.J. & BREKKE, D.W. 1994. New analysis techniques help control boiler fouling. *Power Engineering,* 35-38, March.

KONDRATIEV, A. & JAK, E. 2001. Predicting coal ash slag flow characteristics (viscosity model for the Al_2O_3 – CaO – FeO – SiO_2 system). *Fuel,* 80(2001):1989-2000.

KRISTIANSEN, A. 1996. Understanding coal gasification. London: IEA Coal Research. 69p.

LOUGHNAN, F.C. 1978. Flint, Clays, Tonsteins and the Kaolinite Clay Rock Facies. *Clay Minerals*, 13(1978):387-400.

MACHIN, J.S. & HANNA, D.L. 1945. Viscosity studies of system CaO-MgO-Al_2O_3-SiO_2: I, 40% SiO_2. *Journal of the American Ceramic Society*, 28(11):310-316.

MACHIN, J.S., YEE, T.B. & HANNA, D.L. 1952. Viscosity studies of system CaO-MgO-Al_2O_3-SiO_2: III, 35, 45 and 50% SiO_2. *Journal of the American Ceramic Society,* 35(12):322-325.

MAGASINER, L.B., VAN ALPHEN, C., INKSON, M.B. & MISPLON, B.J. 2001. Characterising fuels for biomass – Coal fired cogeneration. *Proceedings of 75th Annual Congress of the S.A. Sugar Technologists Association, South Africa.*

MAYORAL, M.C., IZQUIERDO, M.T., ANDRÉS, J.M. & RUBIO, B. 2001. Different approaches to proximate analysis by thermogravimetry analysis. *Thermochimica Acta,* 370(2001):91-97.

MAYORAL, M.C., IZQUIERDO, M.T., ANDRÉS, J.M. & RUBIO, B. 2002. Mechanism of interaction of pyrite with hematite as simulation of slagging and fireside tube wastage in coal combustion. *Thermochimica Acta,* 390(2002):103-111.

MCCAMMON, C.A. 2000. Insight into phase transformations from Mössbauer spectroscopy. (*In* Redfern, S.A.T. & Carpenter, M.A. *eds.* Transformation processes in minerals. Washington DC: Mineralogical Society of America. 361p.) (Reviews in mineralogy and geochemistry, vol.39.)

MCMURRY, J. 2000. Organic Chemistry. 5th ed. California: Brooks/Cole. 1284p.

MURAD, E. & CASHION, J. 2004. Mössbauer spectroscopy of environmental materials and their industrial utilization. Massachusetts: Kluwer Academic Publishers. 417p.

NATIONAL ENERGY TECHNOLOGY LABORATORY. 2008. Gasification: Reference shelf – Images and photos. [Web:] http://www.netl.doe.gov/technologies/coalpower/gasification/pubs/photo.html [Date of access: 15 Aug. 2008].

NEAVEL, R.C. 1981. Coal structure and coal science: overview and recommendations. *Coal structure ACS,* p. 1-13.

NINOMIYA, Y. & SATO, A. 1997. Ash melting behaviour under coal gasification conditions. *Energy and conversion management,* 38(10-13):1405-1412.

NOWACKI, P. 1981. Coal gasification processes. *Energy Technology review,* No. 70.

PATTERSON, J.H. & HURST, H.J. 2000. Ash and slag qualities of Australian bituminous coals for use in slagging gasifiers. *Fuel,* 79(2000):1671-1678.

RAM, L.C., TRIPATHI, P.S.M. & MISHRA, S.P. 1995. Mössbauer spectroscopic studies on the transformations of iron – bearing minerals during combustion of coals: Correlation with fouling and slagging. *Fuel Processing Technology,* 42(1995):47-60.

PROBSTEIN, R.F. & HICKS, R.E. 2006. Synthetic Fuels. New York: Dover Publications, Inc. 490p.

REIFENSTEIN, A.P., KAHRAMAN, H., COIN, C.D.A., CALOS, N.J., MILLER, G. & UWINS, P. 1999. Behaviour of selected minerals in an improved ash fusion test: quartz, potassium feldspar, sodium feldspar, kaolinite, illite, calcite, dolomite, siderite, pyrite and apatite. *Fuel,* 78(1999):1449-1461.

RENTON, J.J., 1982, Mineral matter in coal, *in* R.A. Meyers, ed., Coal structure: New York, Academic Press, p. 283-326.

SABS (The South African Bureau of Standards). 1996. Solid mineral fuels – Determination of fusibility of ash – High-temperature tube method. *ISO540:1995(E),* p. 1-5.

SCHILING, H.D., BONN, B. & KRAUSS, U. 1979. Coal gasification – existing processes and new developments.

SEGGIANI, M. 1999. Empirical correlations of the ash fusion temperatures and temperature of critical viscosity for coal and biomass ashes. *Fuel,* 78(1999):1121-1125.

SKOOG, D.A., HOLLER, F.J. & NIEMAN, T.A. 1998. Principles of instrumental analysis. 5th ed. Harcourt Brace & Company. 850p.

SLAGHUIS, J.H. 1993. Coal Gasification: A study guide for the national diploma in coal technology. Coal Processing III, Part A, 81p.

SLEIGER, W.A., SINGLETARY, J.H. & KOHUT, J.F. 1988. Application of a microcomputer to the determination of coal ash fusibility characteristics. *Journal of Coal Quality,* 7(2):48-54, Apr – Jun.

STACH, E., MACKOWSKY, M.-TH., TEICHMULLER, M., TAYLOR, G.H., CHANDRA, D. & TEICHMULLER, R. 1982. Stach's Textbook of Coal Petrology. 3rd ed. Berlin, Stuttgart: Gebrüder Borntraeger. 535 p.

STEVENS, J. G., KHASANOV, A. M., MILLER, J. W., POLLAK, H. & LI,Z. (eds). 1998. Mössbauer Mineral Handbook, Mössbauer Effect Data Centre, University of North Carolina, Asheville, USA. 527 p.

TIEDT, L.R. & PRETORIUS, W.E. 2006. An introduction to electron microscopy and x-ray microanalysis – NWU information pamphlet.

TOMECZEK, J. & PALUGNIOK, H. 2002. Kinetics of mineral matter transformation during coal combustion. *Fuel,* 81(2002):1251-1258.

VAN DYK, J.C., BAXTER, L.L., VAN HEERDEN, J.H.P. & COETZER, R.L.J. 2005. Chemical fractionation tests on South African coal sources to obtain species - specific information on ash fusion temperatures (AFT). *Fuel,* 84 (2005):1768-1777.

VAN DYK, J.C. 2006. Manipulation of gasification coal feed in order to increase the ash fusion temperature of the coal to operate the gasifiers at higher temperatures. Potchefstroom:NWU. (Ph.D. thesis). 147p.

VAN DYK, J.C., MELZER, S. & SOBIECKI, A. 2006. Mineral matter transformation during Sasol – Lurgi fixed bed dry bottom gasification – utilization of HT – XRD and FactSage modelling. *Minerals Engineering,* 19(2006):1126-1135.

VAN DYK, J.C. & WAANDERS, F.B. 2006. Manipulation of gasification coal feed in order to increase the ash fusion temperature of the coal enabling the gasifiers to operate at higher temperatures. *Fuel,* 86(2007):2728-2735.

VASSILEV, S.V., KITANO, K., TAKEDA, S. & TSURUE, T. 1995. Influence of mineral and chemical composition of coal ashes and their fusibility. *Fuel Processing Technology,* 45(1995):27-51.

VASSILEVA, C.G. & VASSILEV, S.V. 1996. General observations on the phase – mineral transformations in inorganic matter of some Bulgarian coals during heating. *Comptes rendus de l'Academie bulgare des Sciences,* 55(7):47-50.

WAANDERS, F.B. & BUNT, J.R. 2007. Transformation of the Fe-mineral associations in coal during gasification. Hyperfine Interactions (2006) 171: 287-292, Feb.

WALL, T.F., CREELMAN, R.A., GUPTA, R.P., GUPTA, S., COIN, C. & LOWE, A. 1996. Coal ash fusion temperatures – New characterisation techniques, and associations with phase equilibria. *Applications of Advanced Technology to Ash – Related Problems in Boilers.* Kluwer Academic Pub. p. 541-556

WARD, C.R. 2002. Analysis and significance of mineral matter in coal seems. *International Journal of Coal Geology,* 50(2002): 135-168.

YONG, K.H. 2007. Method of gasification in IGCC systems. *International Journal of Hydrogen energy,*32(2007): 5088-5093.

ZEVENHOVEN – ONDERWATER, M., BACKMAN, R., SKRIFVARS, B.J. & HUPA, M. 2001. The ash chemistry in fluidised bed gasification of biomass fuels. Part I: predicting the chemistry of melting ashes and ash – bed material interaction. *Fuel,* 80(10):1489-1502.

APPENDIX – EXPERIMENTAL RESULTS

A.1 Ash and coal composition

Table A.1: Composition of the coal in percentage elements present

Sample	O	Na	Mg	Al	Si	P	S	K	Ca	Ti	Fe	Total
Sample A original	48.77	0.59	0.74	16.27	24.51	-	1.90	0.88	3.43	1.21	1.71	100
Sample A 2% iron	48.54	0.48	0.79	15.86	24.42	-	1.88	1.19	3.54	1.35	1.97	100
Sample A 5% iron	48.58	0.62	0.65	16.52	24.00	-	1.85	0.83	3.39	1.55	2.03	100
Sample A 10% iron	48.18	0.37	0.62	16.22	23.64	-	1.97	1.28	3.97	1.10	2.65	100
Sample A 15% iron	47.77	0.56	0.58	15.66	23.07	-	2.29	1.35	3.44	1.04	4.25	100
Sample A 20% iron	46.37	0.30	0.67	14.89	22.04	-	1.84	0.91	2.98	1.22	8.77	100
Sample B Original	48.14	0.61	0.84	14.02	24.42	0.27	1.97	0.90	5.13	1.28	2.42	100
Sample B 2% iron	46.56	0.62	1.03	12.88	22.69	0.25	2.12	0.71	5.13	0.98	5.03	100
Sample B 5% iron	46.17	0.61	0.79	14.03	22.17	0.36	1.63	0.84	4.16	0.84	8.41	100
Sample B 10% iron	44.72	0.68	0.82	12.60	21.04	0.34	1.47	0.92	4.5	1.15	11.75	100
Sample B 15% iron	42.69	0.50	0.85	11.70	18.37	0.35	1.78	0.67	3.65	0.88	18.35	100
Sample B 20% iron	46.07	0.37	1.10	13.01	21.71	0.31	1.97	0.60	5.77	1.38	21.71	100
Sample C original	48.64	0.50	0.85	15.05	24.56	0.40	1.93	1.29	4.53	1.08	1.16	100
Sample C 2% iron	48.24	0.70	0.80	14.18	23.98	0.63	2.09	0.88	4.77	1.16	2.58	100
Sample C 5% iron	47.07	0.62	1.02	13.82	22.15	0.58	2.19	0.77	5.53	1.25	5.00	100
Sample C 10% iron	44.74	0.42	0.58	12.67	20.20	0.62	1.87	0.82	4.80	1.15	12.14	100
Sample C 15% iron	43.62	0.69	0.92	12.38	19.77	-	1.64	0.56	4.20	0.91	15.30	100
Sample C 20% iron	41.73	0.36	1.14	11.32	17.00	0.53	1.27	0.48	3.57	0.95	22.01	100

Table A.2: Composition of the coal ash in percentage elements present

Sample	O	Na	Mg	Al	Si	P	S	K	Ca	Ti	Cr	Ni	Fe	Total
Sample A original	47.95	0.72	0.71	17.48	22.92	0.27	1.23	1.01	4.53	1.19	-	-	1.05	100
Sample A 2% iron	47.56	0.64	0.78	17.22	22.88	0.30	0.80	0.82	4.77	1.48	-	-	1.74	100
Sample A 5% iron	47.22	0.75	0.94	16.51	22.03	0.31	1.28	0.90	5.79	1.39	-	-	2.88	100
Sample A 10% iron	47.15	0.72	0.86	16.89	22.68	0.33	1.22	0.89	4.05	1.29	-	-	5.35	100
Sample A 15% iron	47.05	0.72	0.83	16.75	22.00	0.34	1.06	1.18	4.86	1.55	-	-	7.67	100
Sample A 20% iron	46.91	0.82	0.69	16.98	23.05	0.19	0.94	1.43	3.37	1.09	-	-	9.13	100
Sample B Original	47.86	0.90	1.04	15.65	23.45	0.32	1.39	1.15	5.16	1.45	-	-	1.63	100
Sample B 2% iron	47.16	0.62	1.34	15.60	22.93	0.42	0.68	0.92	7.09	1.46	-	-	1.78	100
Sample B 5% iron	46.85	0.75	1.07	15.28	22.11	0.38	1.24	0.92	6.31	1.55	-	-	3.53	100
Sample B 10% iron	46.79	0.77	1.01	14.91	22.48	0.33	1.25	0.84	5.52	1.48	-	-	4.63	100
Sample B 15% iron	45.44	0.78	0.98	14.57	20.84	0.38	1.08	0.92	5.37	1.62	-	-	8.03	100
Sample B 20% iron	45.24	0.73	1.10	15.62	22.97	0.30	1.04	1.05	5.63	1.48	-	-	9.84	100
Sample C original	48.18	0.70	1.06	16.39	23.53	0.44	1.15	0.85	5.01	1.60	-	-	1.09	100
Sample C 2% iron	47.36	0.68	1.06	15.66	22.48	0.35	1.51	0.68	5.28	1.35	-	-	1.59	100
Sample C 5% iron	47.34	0.66	1.17	15.23	22.80	0.36	1.33	0.78	5.80	1.53	-	-	3.00	100
Sample C 10% iron	47.03	0.76	1.10	15.85	22.96	0.56	1.38	0.84	4.88	2.20	-	-	5.44	100
Sample C 15% iron	46.30	0.68	0.97	15.37	21.03	0.46	1.39	0.93	5.00	1.79	-	-	6.08	100
Sample C 20% iron	45.25	0.76	1.21	14.50	20.60	0.25	1.70	0.87	5.64	1.44	-	-	7.78	100

The percentage iron indicated in Tables A.1 and A.2 present within the sample indicates the iron content on a mass percentage basis.

A.2 AFT analysis on iron – added samples

The elemental iron was added to the three different coal samples in the following quantities: 2, 5, 10, 15 and 20 mass percentage.

A total of 15 sub-samples were thus obtained. Each one of these sub-samples was then subjected to AFT analysis under oxidizing and reducing conditions. The results of these analyses are given in Tables A.3–A.12.

Table A.3: Result of AFT analysis conducted on sample with 2 mass percentage iron added under oxidizing conditions

Sample	IDT (°C)	HT (°C)	ST (°C)	FT (°C)
Sample A	1220	1240	1260	1290
Sample B	1220	1230	1250	1260
Sample C	1230	1240	1260	1280

Table A.4: Result of AFT analysis conducted on sample with 5 mass percentage iron added under oxidizing conditions

Sample	IDT (°C)	HT (°C)	ST (°C)	FT (°C)
Sample A	1140	1170	1200	1240
Sample B	1150	1170	1200	1250
Sample C	1170	1180	1190	1240

Table A.5: Result of AFT analysis conducted on sample with 10 mass percentage iron added under oxidizing conditions

Sample	IDT (°C)	HT (°C)	ST (°C)	FT (°C)
Sample A	1120	1130	1140	1190
Sample B	1120	1130	1140	1150
Sample C	1110	1120	1130	1140

Table A.6: Result of AFT analysis conducted on sample with 15 mass percentage iron added under oxidizing conditions

Sample	IDT (°C)	HT (°C)	ST (°C)	FT (°C)
Sample A	1120	1130	1140	1190
Sample B	1110	1130	1140	1150
Sample C	1100	1110	1120	1130

Table A.7: Result of AFT analysis conducted on sample with 20 mass percentage iron added under oxidizing conditions

Sample	IDT (°C)	HT (°C)	ST (°C)	FT (°C)
Sample A	1110	1120	1130	1150
Sample B	1100	1110	1120	1130
Sample C	1110	1120	1130	1140

Table A.8: Result of AFT analysis conducted on sample with 2 mass percentage iron added under reducing conditions

Sample	IDT (°C)	HT (°C)	ST (°C)	FT (°C)
Sample A	1200	1220	1240	1250
Sample B	1210	1220	1240	1260
Sample C	1220	1230	1250	1270

Table A.9: Result of AFT analysis conducted on sample with 5 mass percentage iron added under reducing conditions

Sample	IDT (℃)	HT (℃)	ST (℃)	FT (℃)
Sample A	1130	1160	1190	1240
Sample B	1140	1160	1190	1240
Sample C	1160	1170	1180	1230

Table A.10: Result of AFT analysis conducted on sample with 10 mass percentage iron added under reducing conditions

Sample	IDT (℃)	HT (℃)	ST (℃)	FT (℃)
Sample A	1110	1120	1130	1150
Sample B	1110	1120	1130	1140
Sample C	1100	1110	1120	1130

Table A.11: Result of AFT analysis conducted on sample with 15 mass percentage iron added under reducing conditions

Sample	IDT (℃)	HT (℃)	ST (℃)	FT (℃)
Sample A	1110	1120	1130	1150
Sample B	1100	1110	1120	1140
Sample C	1090	1100	1110	1120

Table A.12: Result of AFT analysis conducted on sample with 20 mass percentage iron added under reducing conditions

Sample	IDT (℃)	HT (℃)	ST (℃)	FT (℃)
Sample A	1100	1110	1120	1140
Sample B	1090	1100	1110	1120
Sample C	1100	1110	1120	1130

A.2 Mössbauer spectroscopy

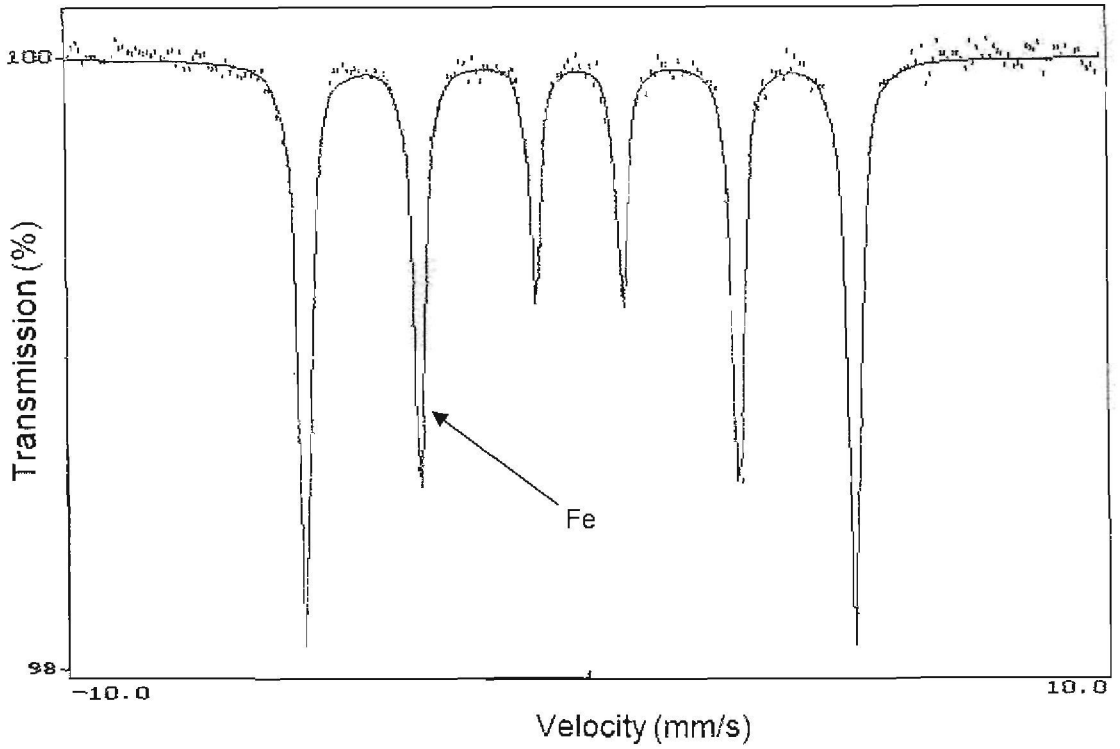


Figure A.1: The Mössbauer spectrum for the calibration sample
(100 mass percentage Fe)

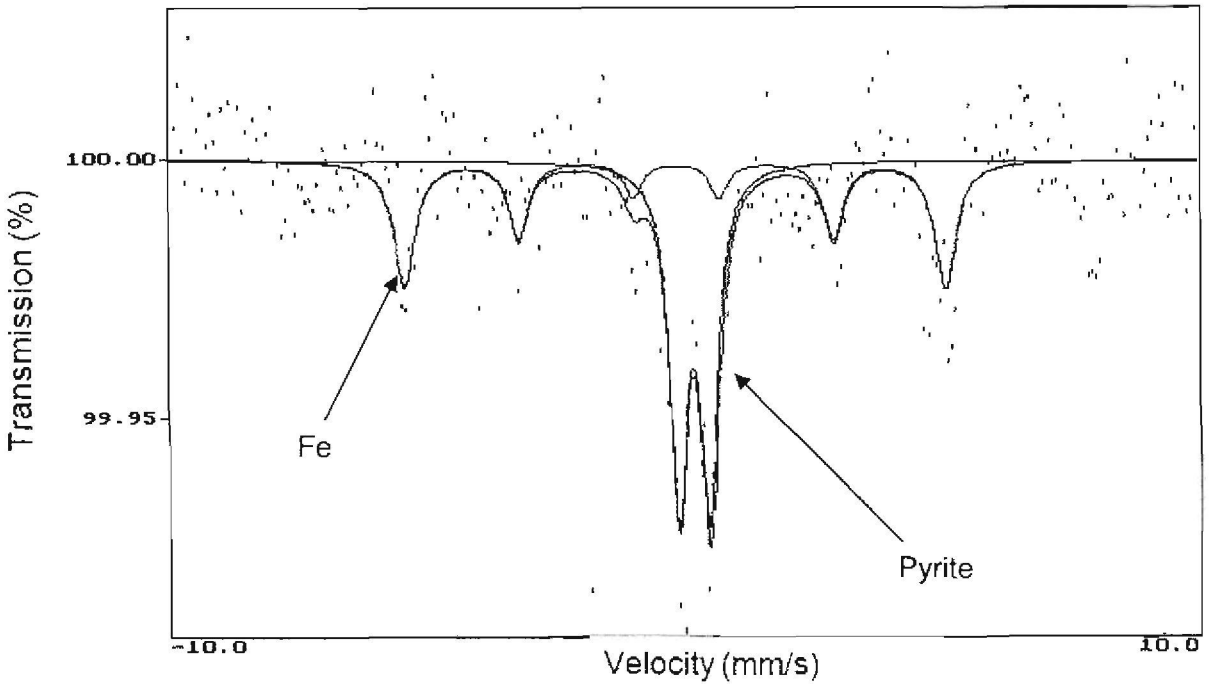


Figure A.2: The Mössbauer spectrum for Sample A coal
(2 mass percentage Fe added)

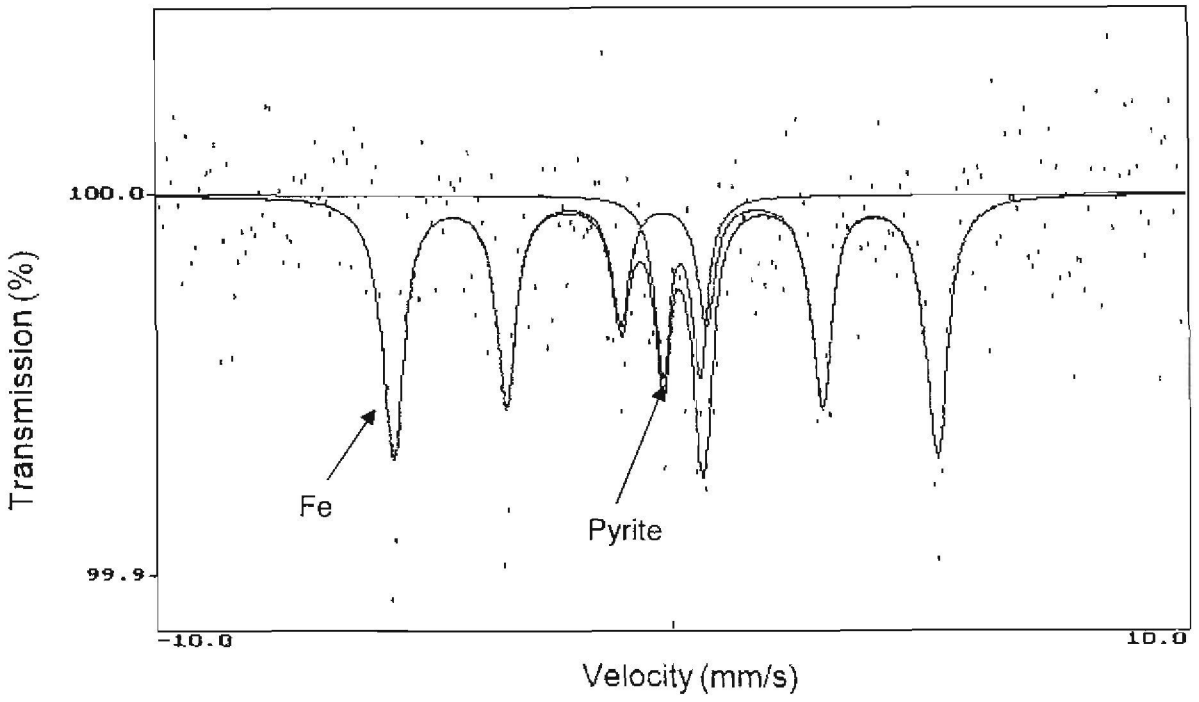


Figure A.3: The Mössbauer spectrum for Sample A coal
(5 mass percentage Fe added)

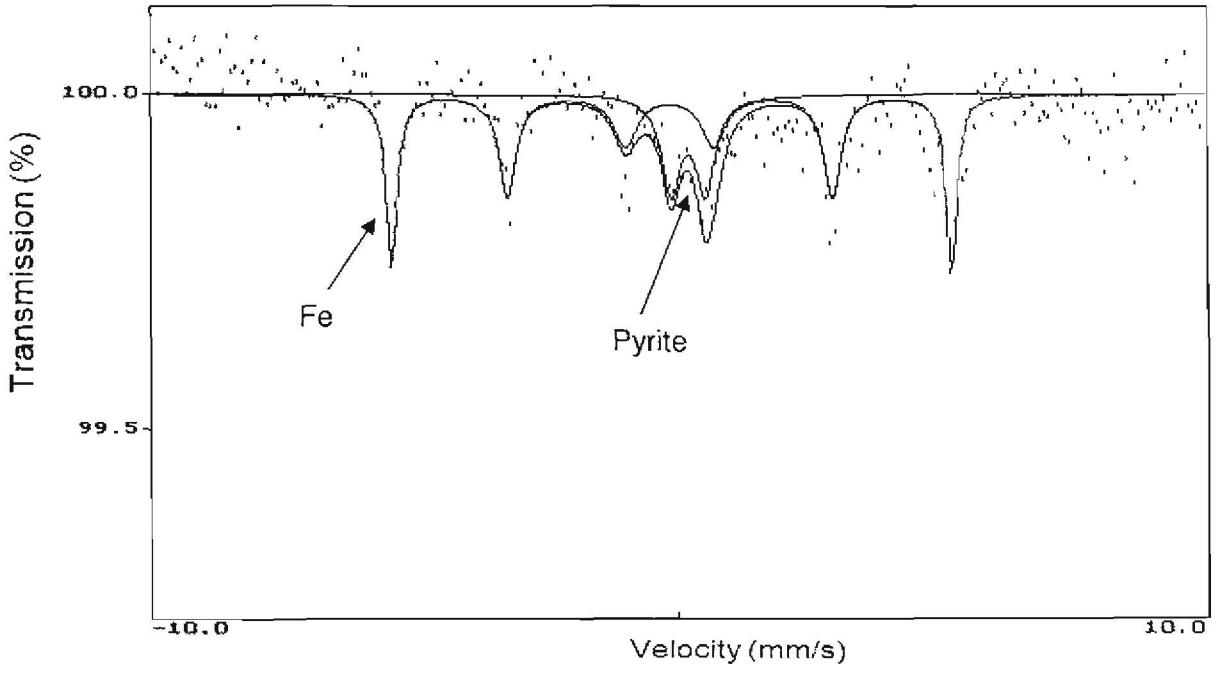


Figure A.4: The Mössbauer spectrum for Sample A coal
(10 mass percentage Fe added)

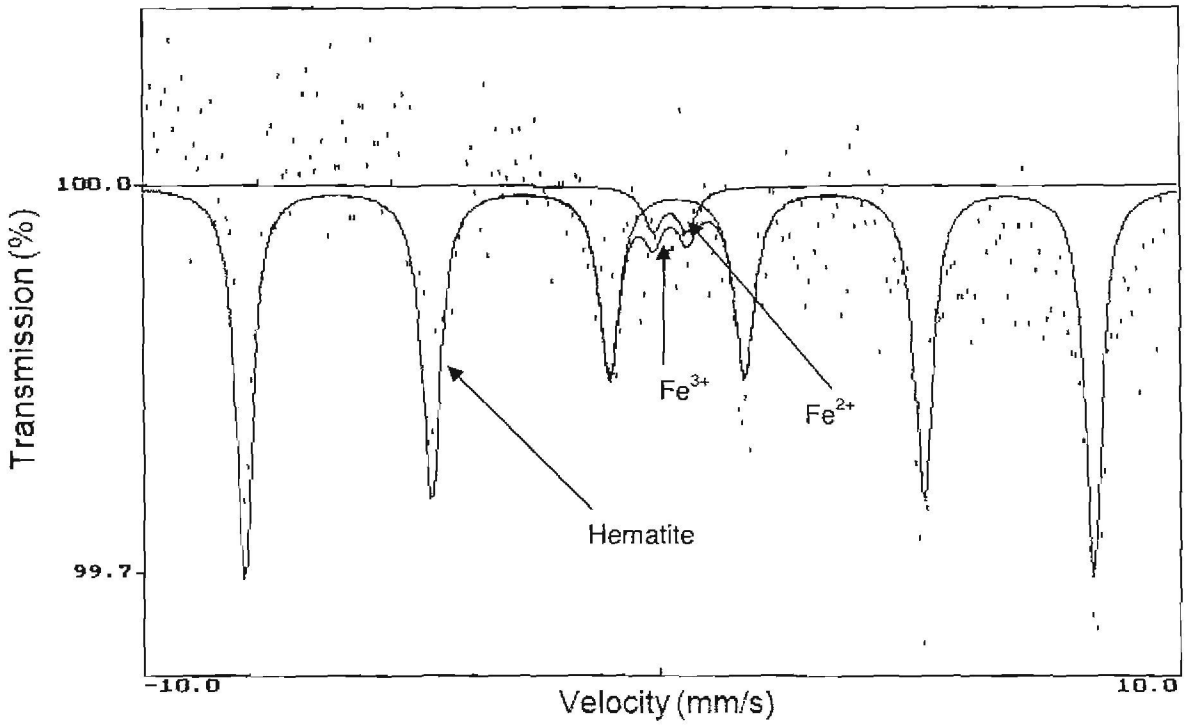


Figure A.5: The Mössbauer spectrum for Sample A ash
(2 mass percentage Fe added)

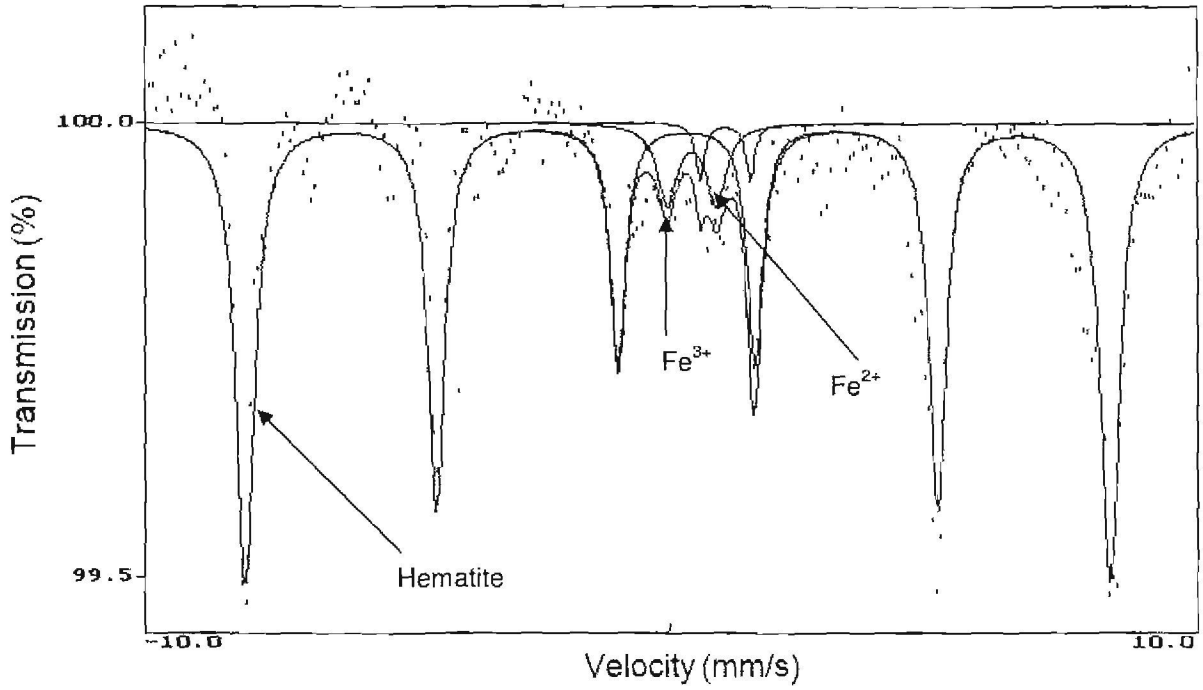


Figure A.6: The Mössbauer spectrum for Sample A ash
(5 mass percentage Fe added)

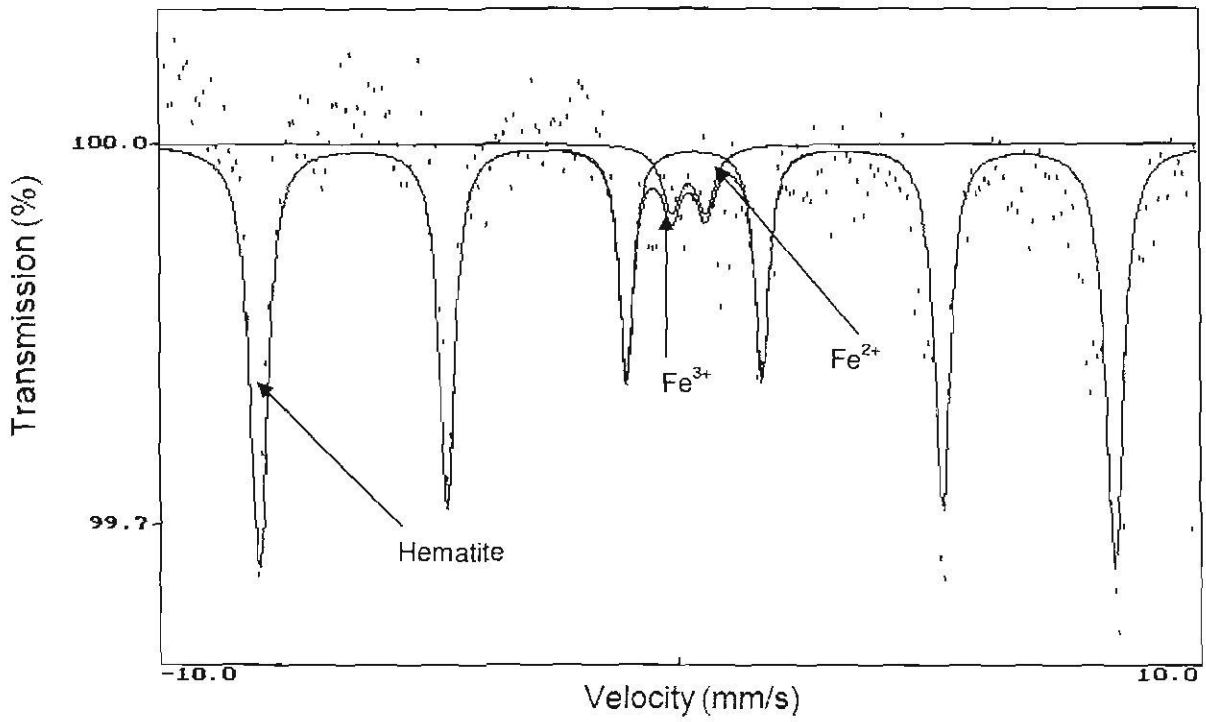


Figure A.7: The Mössbauer spectrum for Sample A ash
(10 mass percentage Fe added)

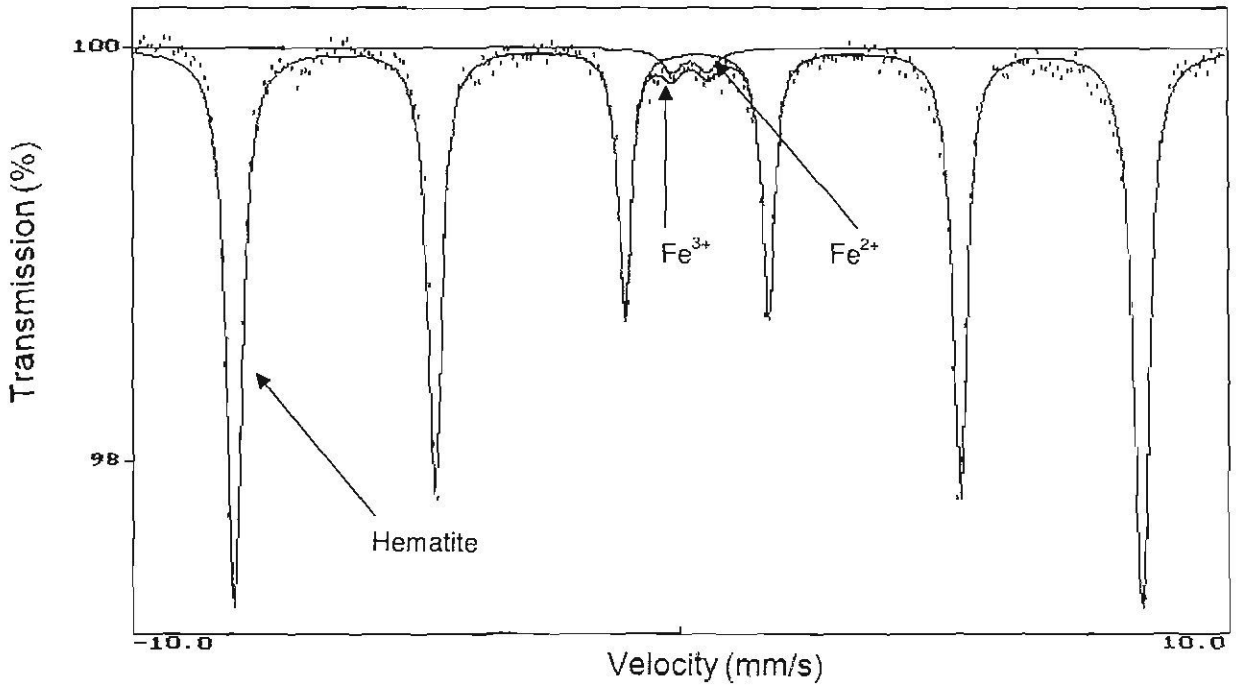


Figure A.8: The Mössbauer spectrum for Sample A ash
(15 mass percentage Fe added)

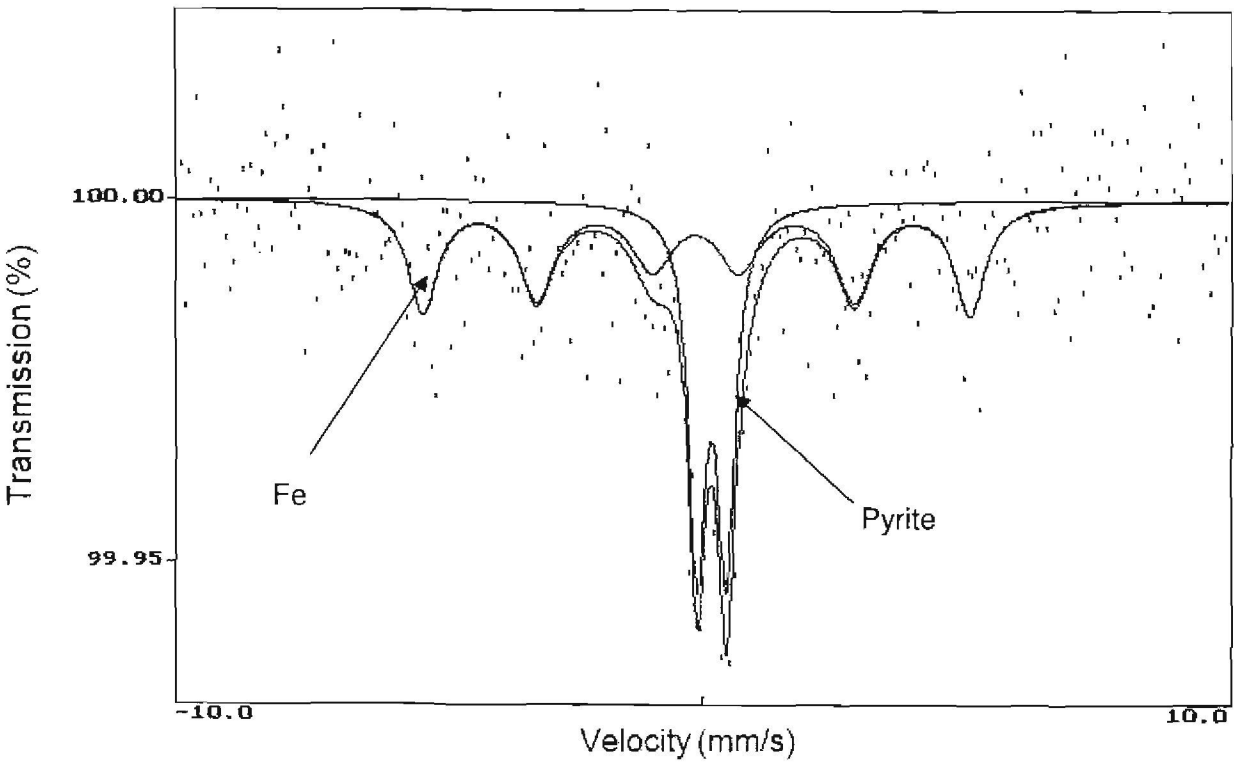


Figure A.9: The Mössbauer spectrum for Sample B coal
(2 mass percentage Fe added)

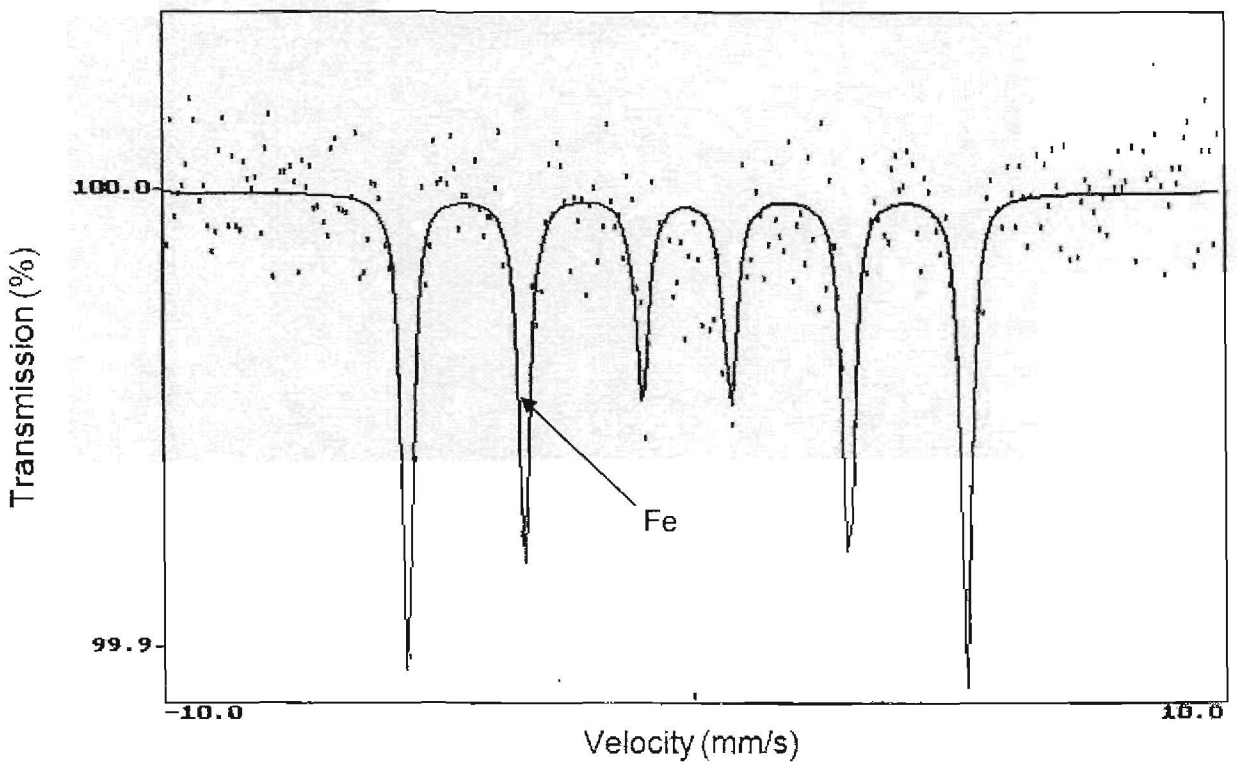


Figure A.10: The Mössbauer spectrum for Sample B coal
(5 mass percentage Fe added)

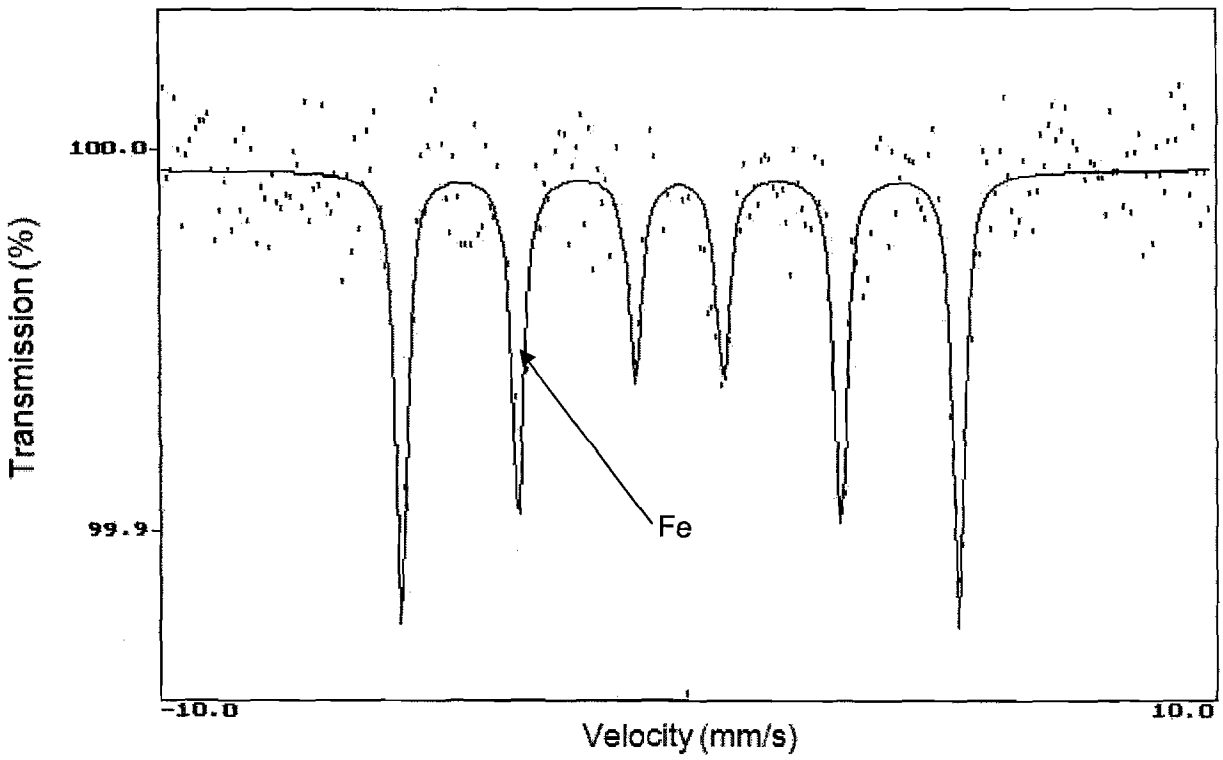


Figure A.11: The Mössbauer spectrum for Sample B coal
(10 mass percentage Fe added)

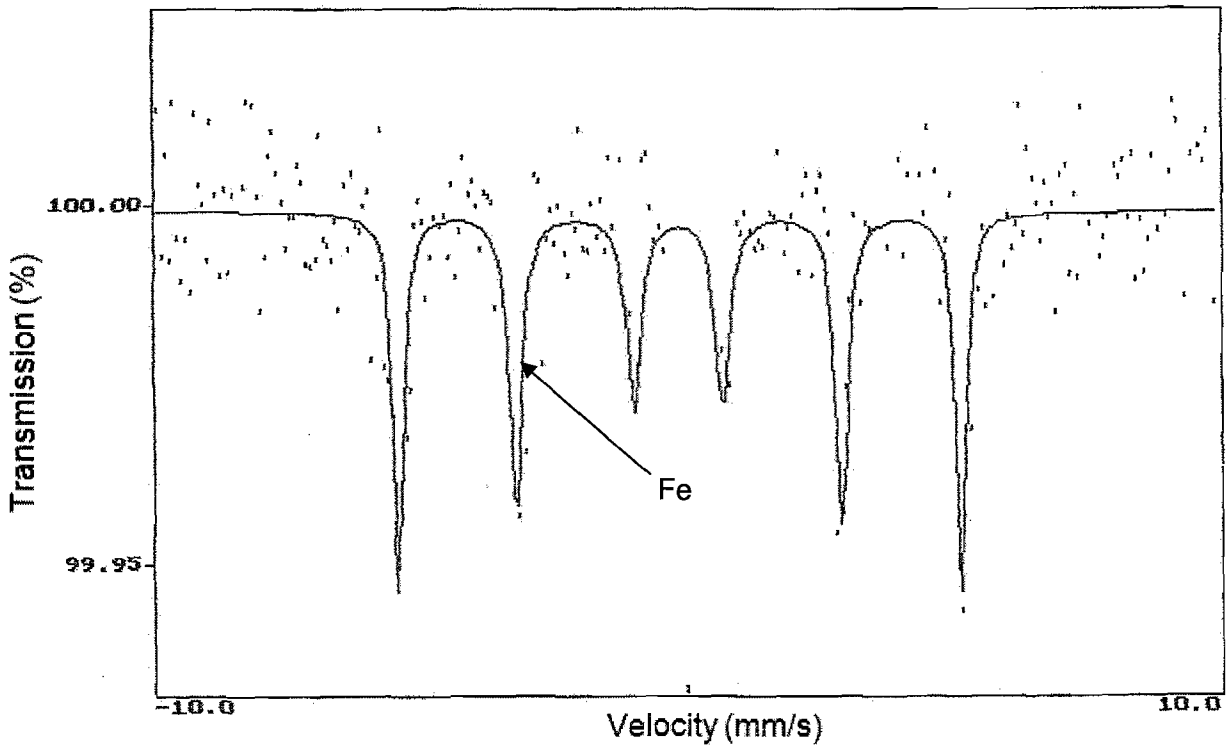


Figure A.12: The Mössbauer spectrum for Sample B coal
(15 mass percentage Fe added)

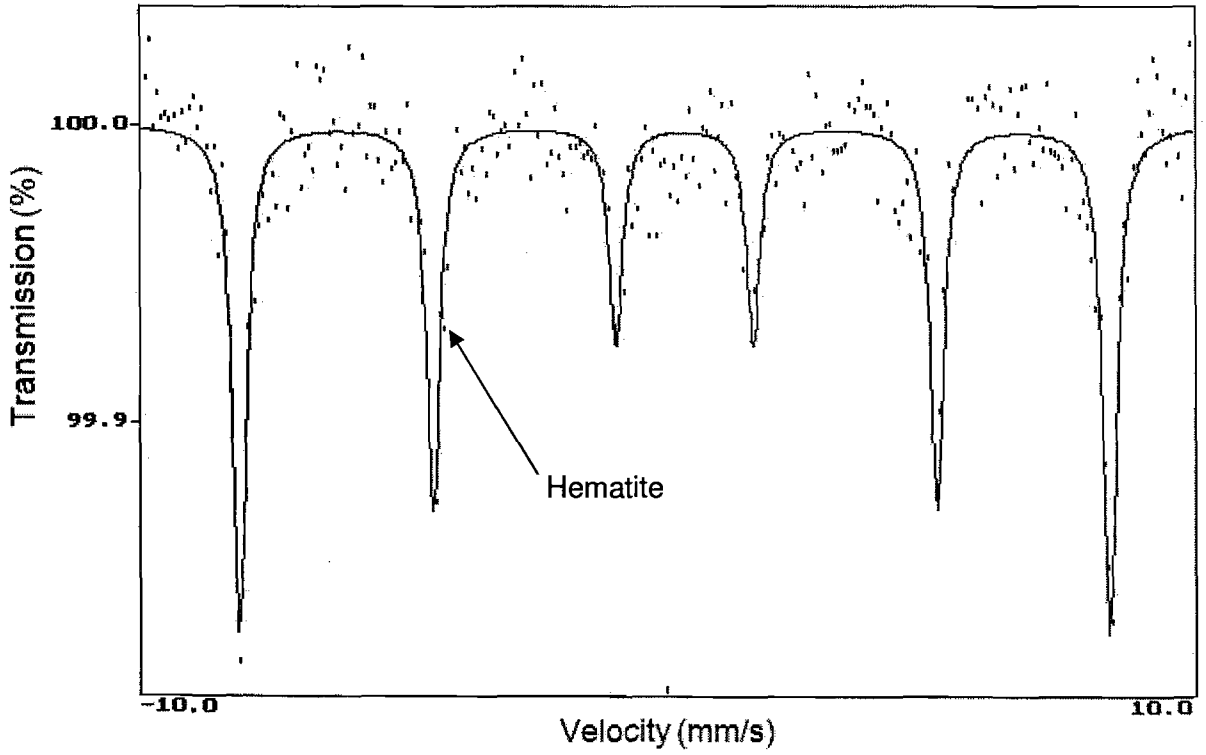


Figure A.13: The Mössbauer spectrum for Sample B ash
(2 mass percentage Fe added)

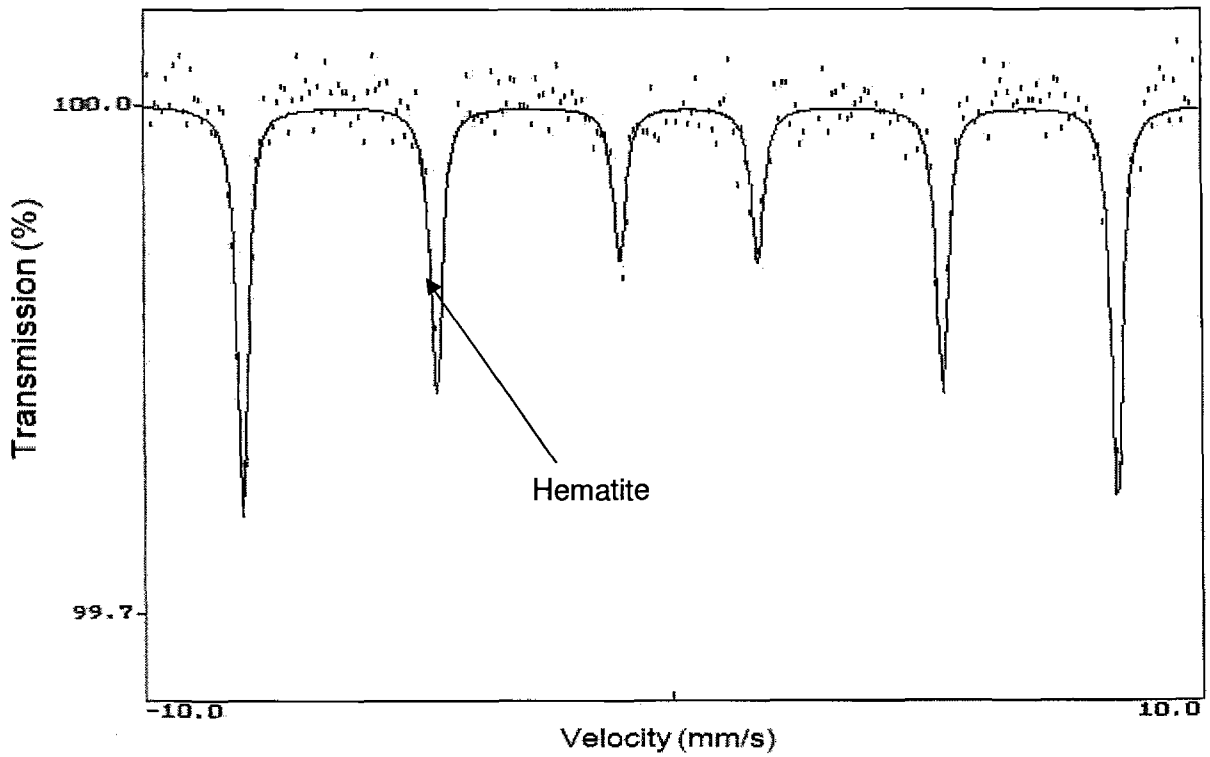


Figure A.14: The Mössbauer spectrum for Sample B ash
(5 mass percentage Fe added)

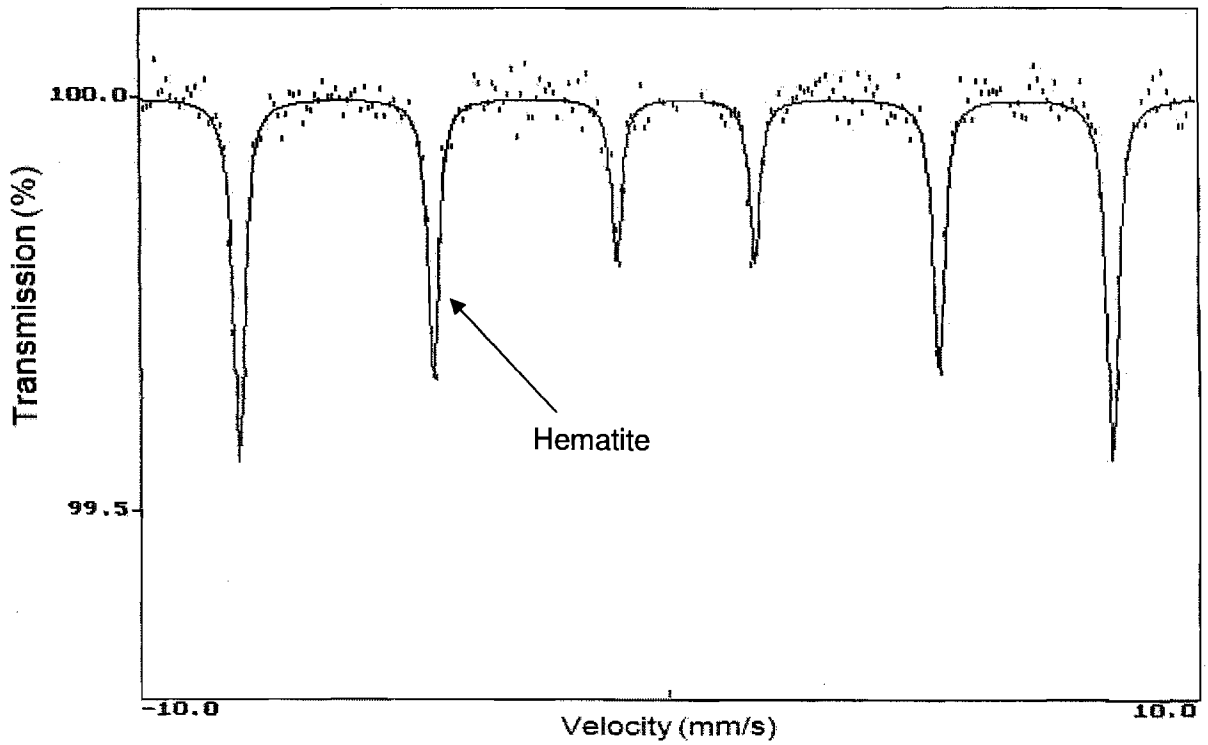


Figure A.15: The Mössbauer spectrum for Sample B ash
(10 mass percentage Fe added)

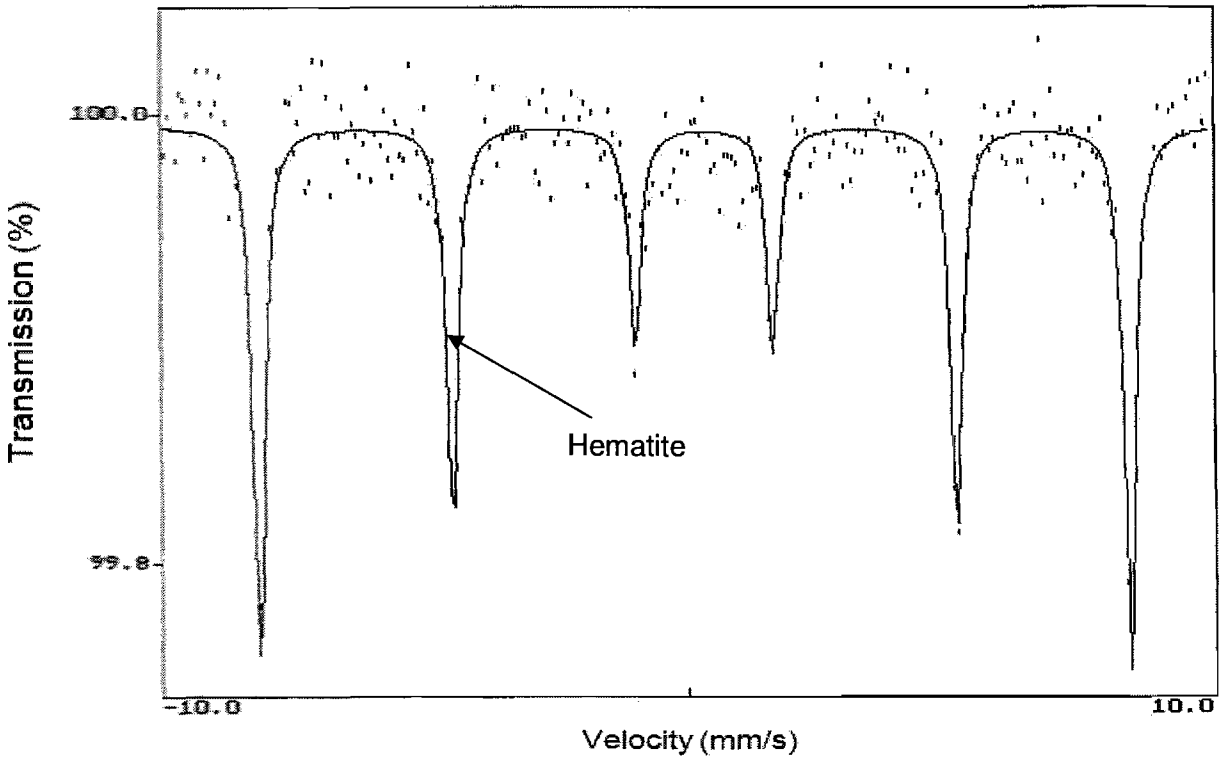


Figure A.16: The Mössbauer spectrum for Sample B ash
(15 mass percentage Fe added)

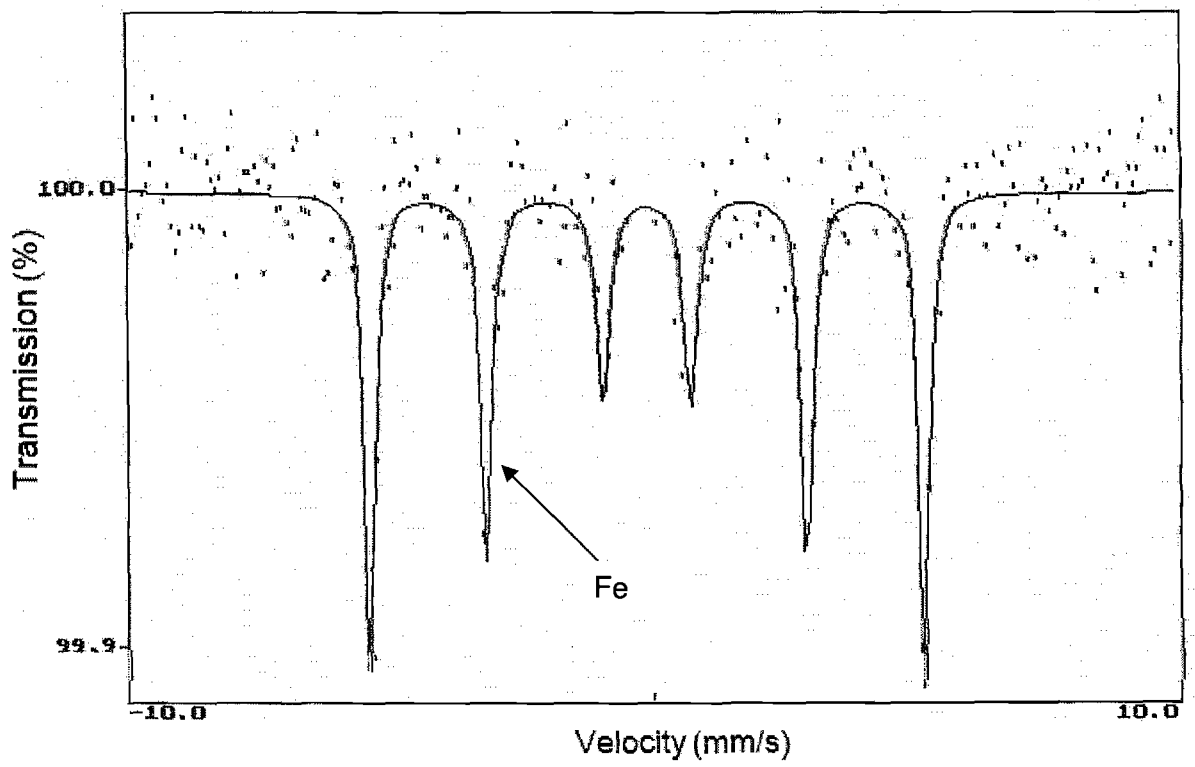


Figure A.17: The Mössbauer spectrum for Sample C coal
(5 mass percentage Fe added)

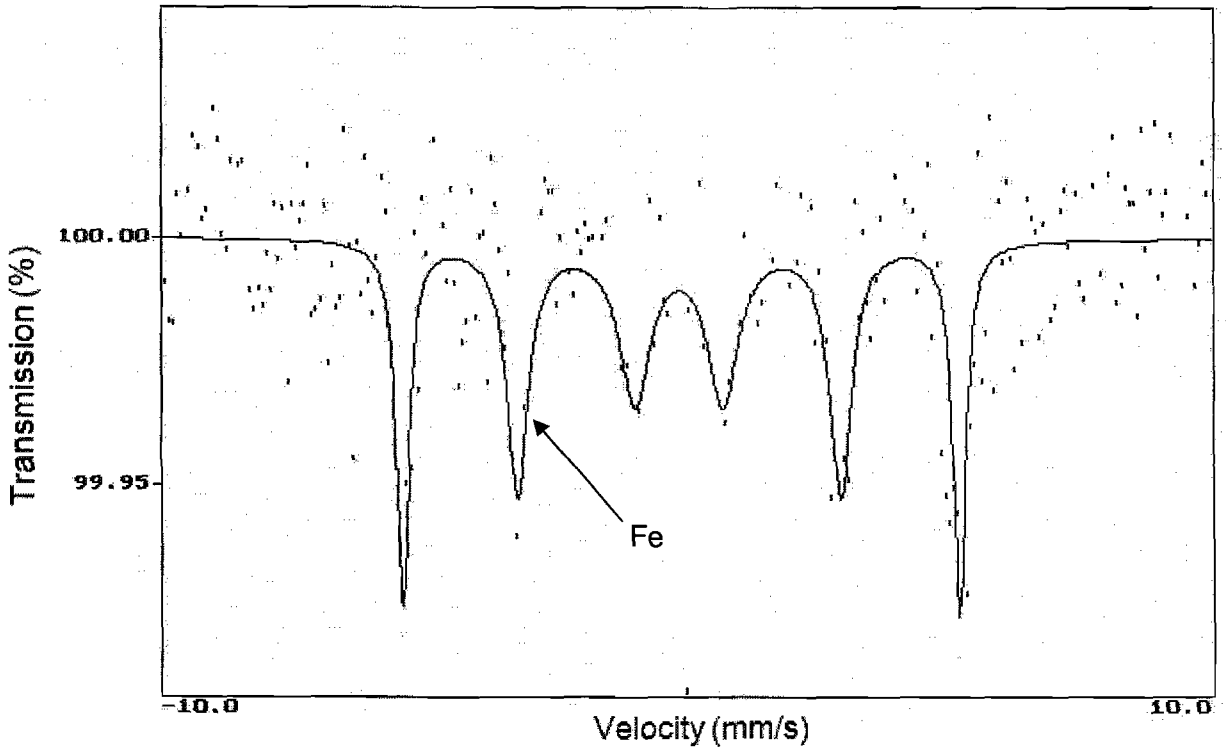


Figure A.18: The Mössbauer spectrum for Sample C coal
(10 mass percentage Fe added)

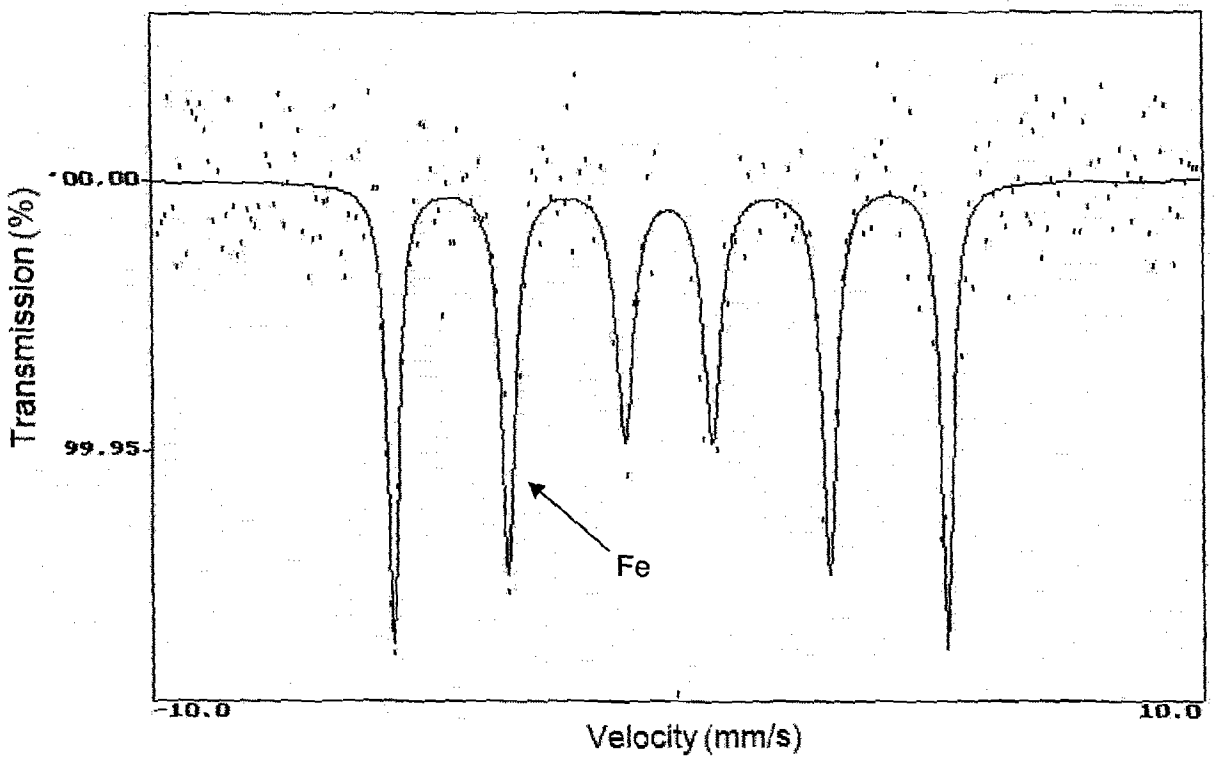


Figure A.19: The Mössbauer spectrum for Sample C coal
(15 mass percentage Fe added)

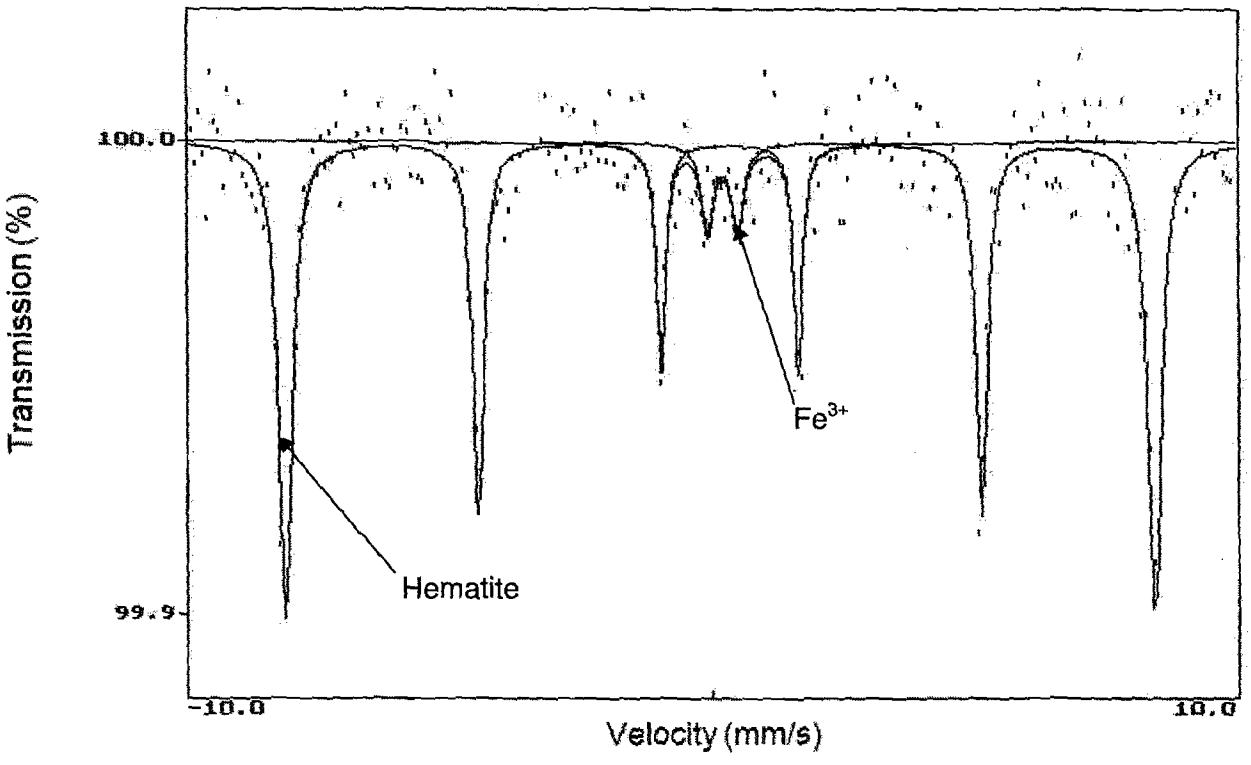


Figure A.20: The Mössbauer spectrum for Sample C ash
(2 mass percentage Fe added)

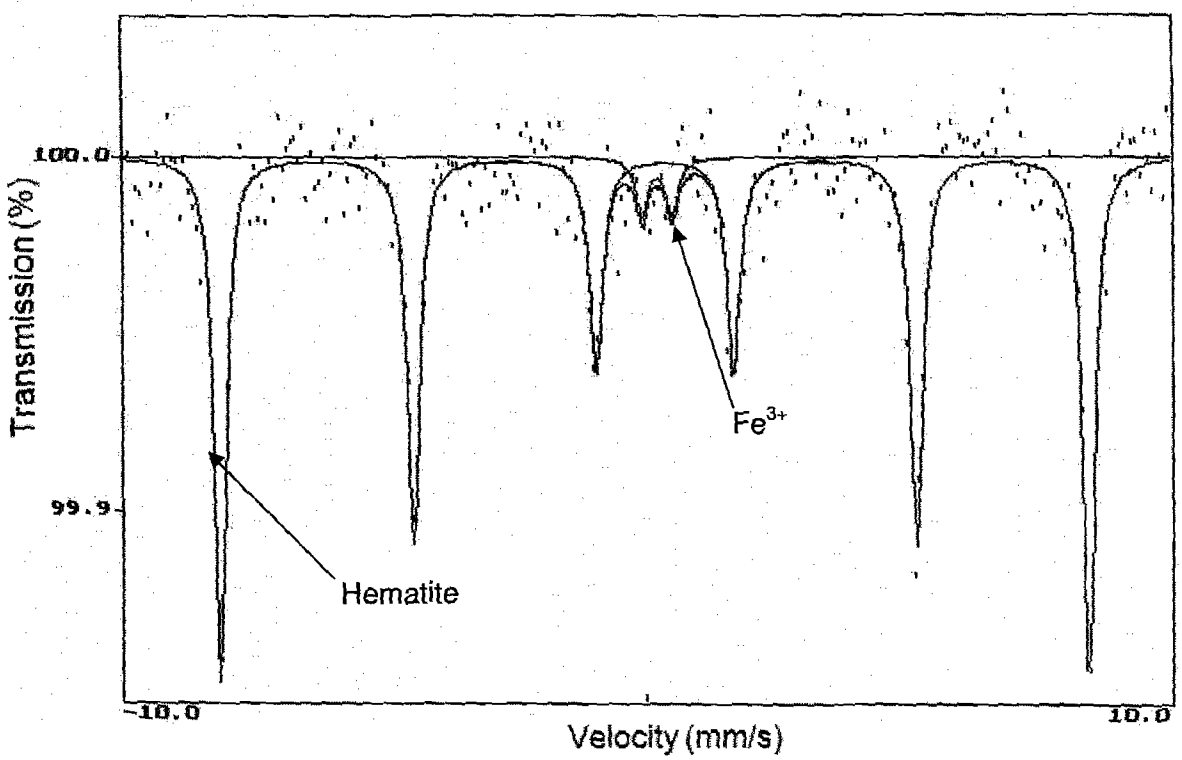


Figure A.21: The Mössbauer spectrum for Sample C ash
(5 mass percentage Fe added)

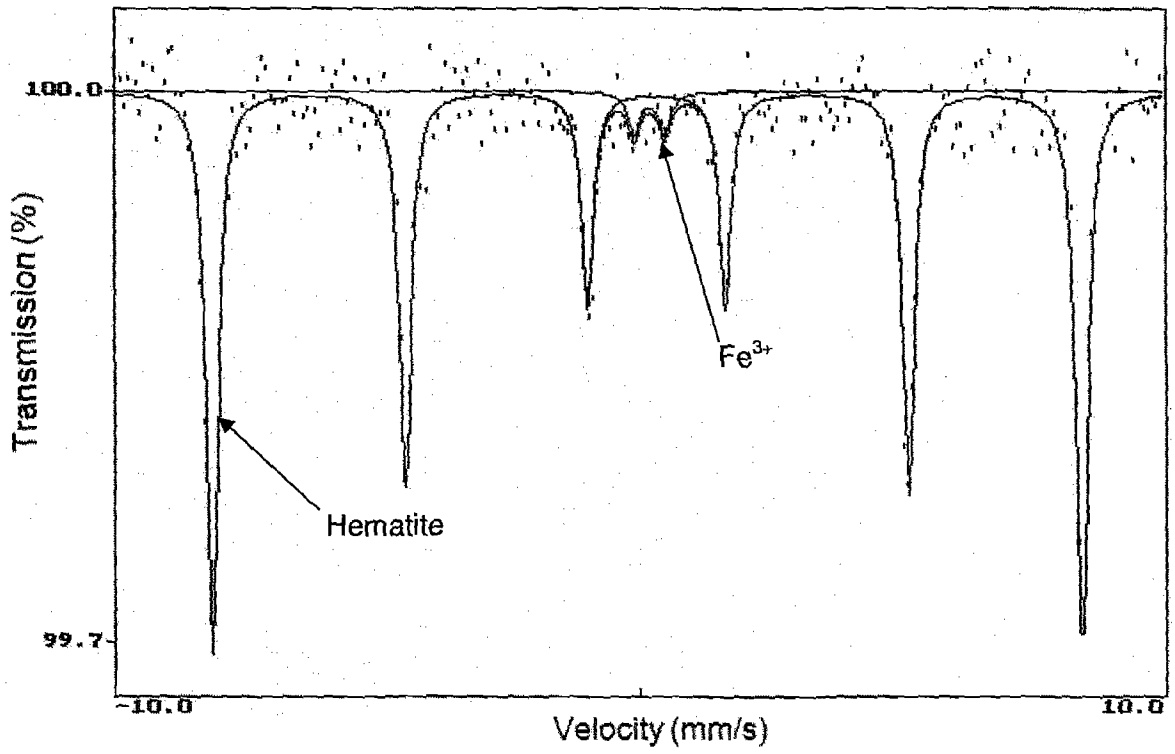


Figure A.22: The Mössbauer spectrum for Sample C ash
(10 mass percentage Fe added)

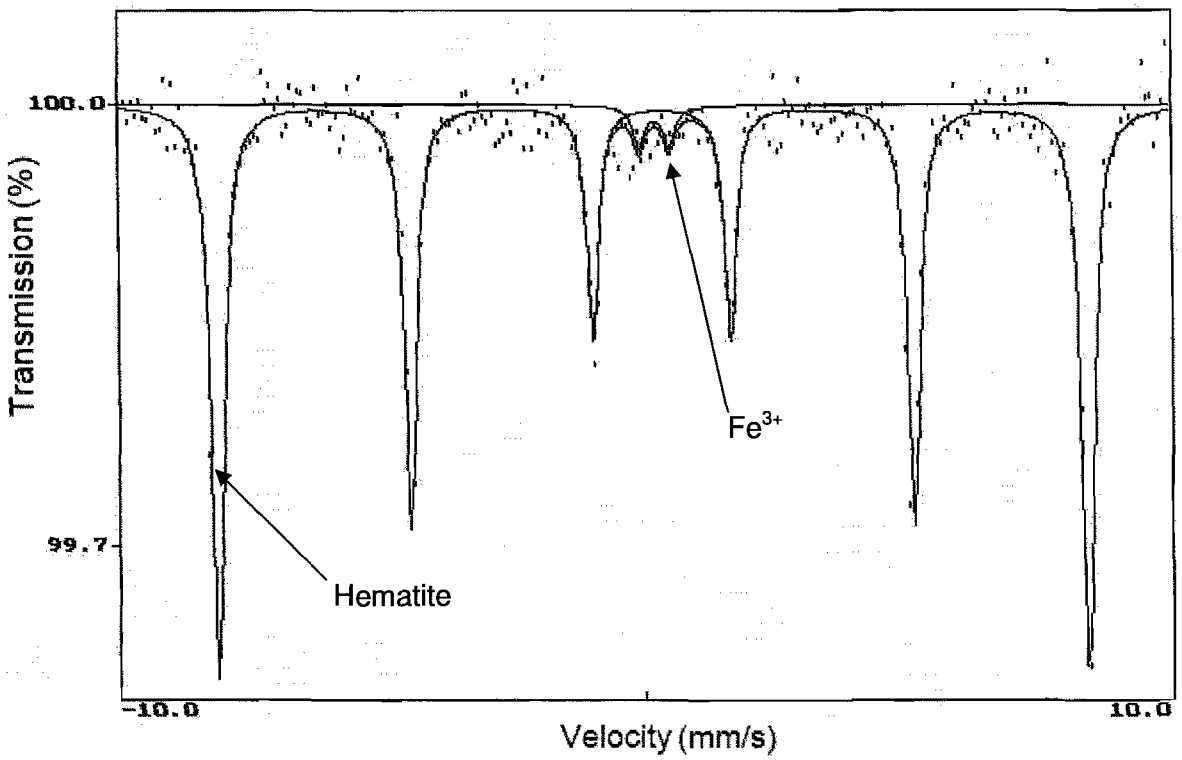


Figure A.23: The Mössbauer spectrum for Sample C ash
(15 mass percentage Fe added)